Universidade de Aveiro Departamento de Química
2011-2012

JOAO RAFAEL RIBEIRO MARQUES

ESTUDO DE PREPARACOES DE FERRO PARA ADMINISTRACAO INTRAVENOSA

Universidade de Aveiro Departamento de Química
2011-2012

JOAO RAFAEL RIBEIRO MARQUES

ESTUDO DE PREPARACOES DE FERRO PARA ADMINISTRACAO INTRAVENOSA

Dissertação apresentada à Universidade de Aveiro para cumprimento dos requisitos necessários à obtenção do grau de Mestre em Bioquímica Clínica, realizada sob a orientação científica do Doutor Nuno Faria, Investigador do Medical Research Council – Human Nutrition Research
e do Doutor Brian Goodfellow, Professor auxiliar do Departamento de Química da Universidade de Aveiro.

o júri

presidente

Doutor Pedro Miguel Dimas Neves Domingues
Professor auxiliar – Departamento de Química – Universidade de Aveiro

Doutora Teresa Margarida dos Santos
Professora auxiliar – Departamento de Química – Universidade de Aveiro

Doutor Nuno Jorge Rodrigues Faria
Investigador Medical Res- Biominerals Resarch Section – Medical Research Council - Human Nutrition Research, Cambridge, U.K.

agradecimentos

Quero agradecer ao instituto MRC-HNR pelo caloroso acolhimento e pela experiencia de vida e profissional que me proporcionaram durante 10 meses de trabalho árduo. A universidade de Aveiro merece, igualmente, uma grande palavra de apreço, porque desde 2007 deu-me todas as condições para evoluir como Bioquímico e como Homem. Em destaque, agradeço ao doutor Nuno Faria e ao doutor Brian Goodfellow pela orientação prestada, ao doutor Jonathan Powell (chefe da “Biomineral Research Section”) por me ter feito sentir que pertencia à família do grupo, e também agradeço a todos os colegas e amigos que deixei em Cambridge, pelo convívio e gargalhadas. Finalmente, queria destacar o papel indispensável da minha família porque foram o pilar que me segurou nos melhores e piores momentos durante toda esta “aventura”, e sem eles a realidade seria outra.

Palavras-chave Deficiência de ferro, ferro, nanopartículas, ferro intravenoso, labilidade, fase mineral, aglomeração, reacções adversas,

Resumo

Introdução: A deficiência de ferro é um dos problemas nutricionais mais comuns no Mundo. Ao longo dos anos, o ferro intravenoso tem-se tornado o tratamento de eleição para a recuperação dos níveis de ferro e para estimular a eritropoiese em casos de deficiência de ferro severa. Os produtos comercialmente disponíveis partilham a mesma composição e estrutura no núcleo de ferro mas diferem na composição da cobertura carbohidratada e nas suas propriedades físicas (tamanho da nanopartícula, aglomeração) e químicas (comportamento em condições de dissolução, valência do ferro do núcleo), o que confere diferenças substanciais no comportamento farmacológico, e fundamentalmente na sua eficácia e segurança. Contudo, esta relação não esta bem compreendida.
Objectivo: Caracterização das propriedades físico-químicas dos quatro produtos de ferro intravenoso disponíveis no Reino Unido (Cosmofer ®, Venofer®, Ferinject® e Monofer®) e estabelecer uma relação entre essas propriedades e a sua eficácia e segurança.
Métodos: O perfil de dissolução de cada produto foi determinado por um ensaio de dissolução lisosómica que foi desenvolvida para simular a dissolução lisosómica de ferro nanoparticulado intravenoso. O estudo da aglomeração das nanopartículas foi determinado por 'particle sizing' e por 'zeta potential' em soluções que simularam as condições no soro. A fase mineral foi determinada por XRD e a valência do ferro do Venofer® foi estudada por voltametria linear.
Resultados e discussão: Todos os produtos apresentaram sinais de aglomeração em condições fisiológicas, mas, entre eles, o Venofer apresentou a mais forte evidência de aglomeração, tanto em soro bovino fetal como em solução de cálcio e fosfato. Venofer exibiu, igualmente, a maior labilidade de ferro, enquanto que o Ferinject® revelou o comportamento menos lábil. O Ferinject® foi o único material a demonstrar carga positiva na sua superfície em suspensão aquosa, e o único que apresentou akaganeite como sendo a fase mineral presente no núcleo de ferro enquanto que o Cosmofer e o Monofer demostraram um perfil mais amorfo. Com a voltametria linear, um conteúdo ferroso maior do que o férrico foi inicialmente detectado no Venofer mas após a correcção da deposição da espécie ferrosa na superfície do eléctrodo, a espécie férrica foi a única a ser detectada.
Conclusão: A metodologia estudada permitiu o estudo dos diferentes comportamentos dos produtos estudados em termos de labilidade de ferro, da relação entre a diminuição do tamanho da partícula e do aumento da amorficidade do núcleo com a facilidade e rapidez de disponibilização de ferro e com a consequente maior incidência de reacções anafilactóides após administração. Cargas positivas na superfície das nanopartículas poderão incrementar a afinidade com o fosfato sanguíneo, o que justifica os vários relatos de hipofosfatemia associado à administração de Ferinject. As fortes evidências de aglomeração verificadas com o Venofer aliadas à sua baixa robustez comprovam a sua formulação de 'iron sucrose' como a mais preocupante do ponto de vista da segurança. Apesar dos resultados não tao clarificadores quanto à valência do ferro no Venofer, a voltametria linear tem potencial para poder estudar a dissolução das nanopartículas de uma forma mais progressiva e com menos variabilidade.

Keywords Iron deficiency, Iron nanoparticles, ferric, ferrous, intravenous iron, lability, mineral phase, agglomeration, adverse reactions.

Abstract

Introduction: Iron deficiency is one of the most common nutritional deficiencies worldwide. Over the years, intravenous iron has become the preferred iron repletion and erythropoiesis treatment to severe iron deficiency. The intravenous iron products available commercially share the same core chemistry but differ in the composition of the carbohydrate shell, as well as, in physical (particle size, agglomeration) and chemical (dissolution performance, iron valence of the core) properties, which makes them vary substantially in pharmacological behavior, and ultimately, in the efficacy and safety profile. However, this relationship is not well understood.

Aim: Perform a physicochemical characterization of the four IV iron products available in the UK (Cosmofer ®, Venofer®, Ferinject® and Monofer®) and establish a relationship between these properties and their efficacy and safety.

Methods: The dissolution performance of each IV iron material was determined by a lysosomal dissolution assay which was developed to mimic the lysosomal dissolution of nanoparticulated IV iron. The nanoparticle agglomeration was determined by particle sizing assays in serum mimetic solutions, and by zeta potential. The mineral phase of the iron core of the nanoparticles was determined by XRD, and the ferrous/ferric presence in Venofer® was studied by linear voltammetry.

Results and discussion: The four products revealed signs of nanoparticle agglomeration when in physiological conditions but, of these, Venofer exhibited the strongest evidence for agglomeration, in both fetal bovine serum and in a simple calcium and phosphate solution. Venofer also presented the highest iron lability whereas Ferinject had the least labile behavior. Ferinject was also the only material with positive surface charge when in a water suspension and with akaganeite as the mineral phase in the iron core, while Monofer and Cosmofer resembled a more amorphousness mineral phase. Indications of greater ferrous iron content than ferric were initially detected in Venofer but after the correction of the ferrous deposition in the electrode, the ferric specie became exclusive.

Conclusion: The methodology developed allowed the study of the different behaviors of the four studied products in terms of iron lability, the relationship of the decrease of particle size and the increase of amorphousness with the ease and quickness of iron mobilization and bioavailability, and with the consequent higher incidence of anaphylactoid type reactions after administration. Positive surface charges might increase the affinity to serum phosphate, which justify the commonly reported hypophosphatemia associated to the administration of Ferinject. The strong evidences of agglomeration with Venofer and its poor robustness makes the iron sucrose material the most concerning in safety matters. Although the uncertain results regarding the iron valence of Venofer, linear voltammetry has the potential to assess the nanoparticulate dissolution more progressively and reliably.

Index

Abbreviations:

AE = Adverse events

DLS = Dynamic light scattering

DME = Dropping mercury electrode

DTS = Dispersion tecnhology software

DMT-1 = Divalent metal transporter 1

ESA = Erythropoiesis-stimulating agent

FDA = Food and Drug Administration

FGF-23 = Fibroblast growth factor 23

GI = Gastrointestinal

HDD-CKD = Haemodialysis dependent-chronic kidney disease

HMW-ID = High molecular weight Iron dextran

IRE/IRP = Iron response element/iron response protein

ICDD = International Centre for Diffraction Data

ICP-OES = Inductively Coupled Plasma - Optical Emission Spectrometer

IV = Intravenous

LIP = Labile iron pool

LMW-ID = Low molecular weight Iron dextran

NTBI = Non-transferrin bound iron

PCS = Photon correlation spectroscopy

QELS = Quasi-elastic light scattering

RDE = Rotating disk electrode

TIBC = Total iron binding capacity

TDI = Total dose infusion

Tf = Transferrin

TfR1 = Transferrin receptor 1

1. Iron Homeostasis

1.1 Iron distribution in Humans

The Human body contains approximately 3-5 g of iron (45-55 mg/kg of body weight in adult women and men, respectively) [1]. The vast majority of body iron (at least 2.1 g in humans [2], 30 mg/kg [3]) is distributed in the haemoglobin of red blood cells and developing erythroid cells. The only other fraction of quantitative significance is storage iron in the liver, amounting to 15 mg/kg (~1g) in the adult male [4]. Significant amounts of iron are also present in macrophages (up to 600 mg) and in the myoglobin of muscles (~300 mg) to a large extent within ferritin and its degradation product hemosiderin *(Figure 1)* [2]. The remaining body iron is primarily localized in cytochromes and iron-containing enzymes [1].

Since humans maintain a precise iron balance during adulthood, the normal loss of about 0.9 mg/day in the adult male is derived from the gastrointestinal (GI) tract (0.6 mg), from the desquamated epithelium of skin (0.2 mg) and from the urinary tract (0.1 mg). This iron is absorbed from a diet containing 10 to 20 mg of iron, so that the overall absorption of iron is at a level of about 6% [5]. Women during the childbearing years will lose about twice that amount due to menses and childbirth. The iron wasted in a specific volume of blood loss is greater in iron overload status, and it is reduced in cases of iron deficiency [4]. The body has no active means of excreting iron, and thus regulation of the absorption of dietary iron from the duodenum plays a critical role in iron homeostasis [5].

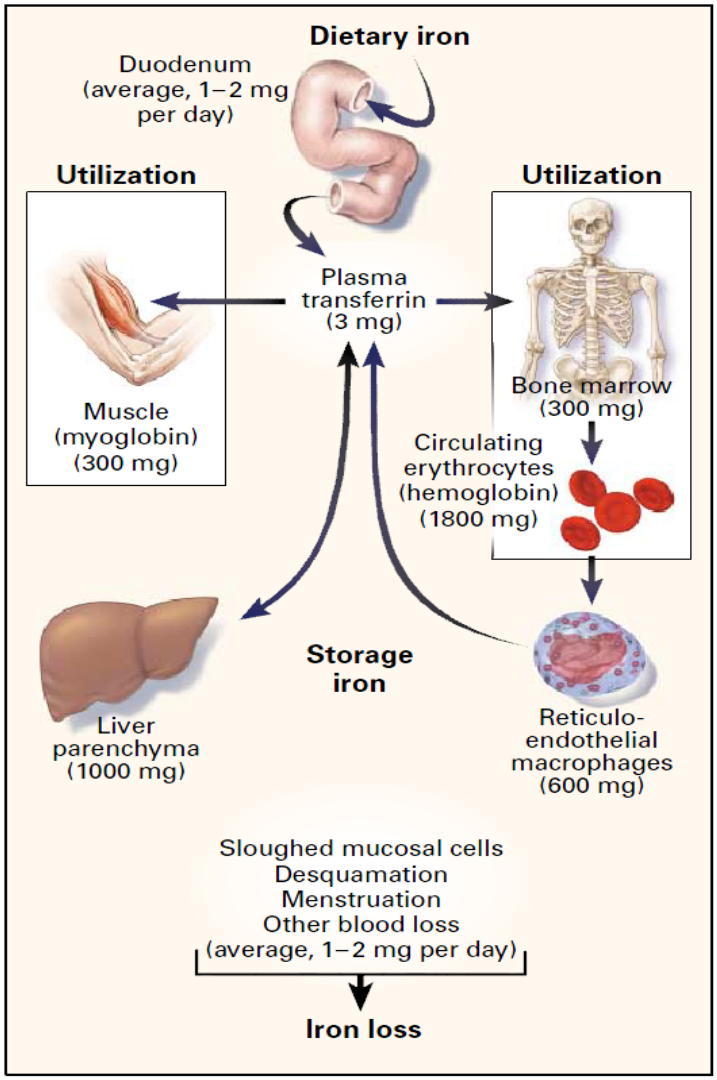

Figure 1 - Iron distribution and loss in the Human [2].

Complex mechanisms have evolved to maintain extracellular iron concentrations in a relatively narrow range and to provide cells with adequate but not excessive iron for their metabolic needs. Blood concentration of iron is determined by iron absorption in duodenum, recycling of iron from aged erythrocytes by macrophages, iron storage by hepatocytes, iron utilization mainly by the bone marrow and iron losses by the faeces [3]. When one of these homeostatic mechanisms of iron is disrupted, the consequent iron imbalance could result in changed iron bioavailability and associated toxicology.

1.2 Iron Deficiency

Iron deficiency is a major problem health with 40% of the world's population affected (1 to 2 billion people [6]) and it can be either functional or absolute. The first one is defined as a condition in which there is a failure to release iron rapidly enough to keep pace with the demands of the bone marrow for erythropoiesis, despite adequate total body

iron stores (ferritin with normal levels). This condition is commonly associated with erythropoiesis-stimulating agent (ESA) usage, because in this situation, iron uptake by erythroid cells is increased to meet the demand of increased red blood cells production, thereby preventing macrophages to release stores of iron fast enough to meet that demand. Another case might be associated with chronic inflammation where the iron transport across cell membranes is inhibited (e.g. by hepcidin in anaemia of chronic disease) which decreases accessibility of storage iron and G) absorption, leading to an increased frequency of iron-restricted erythropoiesis. Absolute iron deficiency occurs when total body iron stores become depleted, that is, the amount of stored iron is no longer adequate to meet the demands for erythropoiesis (e.g. chronic blood losses) [7, 8].

Anaemia emerges in cases where severe iron deficiency impairs oxygen-carrying capacity of the red blood cells, and it is the most familiar clinical means by which iron deficiency is recognized as well as explains the common fatigue and pallor associated [7, 8]. Iron deficiency may also reduce exercise performance, lead to an abnormal neurotransmitter function and result in altered immunological and inflammatory defences. In children, it can cause developmental delays and cognitive abnormalities, whereas in pregnant women, the likelihood of premature and low-birth-weight delivery is increased [9].

1.2.1 Causes

Iron deficiency will result from any condition in which dietary iron intake does not meet the demands of the body and also when there is deprived iron absorption and on-going blood losses. A list of the causes of iron deficiency is shown in *Table 1* [1, 2].

Table 1 – The four main causes of iron deficiency and the respective examples (adapted from [1, 2]).

CAUSES	EXAMPLES
Increased iron demands	Pregnancy
	Infancy
	Patients treated with ESA
Insufficient intake	Chronic alcoholism
	Poor nutrition
	Inappropriate diet with deficit in iron and ascorbic acid
Inadequate iron absorption	Poor bioavailability
	High gastric pH
	Excess dietary tannin, phytates, or starch
	Competition from other metals (e.g. copper, lead)
	Loss of dysfunction or absorptive enterocytes
	Bowel resection
	Helycobacter pylori infection
	Inflammatory bowel disease, Chron's disease, Celiac disease, ulcerative colitis
Increased iron loss	Gastrointestinal bleeding (ulcer, varices, epistaxis)
	Genitourinary bleeding
	Pulmonary bleeding
	Other blood loss (surgery, blood donation, trauma, excessive phlebotomy, large vascular malformations, haemodialysis patients with chronic kidney disease)

1.2.2 Assessment of Iron Deficiency

Laboratory tests, such as haemoglobin concentration can be used to screen for iron deficiency, whereas serum ferritin concentration can be used to confirm iron deficiency. A low ferritin level is reliably indicative of depletion of iron stores ("absolute iron deficiency") and normal or even high level may be associated with underlying iron deficiency in sick patients ("functional iron deficiency"). Other tests may be needed, such as haematocrit, erythrocyte zinc protoporphyrin concentration, transferrin (Tf) concentration, total iron binding-capacity capacity (TIBC) and serum iron concentration (*Table 2*) [10]. However, these parameters might be affected in other conditions (e.g. ferritin concentration elevated in patients with infectious, inflammatory, and neoplasic conditions). Bone marrow examination is a painful and invasive method but accurately shows the absence of stainable iron so it is the definitive method for diagnosing iron deficiency. Alternatively, if the cause is also identified, the clinical judgment in

combination with the measurement of haemoglobin and ferritin usually provides an accurate interpretation and leads to the necessary action [11, 12].

Table 2 - Parameters accepted to the assessment of iron deficiency. *EP* is the erythrocyte zinc protoporphyrin concentration, *Tf* is transferrin, *TIBC* is the total iron binding capacity, *Hb* refers to the haemoglobin concentration, *Hct* is the haematocrit and *N* means normal values (adapted from Trost et al, 2006 [10]).

	Body iron content			**Storage iron**	**Transport iron**				**Functional iron**
Iron status	Storage iron	Transport iron	Functional iron	Serum ferritin	EP	Tf conc/TIBC	Tf saturation	Serum iron	Hb, Hct
Iron overload	↑	↑	N	↑	N	↓	↑	↑	N
Normal	N	N	N	N	N	N	N	N	N
Iron depletion	↓	N	N	↓	N	N/↑	N/↓	N/↓	N
Iron-deficient erythropoiesis	↓	↓	N	↓	↑	↑	↓	↓	N
Iron deficiency anaemia	↓	↓	↓	↓	↑	↑	↓	↓	↓

1.2.3 Treatment: Oral iron vs Intravenous iron

Safety

Oral iron supplementation is a commonly used strategy to meet the increased requirements of risk groups, such as women of childbearing age. It has the advantage of being simple and cheap but it is limited by side effects (56%), poor adhesion to the intestinal walls, poor absorption and low efficacy [13]. Side effects of oral iron supplementation on GI tract may be troublesome, because replacement therapy takes a long time to replenish body iron stores and some patients have difficulty tolerating iron salts because these substances tend to cause GI distress and toxicity, forcing the discontinuation of treatment. Plus, liquid iron salt preparations, given to young children, may cause permanent staining of the teeth and are one of the causes of non-compliance. If provided in excess, oral iron may induce mucosal absorption block [14], peroxidative damage through production of ROS resulting in mucosal cell death, loss of functional integrity and decreased turnover of epithelial cells [9, 11].

Intravenous (IV) iron is the best means of guaranteeing delivery of readily available iron to the bone marrow and it is more efficacious than oral iron because, since the GI tract is bypassed, IV delivery promotes a more rapid and reliable repletion of iron stores with faster normalization of haemoglobin levels, it has better acceptance by the organism and less incidence and frequency of side effects. It has also the ability to keep pace with

continuous blood loss and sustain iron adequacy resulting in lower transfusion requirements and shorter length of hospital stay [15, 16]. However, IV iron requires great clinical supervision and there still remain concerns about iron overload, the acute safety profiles of the available IV products and the potential for long-term harm from repeated administration because all IV iron cause acute severe reactions [17]. *Table 3* shows a practical example of the better safety profile of IV delivery in a study trial [18].

Table 3 - List of adverse events occurred possibly or definitely related to ferric gluconate administrated in cancer patients with chemotherapy-related anemia and functional iron deficiency. *FG* stands for sodium ferric gluconate [18].

Adverse event, no. of patients (%)	FG (n = 63)	Oral iron (n = 61)
Constipation	2 (3.2)	11 (18.0)
Nausea	2 (3.2)	3 (4.9)
Dyspepsia	1 (1.6)	3 (4.9)
Asthenia	1 (1.6)	2 (3.3)
Anorexia	0	2 (3.3)
Abdominal pain	0	2 (3.3)
Diarrhea	1 (1.6)	0
Hypotension	1 (1.6)	0
Vasodilation	1 (1.6)	0
Angina pectoris	1 (1.6)	0
Tremor	1 (1.6)	0
Pain at injection site	1 (1.6)	0
Vomiting	0	1 (1.6)
Back pain	0	1 (1.6)
Dehydration	0	1 (1.6)
Dizziness	0	1 (1.6)
Taste perversion	0	1 (1.6)
Melena	0	1 (1.6)
Tinnitus	0	1 (1.6)
Total[a]	8 (12.7)	19 (31.1)

[a] Patients may have experienced more than one adverse event.

When to use

Because of its limitations, oral iron is administrated in non-urgent iron repletion where minor iron deficiency is noted in patients with other conditions that would not be compromised by the presence of iron deficiency [7].

IV iron is indicated specially for treatment of severe iron deficiency where there is an exacerbated erythropoiesis request or a clinical need to deliver iron rapidly to replenish iron stores. This condition is associated with the following situations [7, 15]:

- Malabsorption of iron e.g. Anaemia of chronic disease, inflammatory bowel disease)
- On-going loss of blood, e.g. Haemodialysis patients with Dependent-Chronic kidney disease (HDD-CKD).
- Increased iron demands (Obstetrics or ESA therapy patients).
- Anaemia heart failure and ischemic heart disease.
- Anaemia associated with poor iron absorption (i.e. anaemia of chronic disease, anaemia associated with cancer).

Sometimes IV iron treatment is required even in mild iron deficiencies when poor absorption, intolerance and non-compliance to oral iron therapy occurs *(Figure 2)* [19].

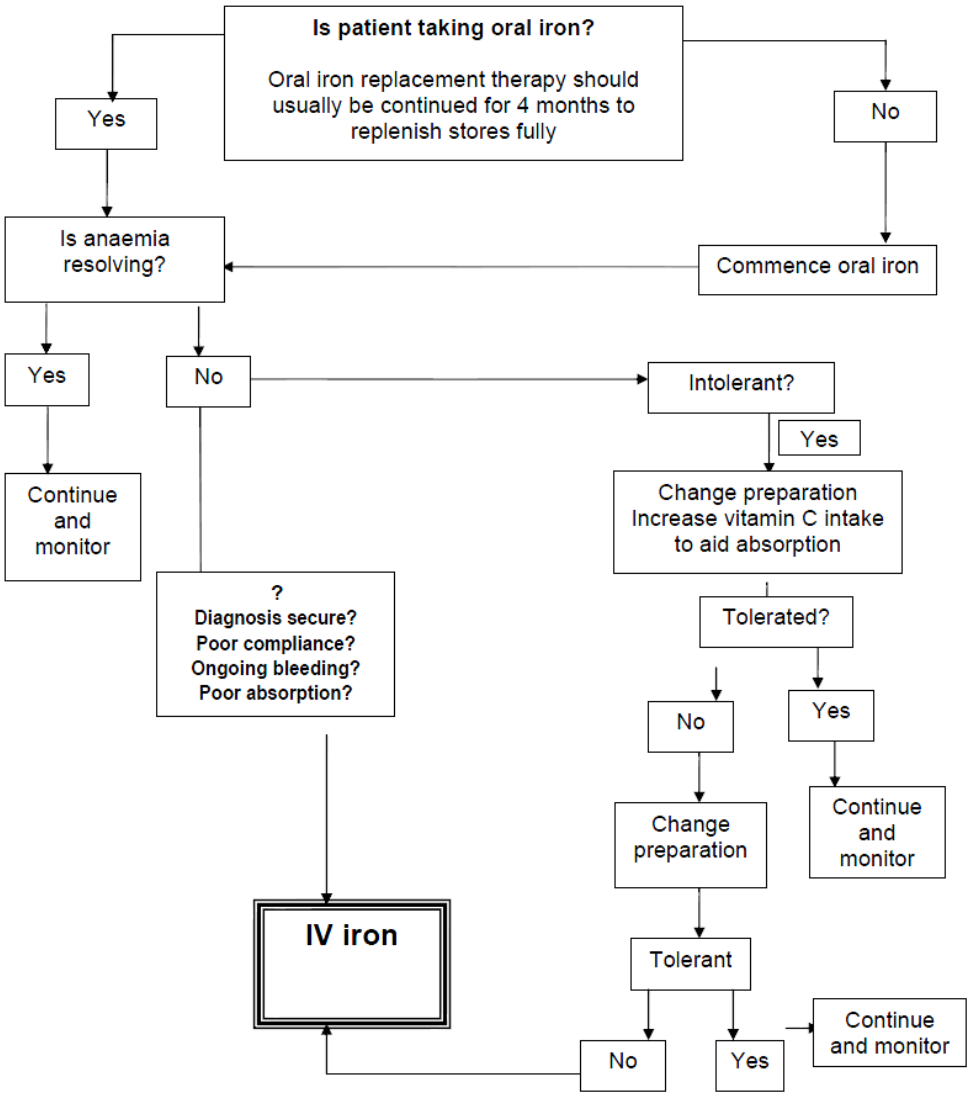

Figure 2 - Flowchart for the use of IV iron in confirmed iron deficiency anaemia, when oral iron cannot resolve the clinical problem [19].

Administration strategy

An IV iron dose requires it to be diluted in 0.9% NaCl before administration by drip infusion or by bolus injection (Venofer® and Ferinject® can be injected undiluted). In case of haemodialysis patients, undiluted injection into the limb of the dialyser can be applied. The cumulative dose required for haemoglobin restoration and repletion of iron stores is calculated by the following Ganzoni formula:

- ***Iron replacement in patients with iron deficiency anaemia:***

Total iron deficit = Weight (kg) x (Target Hb – Actual Hb) (g/l) x 2.4 + Iron stores (mg)

>35 kg Body Weight: **Target Hb=150 g/L**, **iron stores=500 mg.**

- ***Iron replacement for blood loss (no need to replenish the iron stores):***

Total iron deficit = Weight (kg) x (Target Hb – Actual Hb) (g/l) x 2.4

If the required dose exceeds the maximum dose permitted, whether half of the dose is administrated in consecutive days, or the maximum dose in given in the first infusion followed by the reminder in the second infusion.

In general, all IV iron materials are contraindicated in cases of anaemia not attributable to iron deficiency, in iron overload, in disturbances of utilization of iron (e.g. haemosiderosis), history of hypersensitivity to parenteral iron preparations, as well as in patients with a history of asthma, allergic eczema or other atopic allergy [20].

2. Intravenous iron materials

All the current IV iron agents are colloids that consist of small spheroidal iron-carbohydrate nanoparticles with an iron oxyhydroxide core surrounded by a carbohydrate shell that stabilizes the core, slows the release of iron from the core and maintains the resulting particles in a colloidal suspension *(Figure 3)* [21]. All the IV iron agents share the same core chemistry but differ from each other by the particle size and the identity of the surrounding carbohydrate [17, 22, 23].

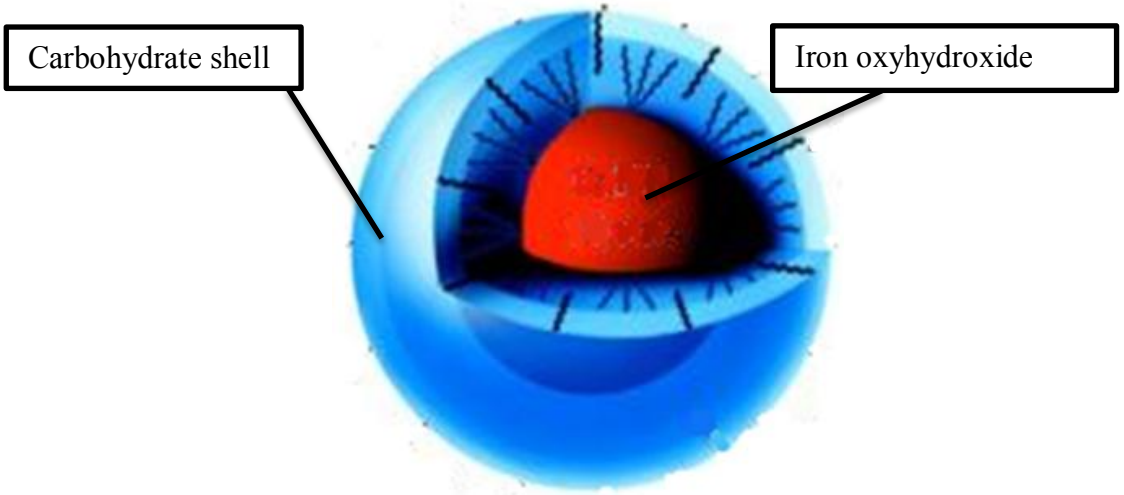

Figure 3 – Schematic of an iron oxyhydroxide nanoparticle present in the intravenous preparations [21].

2.1 Iron core

Ferritin accommodates iron efficiently in an oxyhydroxide ferrihydrite-type solid form and releases it promptly, maintaining an intact structure during this reversible process. Therefore, the IV iron preparations were conceived to have an inorganic core similar to this protein so that its activity as a synthetic iron store in the organism would be ideally similar [24, 25]. The current nanoparticles cores have been identified as iron oxyhydroxide most consistent with a mineral phase of the akaganeite polymorph (β-FeOOH) for all products except for Ferumoxytol, which is thought to have a magnetite and maghemite mixture [26, 27].

Akaganeite resembles the hollandite-like $BaMn_8O_{16}$-type crystal structure with a tetragonal or monoclinic unit cell and it contains "tunnel" shaped cavities occupied by chloride or hydrogen propagating in the c-axis by edge linkages between Fe octahedra. The chloride atoms present in this akaganeite crystal are essential to maintain a stabilized polynuclear ferric oxyhydroxide crystal cell structure, and their complete or partial removal after synthesis leaves channels in the structure that opens core access to ferric ions (*Figure 4*) [24, 28, 29].

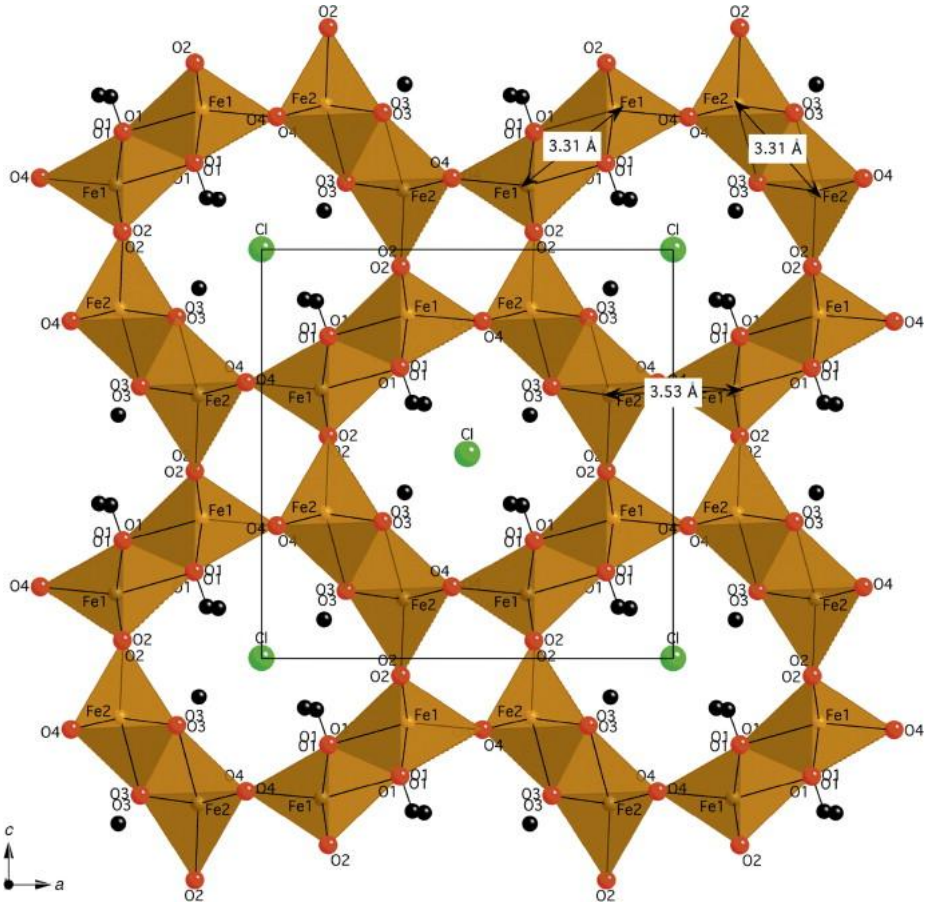

Figure 4 - Akaganeite (β-FeOOH,Cl) structure [28].

The presence of octahedrally coordinated high spin ferric ions were identified coordinated with six oxygen atoms at a Fe–O distance of 1.95 Å, and at the location of a disordered shell of iron ions at a distance of about 3.05 Å. The iron oxyhydroxide crystallite dimensions estimated are generally about 1–5 nm in diameter and the dimensions of the core (which may be larger than the size of the crystalline portion) can range from 3 nm diameter spheres to 5 × 34 nm ellipsoidal particles [26]. In exception of the superparamagnetic Ferumoxytol, the low particle magnetic moments confer the IV iron materials very low magnetic response, consistent to the antiferromagnetic structure of akaganeite.[25].

2.2 Carbohydrate shell

Carbohydrates can be appropriate chelating agents for the stabilization of the iron core by slowing down the release of iron, avoiding the contact to the surrounding molecules and maintaining it as a colloidal suspension. Certain carbohydrates, such as sucrose, present multiple hydroxyl groups in a suitable array to chelate iron, although the binding is weak in neutral aqueous solution. Polymeric carbohydrates such as dextran are also used to stabilize nanoparticles because they present a large number of hydroxyl groups, which can cooperatively chelate the surface of iron oxyhydroxide nanoparticles. For a neutral carbohydrate, the chelation to iron is enhanced at high pH, because the hydroxyl groups may become deprotonated, thus acquiring a negative charge, and interacting more strongly with the cationic iron ion. At neutral pH, inherently anionic carbohydrates such as gluconate are more effective nanoparticle stabilizers. In these cases, a carboxyl group provides the negative charge over a broad pH range. Carboxylic chelation to iron can also drive the deprotonation of nearby hydroxyl groups, further enhancing the complex stability [26]. Each carbohydrate has a surface charge in result to the expose of these hydroxyl and carboxylic groups to the surrounding medium, which can affect nanoparticles biodistribution by limiting or enhancing interactions of nanoparticles with serum proteins, electrolytes, and non-targeted cells [30].

2.3 Mode of action

After injection or infusion of the IV iron material, the distribution and uptake of nanoparticles by the macrophages depends largely on their physicochemical properties such as particle size and surface charge. Thus, when nanoparticles enter the bloodstream, they instantly encounter a complex environment of plasma proteins and phagocytic cells. Nanoparticles tend to adsorb to specific plasma proteins such as immunoglobulins, apolipoproteins, components of Complement System and clotting factors, necessary to mediate nanoparticle recognition and uptake by the macrophages (phagocytosis) [31, 32].

The following intracellular metabolism is yet to be fully understood but phagocytised iron oxide nanoparticles have been shown to be transferred from early to late endosomes (neutral pH) where they may fuse with more acidic lysosomes and become solubilized at lower pH environment, typical of the endolysosome (pH 4.5-5.5), with no

enzymatic involvement. The explanation of this hypothesis can be based on what happens in the normal iron metabolism in the cells. The structure of iron oxide nanoparticles is very similar to that of ferritin because ferritin has an iron oxide core consisted by ferric iron as a solid under physiological pH, coated by a shell. After degradation of ferritin by lysosomal proteases, its iron oxide will be exposed to the surroundings and dissolve. So, it is very likely that the safety of iron nanoparticles is due to degradation of the carbohydrate shell and the iron oxide core in lysosomes, where the iron oxide of the ferritin is degraded *(Figure 5)* [33, 34].

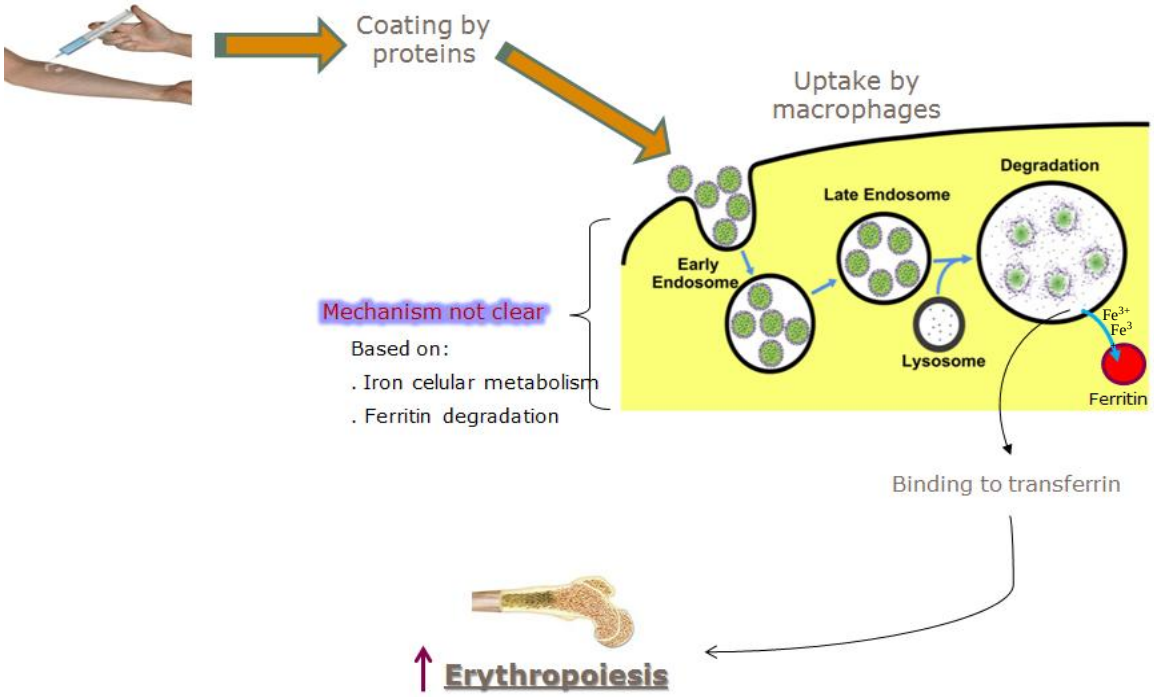

Figure 5 – Processing of IV iron nanoparticles since the product is administrated till the nanoparticles reach the erythroid precursors in the bone marrow.

Moreover, for the release of the free iron from the endolysosome, it should be noted that, in the cellular uptake of iron trough the TfR1 (Transferrin receptor 1) pathway, the transport of iron from the endosome into the cytoplasm involves binding of the iron to various low molecular-weight molecules or transmembrane proteins. Therefore, following the degradation of nanoparticles, it may be speculated that such endogenous Fe(III) chelating compounds facilitate the dissolution and the release of free iron to the Labile Iron Pool (LIP), where it is stored as ferritin/hemosiderin or transported, in lesser extent, out of the cell by ferroportin. Thus, the metabolism of the iron liberated from the core is most probably taken care by the intracellular system for normal iron metabolism [17, 33, 34].

The iron exported out of the cell is bound to transferrin and it is delivered to the transferrin receptor on the surface of erythroid precursors, supporting haemoglobin synthesis and maturation of red blood cell correcting the iron deficiency anaemia. The rate of transfer of iron from the macrophages into the circulation seems to depend mostly on the severity of iron deficiency and the rate of erythropoiesis. When the patient is severely iron deficient, incorporation of iron from IV iron agent into erythroid precursors occurs rapidly whilst in the absence of evidence of iron deficiency, donation of iron from the macrophage to red cells after IV iron administration is blunted, and in patients with cancer or inflammation, little or no erythroid iron uptake may occur. Although every IV iron materials follow this mode of action, there are observations of small fractions that likely bypass the intracellular steps and donate iron directly to transferrin in plasma, which, although not safe, gives a more rapid delivery of iron to the bone marrow [22, 23].

2.4 Chemistry of IV agents & Pharmacologic outcomes

Differences in core size, carbohydrate chemistry and the strength of the iron complex determine pharmacologic and pharmacokinetic differences, including clearance rate after IV administration, rate of release of iron from the ferric hydroxide, maximum tolerated dose and rate of infusion.

2.4.1 Particle size

Size is one of the key parameters in the protein adsorption to the nanoparticles in the plasma (opsonization) and, thus, in the circulation half-life of nanoparticles. When discussing size distribution of particles it is important to remember that it is the hydrodynamic diameter and not the diameter of the metal core that is most important for biodistribution and excretion [33]. Sizes bigger than 30nm suffer a main uptake by the macrophages in the liver, spleen and some uptake by the bone marrow. Nanoparticles with a hydrodynamic radius smaller than 5 nm or polymer nanoparticles with a molecular weight less than 50kDa have higher renal clearance [31, 33].

The relative diameters *(Table 4)* of the iron nanoparticles follow the sequence observed for overall molecular weight (High Molecular Weight-Iron Dextran (HMW-ID) > Ferumoxytol > Iron Carboxymaltose > Low Molecular Weight-Iron Dextran (LMW-ID) > Iron isomaltoside > ferric gluconate ≈ iron sucrose) and further establishes that the relative

diameters of the mineral cores follow the same sequence as those of the complete nanoparticle. This has important implications for core surface area available for bioactive iron release [22, 35]. Likewise, the core radius gives a potential explanation to the rate of release of iron and to the magnitude of the labile iron effect as well as to the dose and rate of infusion. Since all IV iron materials share the same core crystallinity, the rate of iron release per unit surface area would be most likely similar among materials (differing only by the strength of the carbohydrate ligand-core iron bond). However, for the same total amount of core iron, the surface area available for iron release increases dramatically as core radius decreases because surface area is = $4\pi r^2$, and volume is = $4/3\pi r^3$, then the ratio of surface area to volume is = $3r^{-1}$. In short, a collection of many small spheres exposes a greater total surface area than does a collection of an equal mass of fewer, larger spheres *(Figure 6)* [22, 35, 36].

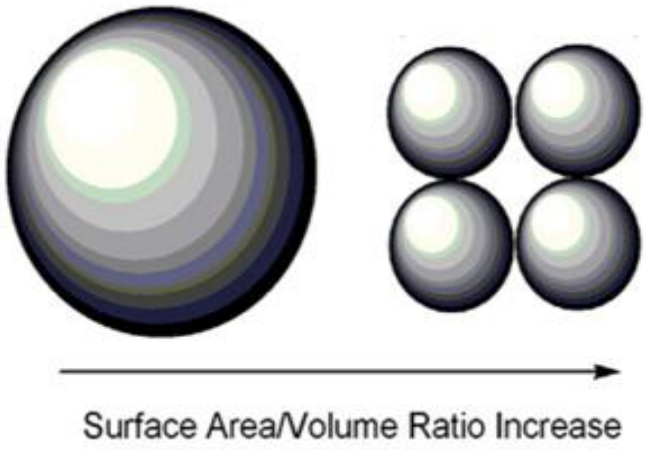

Figure 6 - A simple comparison of surface area between a large iron core and the same mass of smaller iron cores [36].

So, the smaller the particle size, the bigger is the surface area and the bigger is the evidence of labile weakly bound iron as well as more rapid is the iron release. The fraction of labile iron decreases in the order of Iron Sucrose ≈ Iron Gluconate >> Iron Dextran > Iron isomaltoside 1000 ≈ Ferumoxytol > Iron Carboxymaltose. As the labile iron can cause free iron like reactions, the size of the labile iron fraction may be dose limiting, and, if so, then the maximum tolerated dose and rate of administration would be inversely related to labile iron fraction and, consequently, to the particle size, and would follow the sequence LMW-ID ≈ Iron isomaltoside > Iron carboxymaltose > Ferumoxytol > Iron sucrose > Ferric gluconate [22, 35].

Accordingly, the rate of uptake of IV iron into the macrophages depends also on the particle size because, in general, the smaller the size, the more rapid is the clearance of the nanoparticles from plasma after an IV dose as well as the consequent saturation of Tf, which reflects in an inferior half-life too. A long serum half-life will influence the time for continued iron donation and the peak drug concentration achieved, which will result in serious implications after administration of higher than approved doses [22, 35, 37]. It has been suggested that given the same iron loading dose, the rate of metabolism and utilization of IV iron may be lower for agents with higher particle sizes. Prolonged exposure of a product to plasma leads to greater degrees of iron donation. Rapid cellular uptake, characteristic of the smaller nanoparticles, may limit late iron donation in plasma only to augment the intracellular manifestations of labile iron [37]. Although the precise cellular events occurring after iron-carbohydrate compounds are taken up by macrophages have not been elucidated, the observation that plasma clearance of iron dextran follows first-order kinetics after IV doses up to 500 mg but zero-order kinetics at higher doses suggests that the clearance mechanism is saturable [22].

As previously mentioned, iron agents can also donate iron directly to Tf although in a very low extent, and it is suggested by previous *in vitro* work that iron donation to Tf is inversely related to the particle size and directly related to concentration and circulation time [38].

The dose must also be thought accordingly to the volume of distribution of the IV iron in use because when iron is injected intravenously, it is distributed in the plasma space, so that the calculated initial volume of distribution roughly approximates plasma volume. The reported finding that ferric gluconate achieves a peak plasma concentration only half of that expected, prompts the conclusion that the agent is distributed in a volume equal to twice the plasma volume. The resulting conclusion that 50% of the iron in ferric gluconate dissociates immediately from the compound and exits the intravascular space seems quantitatively implausible. Qualitatively, however, the pharmacokinetics of ferric gluconate support that the large labile iron fraction in this agent may be clinically important early, after IV administration [35, 37].

2.4.2 Carbohydrate shell chemistry

Coating carbohydrates limit or delay water access to the core conferring significantly longer degradation rates of the nanoparticles reflected by the increase of the half-life of these particles [39]. Hydrophobic and high surface charged (either negative or positive) nanoparticles have short circulation times due to adsorption of plasma proteins which can lead to recognition by the macrophages followed by removal from circulation. Surface charge is reported to influence the tolerability and bioavailability of iron hydroxide nanoparticles in endocytic membranes, in particular by enhancing adsorption and uptake, probably via electrostatic interaction [30, 40]. As dextran is a neutral hydrophilic polymer whereas sucrose and gluconic acid are negatively charged, this can also explain the lower half-life and the faster uptake of Venofer® (iron sucrose) and Ferrlecit® (Ferric Gluconate) than dextran-like Cosmofer® [40, 41].

2.5 Current IV iron materials

Currently seven parenteral iron preparations are available in the market *(Table 4)*. The first generation preparations were the first ones to be manufactured and are characterized by the dextran nature of the carbohydrate shell, its robustness, the associated high incidence of anaphylaxis and the subsequent slow and high dose administration. The second generation are the smallest iron nanoparticulated materials with high iron lability associated anaphylactoid-type reactions and, thus, with low and slow administrations. The third generation are the newest products, which aims to overcome some of the issues associated with the previous IV irons allowing the administration of higher and faster doses.

Table 4 – The eight current IV iron materials and the respective classification, trade name, launch year and availability

	Active Pharmaceutical Ingredient (API)	Trade name	Manufacturer	Launch year	Availability
1st generation	Low Molecular Iron Dextran	Cosmofer®	Pharmacosmos	1991	Europe
		INFeD®	Watson Pharmaceuticals, Inc	1991	USA
	High Molecular Iron Dextran	Dexferrum®	American Regent, Inc	1996	USA
2nd generation	Ferric Gluconate	Ferrlecit®	Sanofi-Aventis	1999	Europe (not in UK) and USA
	Iron Sucrose	Venofer®	American Regent, Inc	2000	USA
			Vifor Pharma	2000	Europe
3rd generation	Ferric carboxymaltose	Ferinject®	Vifor Pharma	2008	Europe
	Ferumoxytol	Feraheme®	AMAG Pharmaceuticals	2009	USA
	Iron isomaltoside 1000	Monofer®	Pharmacosmos	2010	Europe

The products characterized in this project consisted in Cosmofer® (1st generation), Venofer® (2nd generation), Ferinject® and Monofer® (3rd generation).

2.5.1 Iron Dextran

Dextran is a polysaccharide polymer composed exclusively of α-D-glucopyranosyl units with varying degrees of chain length and branching *(Figure 7)*. An important factor in the choice of dextran appears to be the favourable size of dextran chains, which enables optimum polar interactions (mainly chelation and hydrogen bridges between the hydroxyl dextran groups and the oxide surface of the core) with iron oxide surfaces. Although single hydrogen bridges are relatively weak, the total bonding energy of these hydrogen bonds over the length of a polysaccharide molecule can be very high because of the large number of hydroxyl groups per molecule. The cores of both high and low molecular weight dextran materials resemble akaganeite [42].

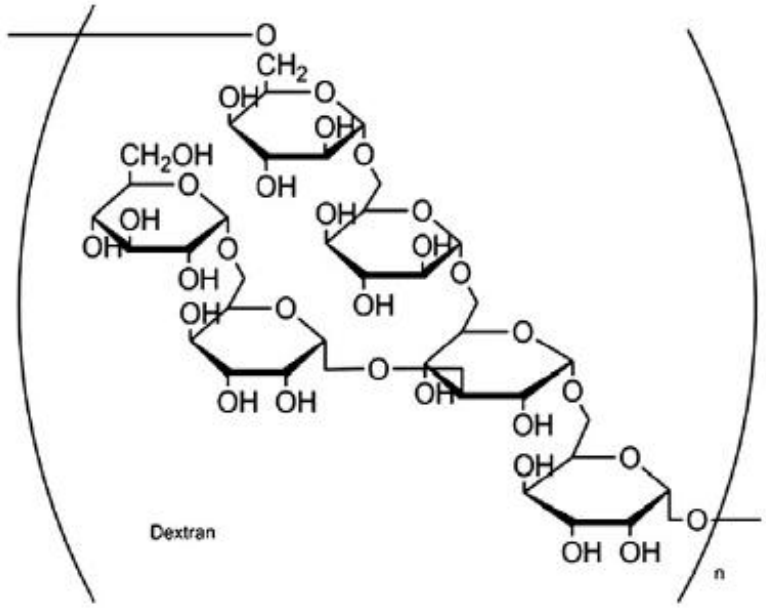

Figure 7 - Structure of the dextran polysaccharide which is used in the coating of the nanoparticles of Dexferrum® and Cosmofer® [36].

High molecular weight iron dextran (Dexferrum®)

Iron dextran was the first IV iron preparation used in haemodialysis patients [43]. HMW-ID became available for IV infusion in the United States after 1971 as "Imferon®" (Fisons pharmaceuticals). This material bypassed the prohibitive toxic reactions associated to the lack of carbohydrate shell of the previous parenteral iron materials (i.e. ferric hydroxide and iron saccharide) because it introduced dextran as a strong and robust iron coating for the iron oxide core, reducing the release of free iron during infusion, which accounted for a lower incidence of adverse reactions and more rapid hematologic responses. Unfortunately, dextran can easily develop antidextran antibodies, in a way that the administration of HMW-ID became associated of severe allergic reactions (even in the test doses [44]) and deaths due to anaphylaxis. Thus, it was withdrawn from the market, until the approval of the next HMW-ID (Dexferrum®) version in 1996 [45, 46].

The currently available Dexferrum® contain spheroid nanoparticles of 265 kDa and a particle size of 30±10 nm [22]. The material is a sterile non-pyrogenic solution that contains 50mg of elemental iron per mL of solution, a pH of 4.5-7.0, and does not contain preservatives. The administration of the undiluted solution must be done slowly, at a rate no greater than 1 mL/min (50 mg/min) and should not exceed 2 mL (100 mg) daily and a

test dose is required because of the dextran nature. After injection, circulating iron dextran follows the macrophage fate described above, with negligible amounts of iron being lost *via* urinary or fecal way. Studies involving intravenously administered iron dextran to iron deficient subjects who had coexisting end-stage renal disease and other clinical problems, have yielded an average half-life value of 58.9 hours [47].

Low molecular weight iron dextran (Cosmofer®)

After realization that the higher molecular weight dextran was the main culprit for allergic reactions, the iron dextran re-emerged in the market in 1991 as LMW-ID (Cosmofer®) which had less variability among the side chains and resulted in 8.1 times fewer adverse events (AEs) likely to occur in comparison to HMW-ID [45]. Besides the advantage of low rate of adverse effects, this material can also be administered in a total dose infusion (TDI) because iron coated with dextran has the advantage of a longer half-life and slow sustained release of elemental free iron into the circulation. This feature allows the administration of a total dose to replenish iron stores at one infusion in a cost-saving way. LMW-ID has been shown to have a comparable safety profile with a number of other non-dextran parenteral iron materials, including iron sucrose and sodium ferric gluconate. In fact, it has been showed that the TDI of LMW-ID was also found to be equally safe compared with infusion of high-dose iron sucrose [46].

Cosmofer® is a material with a molecular weight of 90-165 kDa [17, 48], a 4.4-5.6 nm core and an average hydrodynamic diameter of about 12.2 nm [27]. It is negatively charged and has a stock pH of 5.2-6.5. The vial has a 50 mg/mL of iron and can be administrate, as a conventional series of small IV doses or as a TDI with up to 20 mg/kg of body weight administered over 4-6 hours in one single infusion. Although the plasma half-life is 5 hours for circulating iron and 20 hours for total iron (bound and circulating), an increased haematopoiesis can be observed for the following 6-8 weeks. Due to the size of the complex, CosmoFer® is not eliminated *via* the kidneys and there is minimal removal of iron dextran during haemodialysis which do not warrant a change in the dosage schedule [49].

2.5.2 Ferric Gluconate (Ferrlecit®)

Ferric gluconate rapidly replaced iron dextran as the preferred IV iron preparation. It contains the same iron hydroxide core as iron dextran, but utilizes sucrose and gluconate to stabilize and solubilize the compound [50].

This macromolecular complex (*Figure 8*) has an apparent molecular weight of 164-444 kDa, a mineral sphere core with a diameter of 2-4.1 nm, an average hydrodynamic diameter of about 8.6-10 nm [27].

The manufacturing of the Ferric Gluconate complex is made through the standard procedure, previously described, to originate the iron (III) oxyhydroxide, followed by the reaction of the formed ferric hydroxide with sodium gluconate in a sucrose solution to obtain a crude sodium ferric gluconate complex $Na[Fe_2O_3(C_6H_{11}O_7)(C_{12}H_{22}O_{11})_5]_{n=200}$, which is soluble in a mildly alkaline aqueous sucrose solution [51].

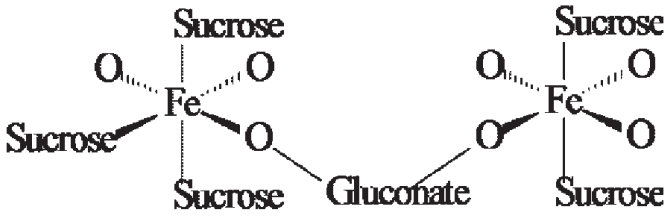

Figure 8 - The proposed structure of Sodium Ferric Gluconate (Ferrlecit®) [51].

Spectroscopic data and elemental analysis suggested that the core resembles akaganeite and it contains 102 repeating Fe(III)OOH centres bound in pseudo-octahedral coordination to 13 gluconate and five loosely associated sucrose molecules [26, 27]. The carboxylate groups in gluconate serve as the bridging group between iron centres with coordinated sucrose molecules bound both directly and weekly to each Fe(III) *(Figure 8)* [51].

Ferrlecit® is supplied in a single ampule or vial containing 62.5 mg of elemental iron in 5 mL (12.5mg/mL) and 20%(w/v) of glucose (195mg/mL). It contains benzylalcohol 0.9% (w/v) (9mg/mL) as preservative. It is negatively charged and it has a pH of 7.7-9.7. The maximum single dose is 10mL of 125mg of iron given over 1h per haemodialysis [52].

The pharmacokinetics in iron-deficient adults who are not on dialysis was described by Seligman *et al* [53]. In that study, it was shown that ferric gluconate-derived

iron was rapidly transferred to Tf, after digestion in the macrophage. Later, Warady *et al* studies on children in haemodialysis were able to define a linear pharmacokinetics where the $[Fe]_{total}$ and the $[\text{ferric gluconate-Fe}]_{serum}$ increased in a dose-dependent manner that was approximately proportional to the administrated dose, whereas K_{el}, clearance, half-life and distribution volume were similarly irrespective of dosage. In contrast, there was a slower and less prominent rise in the concentration of Tf bound iron. This delayed rise was greater after the higher dosage of ferric gluconate, which is reflective of the iron movement in the body whereby ferric gluconate first delivers iron to the macrophage as opposed to direct transfer to Tf [54].

The product does not have dextran content, so it may not share the antigenicity of the iron dextran materials. Therefore no test dose is required. However, it is a much smaller complex than iron dextran and, because of the weakness of the iron complex, it suffers a more rapid dissociation which may enhance the risk of acute toxicity due to a bigger percentage of labile (weakly bound) iron. With fast degradation kinetics and higher percentage of direct release to plasma proteins (apotransferrin, apoferritin, and others), the potential for acute adverse reactions related to labile iron release after IV injection is higher with iron gluconate compared to the other available IV iron preparations and it is caused by oversaturation of the Tf binding capacity [55].

2.5.3 Iron Sucrose (Venofer®)

Iron sucrose, also known as iron saccharate, is a complex of polynuclear iron (III)-hydroxide in sucrose. Iron sucrose has a molecular weight of approximately 34–60 kDa, a particle size of 7-8.3 nm and the proposed structural formula: $Na2[Fe5O8(OH)\cdot 3(H_2O)]n \times m(C_{12}H_{22}O_{11})$ [43], where *n* stands for the degree of polymerization and *m* is the number of sucrose molecules surrounding the iron core [56]. The spherical core has a proposed structure close to 2-line ferrihydrite, possibly mixed with layers of akaganeite, it has an average diameter of 3±2 nm and it contains about 416 FeOOH surrounded by roughly 24 sucroses [26, 27]. Each mL of the vial contains 20mg of elemental iron and 30% sucrose (w/v) (300 mg/mL). It has a pH of 10.5-11.1 and an osmolarity of 1250 mOsmol/L. It contains no preservatives. The administration can occur by slow injection or infusion with a maximum single dose of 200 mg during 2-5 minutes and the usual total iron repletion treatment course of Venofer® is 1000 mg. It requires a test dose only in Europe [57].

In healthy adults treated with IV doses of Venofer®, the iron component exhibits first-order kinetics. Its half-life is 5-6 h, and after a single dose of 100 mg, iron is uptaken rapidly in bone marrow, liver, and spleen, followed by occurrence of injected iron in circulating erythrocytes. The amount of iron transported by Tf, calculated using the Michaelis-Menten model for a single dose containing 100 mg of iron, is around 30 mg Fe^{3+}/24 h and the total erythrocyte uptake accounts for 68% to 97% of injected iron within 2–4 weeks [55, 67]. The total clearance is 1.2 L/h, and the volume of distribution is the central compartment is 3.2 L. The sucrose component and 5% of the total iron are eliminated mainly by urinary excretion [67].

2.5.4 Ferumoxytol (Feraheme®)

Ferumoxytol started a new generation of robust and strong parenteral iron preparations (with ferric carboxymaltose and iron isomaltoside) without the disadvantageous characteristics associated with iron dextran (anaphylaxis) and with iron sucrose and ferric gluconate (high iron lability, ergo dosage limitations, and the long duration of administration). This offers higher single-dose options, no test dose required and all can be rapidly administrated [55].

Ferumoxytol was approved by the Food and Drug Administration (FDA) for iron replacement in patients with iron deficiency anaemia and CKD. Originally developed as a magnetic resonance imaging (MRI) contrast agent due to its magnetic properties [58], ferumoxytol consists in superparamagnetic iron oxide nanoparticles with a polyglucose sorbitol carboxy-methylether coating. It has a molecular weight of 731-750 kDa and a colloidal particle diameter of 23.6-30 nm [17, 27]. The available material is negatively charged, it has an osmolarity of 270-330 mOsm/kg, it does not contain preservatives, and it is a 6-8 pH sterile liquid injection containing 30 mg of elemental iron/mL, with mannitol 44 mg/mL for isotonicity [59]. Ferumoxytol core structure resembles magnetite and maghemite with a diameter of 6.2 ±1.4 nm [27].

Ultrafiltration studies show that the labile iron and free iron content in ferumoxytol injection is the lowest of the available iron injection preparations. Similarly, the use of a bleomycin-detectable iron assay and *ex vivo*/*in vivo* rat experiments measuring free iron release of the various injectable iron products could found the lowest amount of free iron resulting from ferumoxytol. This property explains why ferumoxytol can be safely and

rapidly administrated intravenously in relatively high doses with a maximum single dose of 510 mg administrated in a 17 seconds single push as 1mL (30 mg/s) [60, 61]. Also, in a randomized trial of patients with CKD stages one to five, two 510 mg injections of ferumoxytol administered within a week increased haemoglobin levels significantly higher than in patients receiving oral iron, including those with and without simultaneous ESA therapy [62] . Meanwhile, just one serious AE (anaphylaxis) was observed in a treatment arm in a patient with history of multiple drug allergies, but the patient recovered. The authors concluded that ferumoxytol is well tolerated with decreased immunological allergic reactions, low in other acute AEs and it has a safety profile similar to a placebo saline solution in anaemic patients with CKD [63]. For this reason it does not require test doses.

Regarding the pharmacokinetics, intravenously injected Fe-labelled ferumoxytol was noted to be quickly incorporated into red blood cells in non-anaemic rats. It was detected in red blood cells within 24 hours after injection, and over half of the dose was detected in red blood cells 2-4 weeks after injection contrasting with the iron from sodium ferric gluconate and iron sucrose that, in severe iron deficiency, it is incorporated into red blood cell precursors and is relatively complete 2-4 weeks after administration. It was suggested that the volume of distribution (Vd) of ferumoxytol was consistent with plasma volume and that other pharmacokinetic parameters are dose dependent, such as an increasing half-life, mean maximum observed plasma concentration (C_{max}) and a decreasing total body clearance as the dose increases. The estimated values of clearance and V_d following two 510 mg doses of ferumoxytol administered intravenously within 24 hours were 69.1 mL/h and 3.16 L, respectively. The C_{max} and time of maximum concentration (t_{max}) were 206 mcg/mL and 0.32 h, respectively [60, 64].

2.5.5 Ferric carboxymaltose (Ferinject®)

Ferric carboxymaltose is a stable dextran-free iron complex with low immunogenic potential, and it is administrated at nearly neutral pH (5.0–7.0) and physiological osmolarity. The nanoparticle consists in a polynuclear iron(III)-oxyhydroxide core, structurally in accordance with akaganeite, stabilised with a branched carboxymaltose polysaccharide shell *(Figure 9)* giving an average hydrodynamic diameter of about 23.1 nm and a molecular weight around 150-233.1 kDa [17, 27, 65].

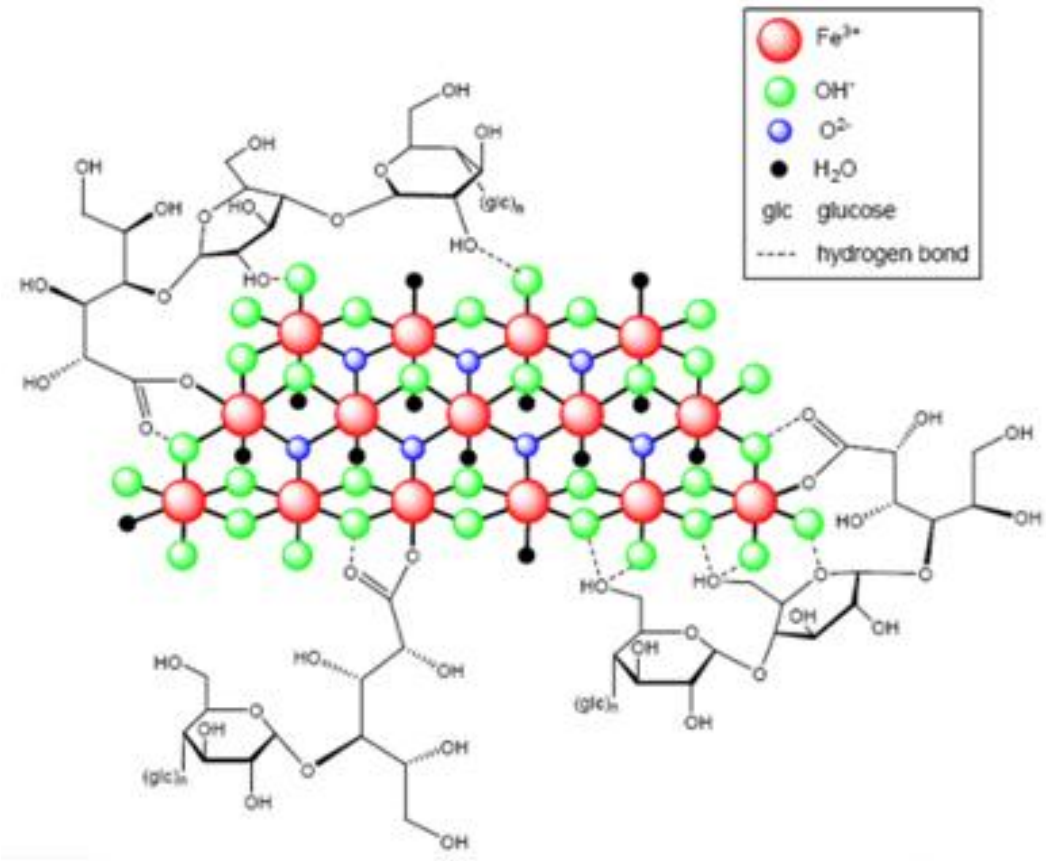

Figure 9 - Model for the proposed molecular structure of ferric carboxymaltose [65].

The robust structure similar to Ferumoxytol makes it possible to administer higher single doses over shorter time periods [61] providing cost saving potential. The preparation has 50 mg of elemental iron per mL of solution allowing doses of 15 mg/kg of body weight (up to a maximum dose of 1000 mg in 15 minutes, per week) to be delivered in a single administration. The other ingredients are aluminium (up to 75 µg/mL), sodium hydroxide and hydrochloric acid for pH adjustment, and water for injection, which may be of concern in dialysis patients and those on sodium-restricted diets [15].

After its administration, the pharmacokinetic characteristics of Ferinject® are similar but not identical to iron dextran. The distribution volume of both preparations corresponds nearly to that of plasma, but the half-life is approximately 7-12h for Ferinject® as compared to 25-30 h for LMW-ID. It seems that Ferinject® is degraded quicker than iron dextran because the plasma it is suggested that the carbohydrate part of Ferinject® is degraded to simple sugars by the enzyme α-amylase in a faster rate than dextran, so maximum concentrations of iron from Ferinject® in plasma are reached in approximately one hour followed by the rapid capture by the macrophages. As a result, the

utilization of iron for erythrocytes increases rapidly up to 6 to 9 days, continuing to increase in a much lower rate. Patients with iron deficiency anaemia showed erythrocyte iron utilization over 90% of the material administered. Different studies on postpartum anaemia, uterine bleeding and in patients doing haemodialysis have confirmed the efficacy and safety of Ferinject®, as the haemoglobin rates quickly increase and the biological stores of iron are quickly refilled with few secondary effects [55, 66].

2.5.6 Iron isomaltoside (Monofer®)

The newest IV iron agent Iron isomaltoside 1000 was introduced in Europe in 2010 as Monofer®, with iron being available in a non-ionic water-soluble form in an aqueous solution with pH between 5.0 and 7.0 with a concentration of 100 mg of elemental iron per mL of solution (vial) [67].

The average hydrodynamic diameter of the nanoparticle is about 9.9 nm (150 kDa [17]). The iron oxyhydroxide core seems to consist of a "mixed layer" similar to akaganeite whereas the carbohydrate is made of spherical shaped particles with a similar structure to dextran with a non-ionic α-1-6 linked glucopyranose units. However, it separates from the dextran because these units are pure linear oligomers arranged in a matrix-like structure with interchanging iron molecules, and with an average size of 5.2 glucose units and an average molecular weight of 1000 Da. The resulting matrix contains about 10 iron molecules per one isomaltoside pentamer in a strongly bound structure that enables a controlled and slow release of bioavailable iron to iron-binding proteins with little risk of free iron toxicity *(Figure 10)* [27].

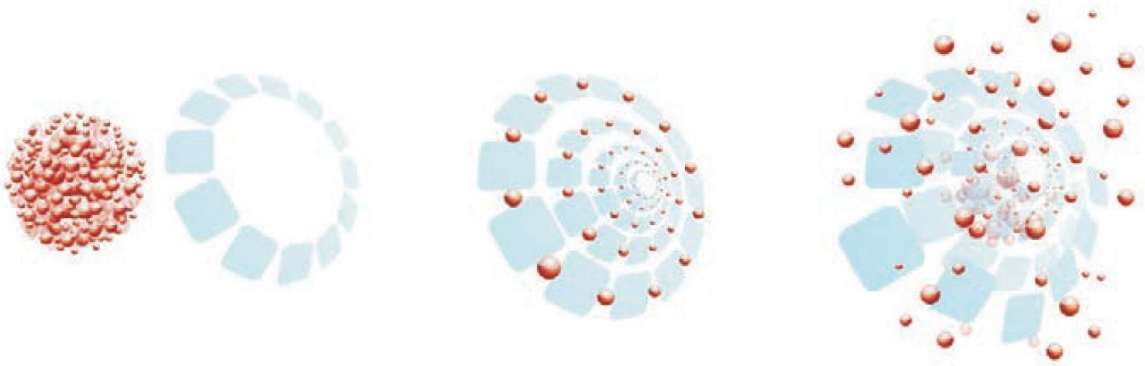

Figure 10 – Matrix structure of Monofer with ferric iron (red balls) layered between the shell oligomers (blue squares) which enables a controlled and slow release of iron [68].

Moreover, the lack of immunogenic branched polysaccharides used in iron Cosmofer® and Dexferrum®, prevent anaphylaxis. This allows iron isomaltoside 1000 to be administered safely as a rapid high dose IV infusion or bolus injection (doses over 1000 mg with a maximum single dose of 20 mg/kg of body weight), without a test dose, (doses over 1000 mg with a maximum single dose of 20 mg/kg of body weight) and it can achieve a 15 minutes administration of 0-5 mg/kg of iron. This can offer considerable dose flexibility, including the possibility of providing full iron repletion in a single infusion, offering convenient one hospital visit for a wide range of patients [27, 67].

Following IV administration, Iron isomaltoside is either metabolized or excreted. Due to the size of the complex, only small quantities of iron are eliminated in urine and faeces. The distribution volume is 3.0-3.5 L [69], the plasma half-life is 5 hours for circulating iron and 20 hours for total iron (bound and circulating) [67].

The main characteristics of each IV iron materials are represented in *Table 5*

Table 5 - Characteristics of the different Iv iron materials (Dexferrum®, Cosmofer®, Ferrlecit®, Venofer®, Feraheme®, Ferinject®, Monofer®). Unless stated otherwise in the table, the values were obtained from two papers on IV iron, [27] and [70].

Product	HMW-ID (Dexferrum®)	LMW-ID (Cosmofer®, USA) (Infed®, Europe)	Ferric Gluconate (Ferrlecit®)	Iron sucrose (Venofer®)	Ferumoxytol (Feraheme®)	Ferric carboxymaltose (Ferinject®)	Iron Isomaltoside (Monofer®)
Mineral phase	Akaganeite[71]	Akaganeite	Akaganeite	Mixture of Akaganeite + 2-line ferrihydrite	Magnetite + Maghemite	Akaganeite	Akaganeite
Core Size (nm)	20-35 [22]	4.4-5.6	2.0-4.1 [8][26]	3.2-5.0	6.2-6.4	4.3	4.2-6.3
Shell	Branched Dextran polysaccharide (α-D-glucopyranosil units)[42]	Branched Dextran polysaccharide (α-D-glucopyranosil units)[42]	Gluconate + loosely associated sucrose	Sucrose	Polyglucose sorbitol carboxymethyl ether	Branched carboxymaltose polysaccharides	Linear α1-6 glucopyranose
NP Size (nm)	30±10 [22]	12.2	10 [51]	7-8.3 [26]	23.6-30 [62]	23.1 [8]	9.9
Molecular Weight	265kDa [22]	96-165kDa [8]	38-444kDa [51]	34-60kDa [8]	731-750kDa [8, 23]	150-233.1kDa [8]	150kDa [8]
Initial distribution volume (L)	3.5	3.5	6	3.4	3.16	3.5	3.4
Plasma Half-Life (h)	60	20	1	6	15	16	20
Labile Iron Release	-	-	+++	+-	-	-	-
Direct iron donation to transferrin (% of injected dose	1-2	1-2	5-6	4-5	<1	1-2	<1
Test dose	Yes	Yes	No	Just in Europe	No	No	No
Iron content (mg/mL)	50	50	12.5	20	30	50	100
Maximal single dose (mg) [27]	20mg/kg	20mg/kg	125mg	200mg	510mg	15mg/Kg Single dose limit: 1000mg	20mg/kg
Pre-medication	Total dose infusion only	No	No	No	No	No	No
Adverse Events	Anaphylaxis, Dyspneia, back pain, chest pain, pruritus, hypotension [72]	Anaphylaxis, Dyspneia, chest pain, hypotension, nausea, vomiting [72]	Dyspneia, Nausea, Chest Pain, Vomiting, Hypotension [72]	Nausea, Vomiting, Hypotension, Dyspneia, Dizziness, Peripheral Edema, Infused related [72]	Diarrhea, nausea, dizziness, hypotension [64]	Headaches, nausea, rash, hypophosphatemia [73]	Arthralgia, myalgia, fever
Life-threatening AEs ($\times 10^6$doses)	11.3	3.3	0.9	0.6	Not known	Not known	Not known

2.6 Negative outcomes of IV iron therapy in clinical practice

Over the years, with the development of new IV iron materials, which have improved safety and efficacy, the benefits of IV iron have been increasingly realised. However, every material is not free from negative outcomes (see *Table 3*) and the reluctance in prescribing this effective treatment could be explained by serious adverse effects of iron dextran, specially associated with repeated injection [56, 74]. Much of the published work regarding adverse reactions focuses on the experience with this material (mostly HMW-ID) with rates of anaphylaxis reported to be as high as 0.6% with adverse reactions seen in up to 26% [75]. In fact, the case fatality rate for iron dextran–associated anaphylaxis was reported to be as high as 15.8% between 1976 and 1996 (31 deaths in 196 allergic events) [76]. These anaphylactic reactions are not dose related and they are mediated by a preformed Immunoglobulin E antibody to the dextran coating, with the majority of symptoms being cutaneous manifestations and respiratory difficulties [75].

Iron gluconate and particularly iron sucrose have a low frequency of side effects in low doses and they are mostly related with the anaphylactoid type reactions which, in opposite to anaphylaxis, are non-IgE-mediated but cause similar symptoms such as breathlessness, wheezing, arthralgia, myalgia, abdominal or back pain, nausea, vomiting and hypotension [13, 56]. This is probably due to the iron component and not to the chemistry of the carbohydrate shell, since the lability profile of these small complexes and the consequent capacity of iron to be released too rapidly may overload the ability of Tf to bind it, leading to the increase of non-transferrin bound iron (NTBI). The high levels of this form of iron is the primary cause of all the free iron reactions and the resulting anaphylactoid symptoms in the second generation of IV irons [77]. NTBI iron becomes highly catalytic and can promote oxidative stress. The one-electron reduction of O_2 by Fe^{2+} results in superoxide formation, which in turn leads to the well-known Haber-Weiss and Fenton reaction generating hydroxyl radical ($OH^{\bullet}$) in the following sequence [78]:

(1) $Fe^{2+} + O_2 \longrightarrow Fe^{3+} + O_2^{-\bullet}$

(2) $2O_2^{-\bullet} + 2H^+ \longrightarrow H_2O_2 + O_2$ (Haber-Weiss Reaction)

(3) $Fe^{2+} + H_2O_2 \longrightarrow OH^{\bullet} + OH^- + Fe^{3+}$ (Fenton Reaction)

The hydroxyl radical is the most powerful oxidant encountered in biological systems and will attack proteins, nucleic acids and carbohydrates, initiate chain-propagating lipid peroxidation [78] resulting in the formation of alkoxyl and peroxyl radicals [79]. NTBI can also cause cytotoxicity from oxidative stress by changes in the iron metabolism especially in the liver where NTBI is taken up preferentially after being cleared from the plasma [35]. The exact mechanism of NTBI-uptake is not known, but it is quite possible that the NTBI transporters such as the endosomal divalent metal transporter 1 (DMT-1) and the membrane putative zinc transporter ZIP14 [80] may be overexpressed under the conditions of iron overload, in a way that it will further increase iron uptake through NTBI and a consequent increase of the intracellular LIP. This will deactivate the iron response element/iron response protein (IRE/IRP) regulatory system, stimulating the cell to increase ferritin synthesis and decrease TfR1 expression. The ultimate outcome is a decreased uptake from Tf-Fe via TfR1 and an enhancement of the oxidative cell damage by the elevated LIP *(Figure 11)* [81].

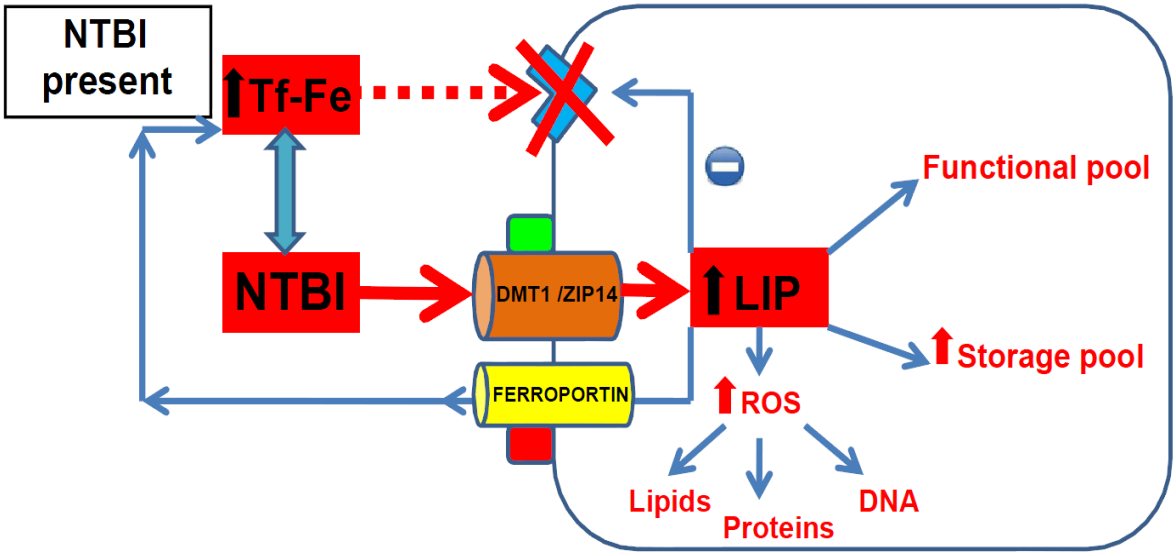

Figure 11 - Cellular outcomes occurring when the serum NTBI is too elevated after IV iron administration [82].

Other *in vitro* and *in vivo* manifestations of the high NTBI levels associated to lability in iron sucrose and ferric gluconate are the direct iron donation to Tf *(Table 5)*, neutrophil dysfunction and bacterial growth enhancement. In fact, even in low doses, iron sucrose has been associated with Tf oversaturation, oxidative stress and enhanced bacterial growth in vitro. Although there is no strong clinical evidence for an association of IV iron with infection, NTBI makes iron more accessible to bacterial growth and can enhance infection [83]. NTBI associated with parenteral iron administration can also promote

neutrophil damage and consequent loss of migration and killing function by the saturation of lactoferrin in iron overload which can decrease the host resistance to bacterial infection. This protease destroys the Gram-bacteria by degradation of the outer membrane [84].

In contrast to the iron dextran-induced anaphylaxis, the "free iron" reactions seem to be dose-related. For example, NTBI occurs to a smaller degree after application of iron sucrose doses of 50 mg or less, but in higher doses, exaggerated iron levels happen more often, maybe due to impaired phagocyte function [85]. Side effects occurred in 0.9% of the patients receiving 100 mg/10 min of iron sucrose, but in 5.9% of the patients receiving 200 mg/10 min iron sucrose [44]. In consequence, ferric gluconate and iron sucrose require multiple and/or relatively time-consuming administration regimens [86] and they are useful for only low-dose administration, because its toxicity limits the dose to a maximum single administration of just 125 mg and 200 mg, respectively, in opposition to the fewer and larger dosage required of ferumoxytol, ferric carboxymaltose and iron isomaltoside [13].

Epidemiologic data have also raised concerns about a possible association between augmented body iron stores and an increased risk of atherosclerosis and cardiovascular disease [87].

Since ferumoxytol, ferric carboxymaltose and iron isomaltoside are robust with a low immunological shell structure, they release minimal detectable free iron compared with other iron agents, they are also well tolerated and have a low incidence of side-effects associated. Similar to iron dextran, they have the advantage of a slower dissociation rate of iron from the complex than iron sucrose and iron gluconate, but they have a lower indication of problems with anaphylaxis [88] due to the non-dextran coating. However, the FDA failed to approve ferric carboxymaltose for distribution in the USA due to unexplained hypophosphatemia [89] and also because of an increased number of adverse cardiac events and an imbalance in death rates in the treatment arm compared to the control arm in different randomized controlled trials [65]. Although not clearly known, ferric carboxymaltose positive surface might be the reason, because, when in circulation, negatively charged phosphate could potentially be trapped by electrostatic interaction with the surface of the material, explaining the mechanism behind the induced hypophosphatemia [27]. On the other hand, it has been suggested that the hypophosphatemia associated with parenteral iron therapy could be mediated by Fibroblast Growth Factor 23 (FGF-23) [68].

Iron isomaltoside is the latest IV iron and it was supposed to overcome most of the negative aspects of the previous IV preparations, and although there is a limited clinical data on its safety, there are already reports of AEs happening after administration of Monofer® to CKD and IBD patients with associated anaemia [69, 90].

Table 6 shows a summary of the FDA's adverse event reports by serious outcome for first and second generation IV iron products since their initial marketing to mid-April 2007 [72].

Table 6 - Number of U.S. cases of Adverse Events Entered in AERS for Selected Parenteral Iron Products, and Types of Outcomes, from Each Product's Marketing to Mid-April, 2007 [5]. ***a*** **= Life threatning,** ***b*** **= Required intervention;** ***c, d, f*** **and** ***g*** **were marketed from 1996, 1992, 1999 and 2000, respectively; and** ***e*** **refer to Dexferrum, INFeD or previously marketed iron dextrans [72].**

Drug	Cases	Serious	Death	Hospitalized	LT[a]	Interv[b]
Dexferrum[c]	698	524	24	160	157	214
INFeD[d]	612	478	43	188	152	90
Iron dextran[e]	124	94	7	42	42	32
Ferrlecit[f]	322	222	11	125	53	72
Venofer[g]	79	64	2	40	8	14

Although the clinical side effects of the IV iron materials are well documented in literature, there is still unexplained occurrence of side effects especially in third generation materials, ergo there is a need to fill these gaps by in depth work about the relationship between the physicochemical properties (i.e. agglomeration, particle size, iron dissolution, mineral phase, redox state of the iron in the core, and surface properties) and the occurrence of these side effects.

2.7 Ideal IV iron

An ideal preparation for IV iron replacement therapy should balance effectiveness and safety.

Such IV iron material would allow the administration of large doses in a short period of time to allow the replenishment of iron stores in one infusion and the reduction of the need for blood transfusions; to improve convenience of treatment and patients management through increased compliance, and, finally, to increase staff efficiency thus reducing costs. As for the latest generation of IV iron preparations, such preparations would lack dextran since this would result in low immunogenicity and no requirement for a

test dose. In addition, a robust core-shell complex would provide a stable binding of the iron to its carrier molecule in serum until it is taken up into the macrophage for transfer to Tf or storage, because the non-specifically binding of labile iron to other serum molecules or the quick saturation of Tf binding site through direct transfer of iron to Tf, could result in free radicals formation leading to oxidative stress and a greater probability of side effects [35, 60].

Although, not fully understood, particle size does seem to impact on the efficiency of iron delivery from IV iron. Preliminary studies seem to imply that a particle with a size greater than 5.5 nm considerably avoids renal clearance and allows a higher macrophage uptake limiting direct iron donation to Tf [31]. In fact, the renal elimination rate should be below 1% of the dose, and there should be practically no iron detectable in the proximal tubule [91]. Sizes above 30 nm are mainly taken by the liver and spleen (i.e. macrophages) which associated with longer circulation times could result in enhanced tissue accumulation or could be internalized in endothelial cells with a lower rate of endocytosis than the macrophages, and it is yet to be understood if this is beneficial [33].

Furthermore, nanoparticles surface charge will also directly influence the extent of cell–nanoparticle interactions and toxic potential of the nanoparticles. In general, cationic particles have been described to be the least stable and exert the greatest cytotoxic effects (e.g. hypophosphatemia). Although the reduction in positive charges might accompany a diminished protein coating in circulation and cellular internalization, it is important to find the optimal balance between a lack of toxicity and internalization efficiency. Moreover, for quantum dots (i.e. nanosized semiconductor materials), it has been shown that the functional groups introduced at the NP surface have a great effect on the nanoparticles toxicity with the carboxyl coatings being the best tolerated by cells [92].

3. Techniques for the characterization of IV iron materials

Cosmofer®, Venofer®, Ferinject® and Monofer® share the same core chemistry but differ in the composition of the carbohydrate shell, as well as, in physical (particle size, agglomeration) and chemical (dissolution performance, redox state of the iron in the core) properties, which makes them vary substantially in pharmacological behaviour, and ultimately, in the efficacy and safety profile.

However, this relationship is not well understood, and the current project aims to fill these knowledge gaps, so a physicochemical characterization of each of the IV iron materials was needed to fill the gaps of information about the relationship about the physicochemical properties of the nanoparticles and the clinical behaviour and safety of the IV iron materials *in vivo* to potentially point out the main flaws of the constitution of a colloidal preparation of IV iron and propose an ultimate safe and efficient material.

To study the physical and chemical properties of the IV iron preparations, particle size analysis in aqueous solutions were conducted to the preparations using water and serum mimetic solutions to study the behaviour of the nanoparticles and to relate to what they would encounter in the circulation *in vivo*. A key *in vitro* assay of lysosomal dissolution was performed to test all four materials in a narrower range of lysosomal conditions to study the kinetics of the preparations, with the assistance of Inductively Coupled Plasma - Optical Emission Spectrometer (ICP-OES). Furthermore, the analysis of the IV iron materials by XRD allowed to determine the mineral phase and crystallinity (linked to iron lability, e.g. iron dissolution) of each IV iron material, gathering a more in depth information about the structure and composition of the IV iron preparations and to consolidate the data already available about this type of characterization [32]. The redox state (i.e. valence) of Venofer® was also carried out by linear voltammetry methods to possibly determine the unexpected presence of ferrous iron in the nanoparticles core and to determine how big its content is in each IV iron.

3.1 *In Vitro* assays

Lysosomal dissolution assays was developed to establish the relative chemical lability of the preparations in the lysosomal compartment which can be useful to

understand how the presence of free iron relates to the likelihood of side-effects and then, their bioavailability. The pH chosen was 4.5, 5.0 and 5.5 because the pH 4.5 and 5.0 are the border values of the physiological lysosomal pH, which is 4.7. A pH above 5.0 might affect lysosomal digestion [93]. However, the pH 5.5 was also selected because the common mechanism for cellular iron uptake dictates that after the internalization of iron bound to Tf, a proton pump promotes acidification of the endosome to pH 5.5, triggering the release of Fe^{3+} from Tf to the endosomal space. The chelating agents used were citrate, isocitrate and phosphate because both the low pH environment of endosomes/lysosomes and the intracellular Fe-chelating substances (i.e., phosphate, nucleotides, dicarboxylic acids (citrate and isocitrate)) are responsible for the solubilisation of iron oxide particles [94]. The iron concentrations of 0.1, 0.5 and 1 mM were preferred because although not physiological values, they are low, ergo permitting a more obvious variation of the percentage of soluble iron with time, and 0.1 is the minimum concentrations that allows the detection and quantification of iron concentrations by the ICP-OES in conditions where small percentages (~5%) of iron are dissolved between two time-points. All the solutions tested were left at 37ºC conditions because it is the temperature that subsists in intracellular conditions [95].

An agglomeration assay was also carried out to determine if any agglomeration can occur locally when IV iron preparations are administrated intravenously. As the agglomeration of iron nanoparticles should not happen in the presence of serum electrolytes after the IV administration, the agglomeration was tested by mixing each IV iron material with a serum mimicking solution of phosphate and calcium. The preparations were also mixed with fetal bovine serum to determine if any nanoparticle agglomeration occurs in a more realistic scenario.

Finally, linear voltammetry was carried out since it is known that the redox state of the iron has substantial impact on the safety of iron treatments. In particular, it is recognised that ferric iron is better tolerated than ferrous iron in the same conditions *in vivo*, and also that the administration of ferrous iron leads to the production of free radical and systemic toxicity [96]. After developing the suitable method, it was applied to Venofer® to accurately characterize the redox state of iron in the stock solution.

3.2 Analytical techniques

3.2.1 Dynamic light scattering (DLS)

Dynamic Light Scattering (DLS) (Zetasizer, Malvern Instruments), sometimes referred to as Photon Correlation Spectroscopy (PCS) or Quasi-Elastic Light Scattering (QELS), is a non-invasive, well-established technique, useful to obtain particle sizes distributions of the four IV iron preparations available in the UK and to measure accurately the hydrodynamic sizes of the IV iron nanoparticles in simple aqueous solutions and in serum mimetic solutions. It can be also applied to *in vitro* assays like the lysosomal dissolution assay.

DLS measure the intensity of light scattered by 0.5 to 6000 nm particles in a sample. The intensity changes with time due to the Brownian motion (random diffusive motion of microscopic particles suspended in a liquid or a gas) of particles in the suspension and this motion increases with decreasing particle size. The intensity fluctuations of the scattered light are detected at a known scattering angle by a fast photon detector. Here, they are converted into electrical pulses, which fed into a digital correlator. A correlation factor from the intensity versus time profile is obtained and this exponentially decaying correlation function $g_2(t)$ provides the diffusion coefficient of the particles. In practice, this means that due to their greater Brownian motion, nanoparticles lose correlation more rapidly which can then be related to their size *(Figure 12)* [97-99].

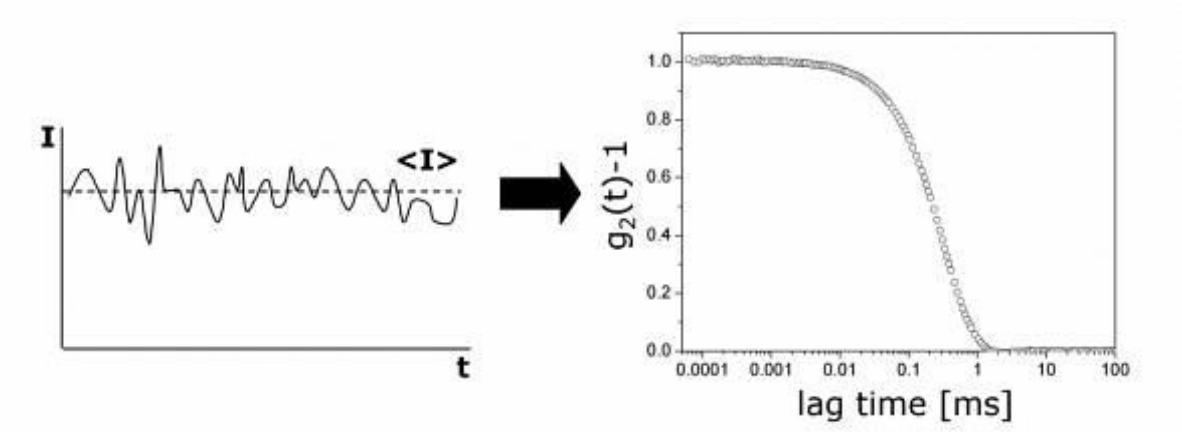

Figure 12 - Correlation of the scattered light fluctuations after detection of the scattered light and the conversion into electrical pulses [99].

The diffusion coefficient, *D*, is then related to the radius *R* of the particles by means of the Stokes-Einstein equation and the instrument calculates the hydrodynamic size of the particle *(Equation 1)* [100].

$$D = \frac{kT}{6\pi R\eta}$$

Equation 1 - Stokes-Einstein equation.

D is the diffusion coefficient, *R* is the radius, *T* is the temperature and η is the viscosity. The translational diffusion coefficient will depend not only on the size of the particle but also on any surface structure and the concentration and type of ions in the medium [98].

The events that take place on the DLS are represented in *Figure 13* [101]. The size obtained by this technique is that of a sphere that has the same translational diffusion coefficient as the particle being measured. DLS produces an intensity distribution *(Figure 14)* from which, assuming a fixed relationship between scattering intensity and volume, a volume distribution can then be estimated.

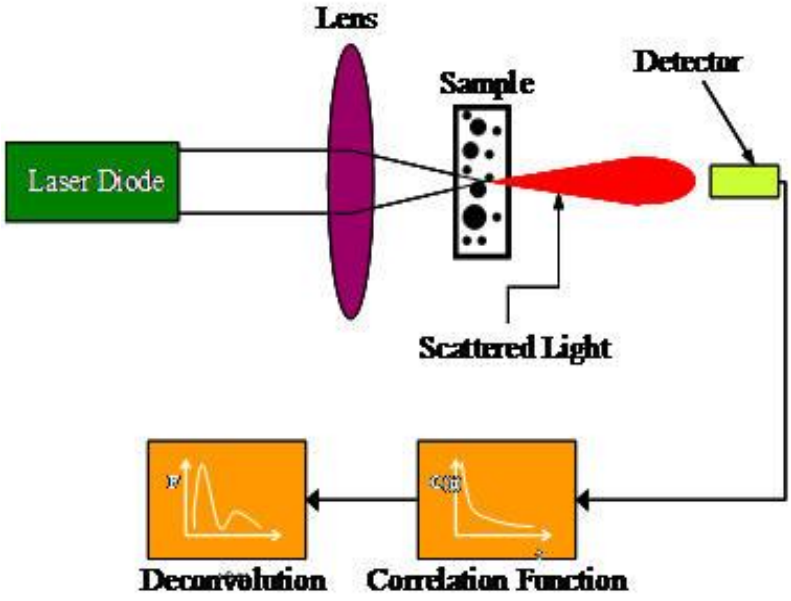

Figure 13 – Schematic diagram of the events that occur in a conventional Dynamic Light Scattering [101].

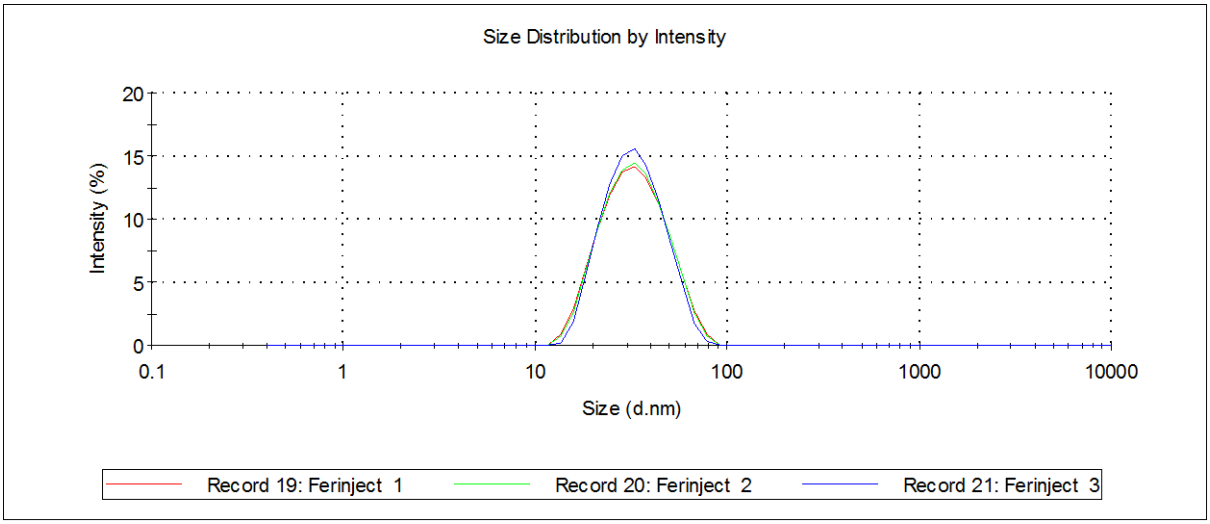

Figure 14 – Example of particle sizing distribution data of Ferinject (Ferric carboxymaltose) by intensity. The current example shows the measurement of three replicates.

3.2.2 Zeta Potential

Zeta potential (Zetasizer, Malvern Instruments) is a measure of the magnitude of the electrostatic or charge repulsion or attraction between particles, and is one of the fundamental parameters known to affect stability. The "Zetasizer" calculates the zeta potential by determining the electrophoretic mobility and then applying the Henry equation *(Equation 2)* [102].

$$U_E = \frac{2\varepsilon z f(ka)}{3\eta}$$

Equation 2 - Henry equation.

Z is the zeta potential, U_E is the electrophoretic mobility, ε is the dielectric constant, $f(ka)$ is the Henry's function (1.0 and 1.5 are usually used to as approximations) and η is the viscosity. An important consequence of the existence of electrical charges on the surface of particles is that they will exhibit certain effects under the influence of an applied electric field. In this case, the determination of zeta potential and ergo the surface charge will be induced by the electrophoretic motion – the movement of a charged particle relative to the liquid it is suspended in, under the influence of an applied electric field. The essence of a classical micro-electrophoresis system is a cell with electrodes at either end to which a

potential is applied. Particles move towards the electrode of opposite charge and their zeta potential is calculated directly from their mobility *(Figure 15)* [102].

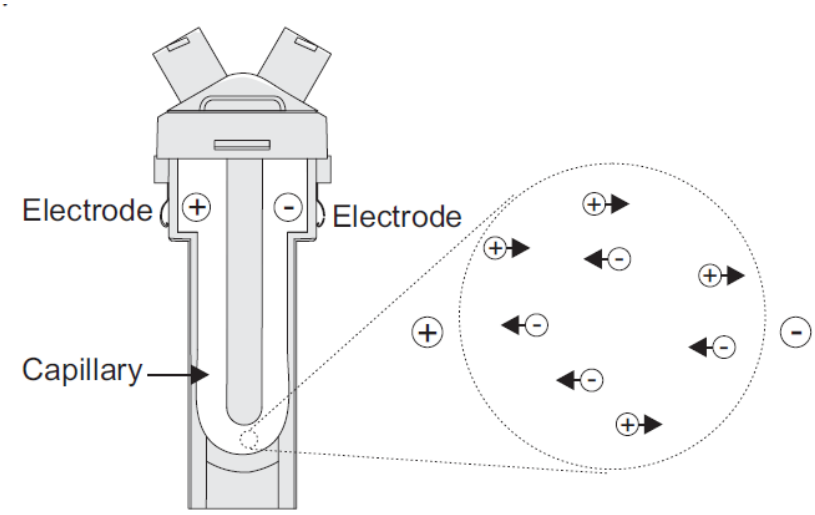

Figure 15 - Disposable folded capillary cell representing the micro-electrophoresis system that permits the differential mobility of particles according to their surface charge[102].

Its measurement brings detailed insight into the causes of dispersion or agglomeration (clumping of nanoparticles together). Ultimately, it will give information about the nanoparticle surface charge at a given pH which may help explaining the data of the agglomeration given by the DLS.

3.2.3 Inductively Coupled Plasma - Optical Emission Spectrometer (ICP-OES)

ICP-OES is a rapid and accurate technique to determine concentrations of a wide range of elements in solution. Metals and metalloids can be determined at the ultra-trace level on µg or µL samples (detection limits of 0.03–10 ng/mL) [103]. In the current project, ICP-OES will allow accurate quantification of iron content in the IV iron materials to detect different phases (i.e. soluble, nanoparticulated or agglomerated) from samples obtained from *in vitro* assays.

The technique requires an initial nebulization of the liquid sample into an aerosol. This aerosol sample is then transported to the plasma where the temperature is sufficiently high (6000–8000 K) so that the sample can be desolvated, vaporized and atomized thus breaking chemical bonds and liberating elements. The plasma promotes then the excitation

of the atoms which when returning to their fundamental state, emit radiation. The frequency of this radiation is characteristic of the element that emitted it and as such can be used for identification purposes. Also, the intensity of the radiation is proportional to the concentration of that element within the solution so it can be used for quantitative purposes [104]. The major events that happen in an ICP run are illustrated in *Figure 16* [105].

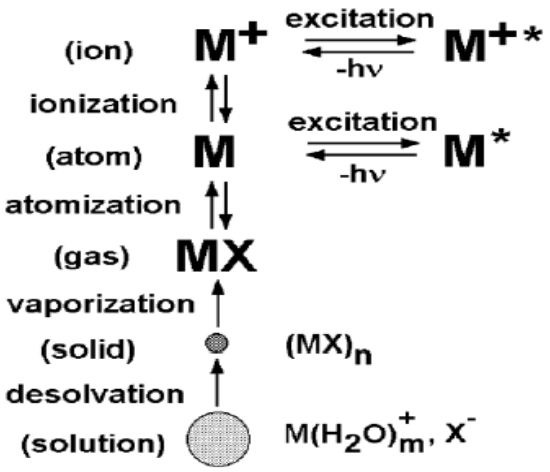

Figure 16 – Chemical events that occur during an ICP-OES run of a sample [105].

3.2.4 Voltammetry

The potentiostat (Autolab/PGSTAT302N) allows electrochemical studies such as voltammetry, for investigations of reaction mechanisms related to redox chemistry. In voltammetry we apply a time-dependent potential to an electrochemical cell and measure the resulting current as a function of that potential.

A modern potentiostat makes use of a three-electrode arrangement – the most common ones are the Ag/AgCl reference electrode, the platinum wire auxiliary electrode and the mercury working electrode. The working electrode can also be replaced by a rotating disc electrode (RDE). The cell also includes a gaseous nitrogen line purge all the oxygen out to avoid oxygen-driven redox reactions and an optional stir bar *(Figure 17)* [106, 107].

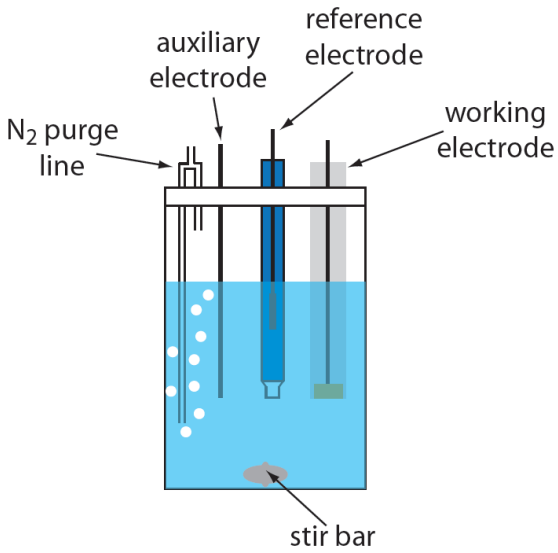

Figure 17 - Typical electrochemical cell for voltammetry: three-elecrode arrangement plus the N_2 purge line, all immersed in the solution where the analytes are present [106]

In voltammetry we apply a time-dependent potential excitation signal to the working electrode changing its potential relative to the fixed potential of the reference electrode, and measure the current that flows between the working and auxiliary electrodes. When we oxidize an analyte at the working electrode, the resulting electrons pass through the potentiostat to the auxiliary electrode, reducing the solvent or some other component of the solution matrix. If we reduce the analyte at the working electrode, the current flows from the auxiliary electrode to the cathode. In either case, the current from redox reactions at the working electrode and the auxiliary electrodes is called a faradaic current, and it is presented as a specific peak which size is directly proportional to the concentration of the analyte specie oxidized/reduced [106, 108].

There are several different voltammetric methods that differ in terms of the type of working electrode, how we apply the potential, and whether we include convection (stirring) as a means for transporting of material to the working electrode. Among the several voltammetric modes, we have the differential pulse polarography which is a frequently used voltammetric determination mode. It uses a Dropping Mercury Electrode (DME) and we obtain a limiting current instead of a peak current. When a Hg drop separates from the working electrode surface and falls to the bottom of the electrochemical cell, it mixes the solution. Each new Hg drop, therefore, grows into a solution whose composition is identical to the bulk solution. The oscillations in the current are a result of the Hg drop's growth, which leads to a time-dependent change in the area of the working electrode where the current is measured twice per cycle: before applying the pulse at the

end of the cycle. The difference in the two currents gives rise to the peak-shaped voltammogram *(Figure 18)* [106].

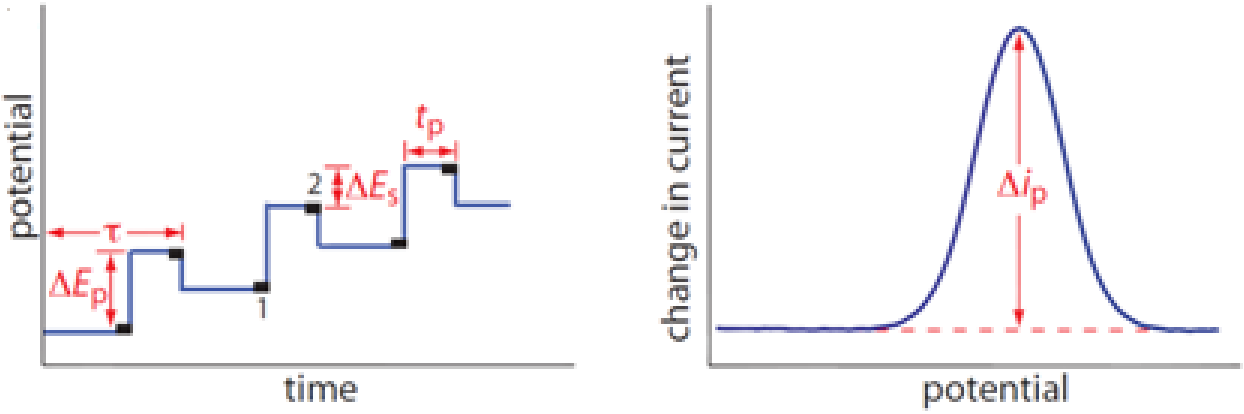

Figure 18 - Potential-excitation signal and voltammogram for a differential pulse polarography scan. When measuring a change in current, Δ*ip*, the current at point 1 is subtracted from the current at point 2. T is the cycle time Δ*E*p is a fixed or variable pulse potential; Δ*E*s is the fixed change in potential per cycle, and *t*p is the pulse time [106].

We call the resulting plot of current versus applied potential a voltammogram *(Figure 19)*, and it is the electrochemical equivalent of a spectrum in spectroscopy, providing quantitative and qualitative information about the soluble species involved in the oxidation or reduction reaction [106, 108].

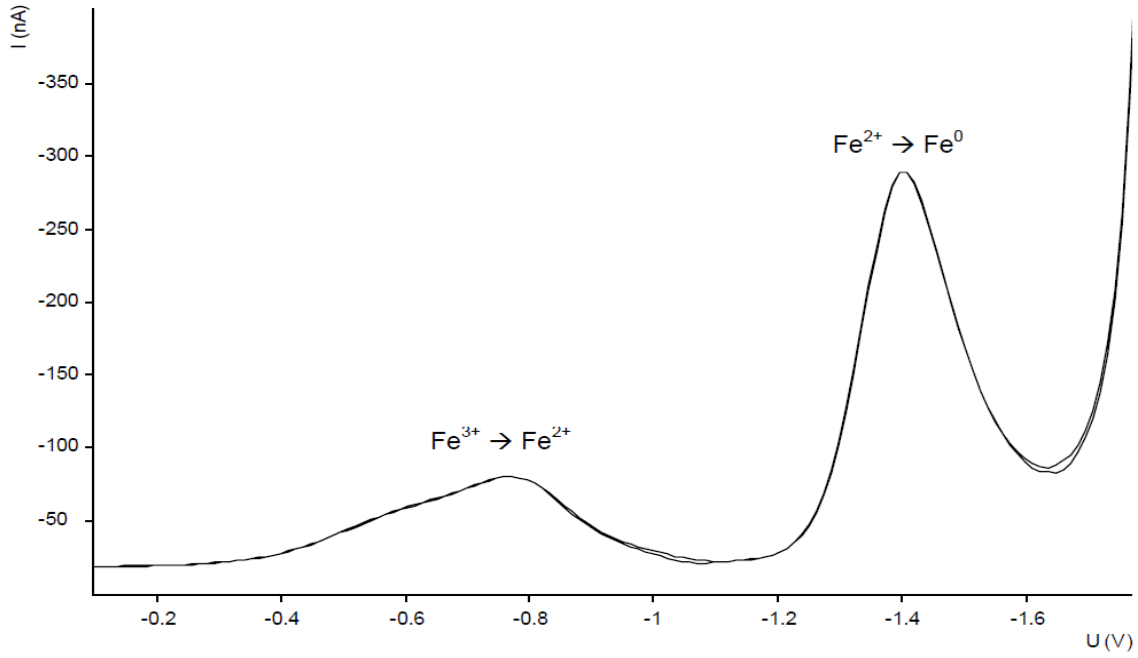

Figure 19 - Typical linear voltammogram regarding an iron valence analysis with the two peaks referred to the soluble ferrous and ferric iron present when reducing potentials are applied. The plot is current I(A) versus potential U(V). Experimental output retrieved from a method of polarographic determination of iron from a sucrose injection solution.

This current vs concentration relationship will allow a quantitative analysis of the ferrous and ferric iron present in the stock solutions of the IV iron preparations by Linear voltammetry simply by applying a potential increasingly negative until it reaches the potential of reduction of Fe^{3+} to Fe^{2+} and then the potential of reduction of Fe^{2+} to Fe^{0}, giving two distinct peaks.

3.2.5 X-ray diffraction

X-ray diffraction is a rapid analytical technique used for phase identification of solid matter, especially crystalline substances. Solid matter can be described as amorphous – where the atoms are arranged in a random way similar to the disorder we find in a liquid –, or as crystalline – that act as three-dimensional diffraction gratings for X-ray wavelengths where the atoms are arranged in a regular pattern, and exist as smallest volume units that by repetition in three dimensions describes the crystal. The smallest volume unit is called a unit cell. The dimensions of the unit cell is described by three axes *a, b and c* and the angles between them *alpha, beta, gamma* [109], which defines the crystallization system.

X-ray diffraction is based on constructive interference of monochromatic X-rays and a crystalline sample. These X-rays are generated by a cathode ray tube, filtered to produce monochromatic radiation and directed toward the sample. The interaction of the incident rays with the sample produces constructive interference (and a diffraction ray) when conditions satisfy Bragg's Law [109, 110]:

$$\mathbf{n\lambda = 2d \sin \theta}$$

λ – Wavelength of the x-ray beam

θ – incident angle

d – distance between atomic layers in a crystal

n – order of the diffraction peak (integer number)

This law relates the wavelength of the electromagnetic radiation (λ) with the diffraction angle (θ) and the lattice spacing between atomic plans (d). These diffracted X-rays are then detected, processed and counted. By scanning the sample through a range of

2θ angles, all possible diffraction directions of the lattice should be attained due to the random orientation of the powdered material. Conversion of the diffraction peaks to d-spacings allows identification of the mineral because each mineral has a set of unique d-spacings. This is compared with standard reference patterns [109, 110].

The sample preparation is easy, and X-ray powder diffraction should be able to quickly identify the mineral phases of all the materials, even if there is a multiplicity of components in a mixture.

4. Materials and Methods

4.1 Materials

Table 7 – List of the compounds used in the lysosomal assay, in the serum mimetic solution and in voltammetry.

Compound	Chemical Formula	Supplier
Sodium Phosphate Dibasic	Na_2HPO_4	Sigma-Aldrich
Calcium Chloride dihydrate	$CaCl_2 \cdot 2H_2O$	Sigma-Aldrich
Sodium Chloride	NaCl	Sigma
Sodium Citrate	$Na_3C_6H_5O_7$	Sigma-Aldrich
Sodium acetate anhydrous	$NaC_2H_3O_2$	Sigma
(+)-Potassium D_s-*threo*-isocitrate monobasic	$KC_6H_7O_7$	Sigma-Aldrich
Citric acid	$C_6H_8O_7$	Sigma-Aldrich
Mercury	Hg	Sigma-Aldrich
Iron(III) chloride hexahydrate	$FeCl_3 \cdot 6H_2O$	Sigma-Aldrich
Iron(II) sulphate hepahydrate	$FeSO_4 \cdot 7H_2O$	Sigma
Sucrose	$C_{12}H_{22}O_{11}$	Sigma
Dextran (1000kDa) from *Leuconostoc mesenteroides*	$(C_6H_{10}O_5)_n$	Sigma-Aldrich
Dextran (5000kDa) from *Leuconostoc mesenteroides*	$(C_6H_{10}O_5)_n$	Sigma-Aldrich
Fetal Bovine Serum	Not available	GIBCO

Table 8 – List of the IV iron preparations used as samples in the experimental work [43, 65].

Compound	Chemical Formula	Supplier
Cosmofer® (LMW-ID)	Not found	Pharmacosmos
Venofer® (Iron Sucrose)	$[Na_2Fe_5O_8(OH)\cdot \mathbf{3}H_2O]n\cdot m(C_{12}H_{22}O_{11})$[48]	Vifor Pharma
Ferinject® (Ferric carboxymaltose)	$[FeO_X(OH)_Y(H_2O)_Z]_n[\{(C_6H_{10}O_5)_m(C_6H_{12}O_7)\}_1]_k$[70]	Vifor Pharma
Monofer® (Iron isomaltoside 1000)	Not found	Pharmacosmos

4.2 Methods

4.2.1 XRD analysis

The four IV iron materials were completely dried at 45ºC and the powders were milled and analysed by X-Ray Diffraction, at the Earth and Environmental Department at the University of Leeds. Each sample was mixed with ethanol and pipetted onto a low background silicon holder. The diffraction data was collected with a Philips PW1050 Powder Diffractometer using Cu K-alpha radiation and a Ge secondary monochromator. The scanning range was 5-70 deg 2 theta at a speed of 0.8 deg/min and a step size of 0.01 deg. TRACES software with the ICDD (International Centre for Diffraction Data) database was used to process the data. The percentage of solid matter was also calculated from the powders obtained.

4.2.2 Iron content determination by ICP-OES

Cosmofer®, Ferinject® and Monofer® were diluted with 5% nitric acid (to completely dissolve the iron) while Venofer® was diluted using a more concentrated solution of nitric acid (70%) because of the difficulty encountered with 5% nitric acid. Nitric acid is necessary because sample preparation for ICP-OES analysis requires acid digestions to avoid the existence of solid analyte in the sample. Subsequently, dilutions were made with 5% nitric acid, in triplicate, for each IV iron to adjust the concentration of iron to the range of the different standards used (0-100 ppm). The IV iron preparations were then analysed by ICP-OES (JY2000, Horiba Jobin Yvon) to determine the iron concentration of the solutions.

4.2.3 Determination of nanoparticle agglomeration

Initially, the preparations were diluted to 50ppm of iron with ultrapure water, in triplicate, using the iron concentrations obtained by ICP-OES (experiment 4.1.2) and were analysed by DLS do determine their partice size in the simplest aqueous solution.

The same procedure as above was repeated, but instead of water, an aqueous solution of 2.4 mmol/L of total calcium ($CaCl_2 \cdot 2H_2O$), 1.3 mmol/L of phosphate (Na_2HPO_4) and 0.9% of NaCl at pH 7.42 was used, to mimic the conditions that the IV iron would face in the circulation [111, 112].

All the samples were analysed by DLS immediately after being prepared, except the serum mimetic solutions. Due to this delay, the pH had to be adjusted again right before the analysis by DLS. The resulting particle size distribution was obtained and processed by the "DTS (Version 4.1)" software (Malvern Instruments Ltd., Malvern, UK).

The concentration of precipitated, nanoparticulated and soluble fractions of calcium and phosphate were determined by ICP-OES to determine if there is aggregation (association of both ions by electrostatic interaction) in electrolyte solutions of calcium and phosphate. For this we used the phosphate and total calcium solution prepared before and a fresh solution with physiological concentrations of phosphate and calcium in its free ionic form, 1.2 mmol/L of calcium ($CaCl_2 \cdot 2H_2O$). To study the fractions of calcium and phosphate in each solution, i. e. soluble, nanoparticulated and precipitated, sets of three aliquots were collected for each fraction. One set of aliquots was used to calculate the total concentration of calcium and phosphate in the solution; a second set was centrifuged 5minutes with 13000 rpm and the supernatant was analysed to get the concentration of the nanoparticulated calcium and phosphate. The third set was ultrafiltred by centrifugation (5 minutes, 13000 rpm) through a membrane of 3 kDa to retain any salt in nanoparticulated form, and then analysed on the ICP-OES to determine the concentration of the soluble calcium and phosphate. All samples were diluted in 5% nitric acid and to get final samples with iron concentrations within the calibration curve (0-5 ppm for calcium and phosphate). The calculations used were:

Fe precipitated (mM): $Fe_{total} - Fe_{supernatant}$

Fe nanoparticulated (mM): $Fe_{supernatant} - Fe_{soluble}$

Fe soluble (mM): $Fe_{total} - (Fe_{precipitated} + Fe_{nanoparticulated})$

Furthermore, each material was diluted to 300 ppm of Fe in Fetal Bovine Serum (FBS) or in 0.9% NaCl. Each suspension was incubated at 37ºC with stirring for 30 minutes, after which aliquots (in duplicate) were transferred to 1000 kDa filter eppendorfs to be centrifuged 15 minutes with 13000 rpm. Both filtrates plus a non-filtrated aliquot were diluted five times in 5% nitric acid and were analysed by ICP-OES using the preferred standard range. The calculations used were:

% Fe agglomerated (1000 kDa): $[(Fe_{total} - Fe_{filtered,\ 1000})/ Fe_{total}] \times 100$

% Fe agglomerated (0.1 µm): $[(Fe_{total} - Fe_{filtered,\ 0.1})/ Fe_{total}] \times 100$

% Fe filtered (100 0kDa): $(Fe_{filtered,\ 1000}/ Fe_{total}) \times 100$

% Fe filtered (0.1 µm): $(Fe_{filtered,\ 0.1}/ Fe_{total}) \times 100$

Additionally, the four IV iron materials were diluted to 1000 ppm in ultrapure water and the zeta potential was measured firstly with no pH adjustment and then with pH = 7.35. The zeta potential was obtained and processed by the "DTS (Version 4.1)" software (Malvern Instruments Ltd., Malvern, UK).

4.2.4 Lysosomal dissolution

The first part of this assay was the determination of the optimal conditions of pH, iron concentration and chelating agent to obtain the most representative results, using Venofer® as the sample. Then, with the method optimized, it was applied to all materials.

Assuming the iron concentration of Venofer® obtained by the ICP-OES in experiment 3.1.2, the necessary dilutions with a 10 mM of fresh citrate buffer were made to get a final iron concentration of 0.1 mM (5584 ppb) in a pH 5.0 environment. Subsequently, the solution was incubated at 37ºC in a water bath for seven days with no further adjustment of the pH. The solution was analysed in the ICP-OES at 0, 15 and 30 min, 1, 2, 4, 6, 24 and 48h and seven days (the 0 min measurement was done using the citrate buffer as sample). At each time-point, aliquots of the solution were taken and prepared for ICP-OES measurement of the precipitated, nanoparticulated and soluble iron the same way as it was done for 4.2.3 for the calcium and phosphate solution.

We used the same protocol to perform further dissolution assays with the following modifications *(Table 9)*:

Table 9 - Four solutions of Venofer® and citrate buffer prepared with different pH and iron concentrations.

Solution	pH	[Fe] (mM)	Chelating agent
2	5.0	0.5	Citrate (10mM)
3	5.0	1.0	
4	4.5	0.1	
5	5.5	0.1	
6	4.5	0.1	Phosphate (10mM)
7	4.5	0.1	Isocitrate (10mM)

Once the pH, chelating agent and iron concentrations were chosen, we deviated from the physiological conditions by performing a more acidic dissolution of Venofer® (pH 2.5 with citric acid as the pH adjuster and chelating agent) to make the dissolution quicker. To understand if the results obtained were due to a pH or chelating agent-driven dissolution, the four IV iron products were dissolved in the same conditions but without citric acid.

Once established the best conditions to a faster and reproducible dissolution a dissolution assay was performed to the four IV irons in the conditions of pH 2.5, 0.1mM of Fe and 10mM of citric acid.

To possibly obtain the same soluble iron yield as the previous dissolution but maintaining a more physiological scenario, we tried to optimize the assay by increasing the concentration of chelating agent. Two dissolutions of Venofer® were made, both at pH 4.5, 0.1 mM of Fe but with different concentrations of citrate: 20 mM and 50 mM. 20 mM regards the sum of the concentrations of all the organic acids in the lysosome assuming the concentration of citrate as being 10 mM, whereas 50 mM is the concentration of citrate in the lysosomes of the rubber tree [113].

The calculations used were:

% Fe precipitated: $[(Fe_{total} - Fe_{supernatant})/ Fe_{total}] \times 100$

% Fe soluble: $(Fe_{soluble} / Fe_{total}) \times 100$

% Fe nanoparticulated: $100 - Fe_{soluble}(\%) - Fe_{precipitated}(\%)$

4.2.5 Linear voltammetry analysis of ferric and ferrous content in Venofer®.

The potentiostat (Autolab/PGSTAT302N) was used to analyse the iron redox state (ferric and ferrous content) of Venofer® by differential pulse polarography (linear voltammetry) using the software *757 VA Computrace* and the method *VA Application Note No. V-127, Polarographic determination of* Fe^{2+} *in iron sucrose injection solution according to USP 26 / NF21* from Metrohm. The working electrode was a Multi-Mode Electrode with the Dropping Mercury mode; the auxiliary electrode was a platinum one and the reference electrode was a Ag/AgCl one. A ferrous sulphate and ferric chloride solution were also analysed to evaluate if the method works. Venofer® was also scanned using a Rotating disk electrode (RDE) instead of a mercury working electrode. The sample conditions in every scans performed was 20 ppm of iron, diluted in the sodium acetate (150 g/L) electrolyte solution. Each analysis was performed in triplicate.

5. Results and Discussion

5.1 XRD analysis

The identification and characterization of synthesized materials was carried out by powder XRD to determine the mineral phase of Cosmofer® (*Figures 20),* Venofer® *(Figure 21),* Ferinject® *(Figure 22)* and Monofer® *(Figure 23),* which, surprisingly, showed akaganeite crystallinity resemblance only in Ferinject®, whereas Cosmofer® and Monofer® exhibited amourphousness, and Venofer's mineral phase profile was masked by the sucrose peaks.

The XRD characterization of each IV iron products can help to explain the results from the lysosomal dissolution because amorphous forms may exhibit distinct physical properties compared to crystalline species of the same molecule, such as different dissolution profiles. The dissolution advantage of amorphous solids can be negated by crystallization due to higher robustness [114]. Particularly, the presence of a crystalline arrangement such as akaganeite confers a higher stability to the core because of the ordered octahedrally high spin Fe(III) ions coordinated with six oxygen atoms, whereas an amorphous solid has the atoms arranged in a random way decreasing the structure order, increasing the surface area and making them more easily dissolved with higher rates of

iron release. For example, it has been proved that amorphous $Fe(OH)_3$ dissolves at least ten times faster than lepidocrocite (γ-FeOOH), which is another oxyhydroxide polymorph like akaganeite (β-FeOOH) [115].

Moreover, a higher level of amorphousness has been linked to an increased capacity to bind anions, and different types of FeOOH polymorphs have different electrolyte affinities, such as the described affinity of akaganeite to phosphate. Thus, not only phosphate binds the nanoparticles according to the surface charge by electrostatic interaction, but also by electrostatic interaction with the surface of the core and by ligand exchange for surface OH groups [116].

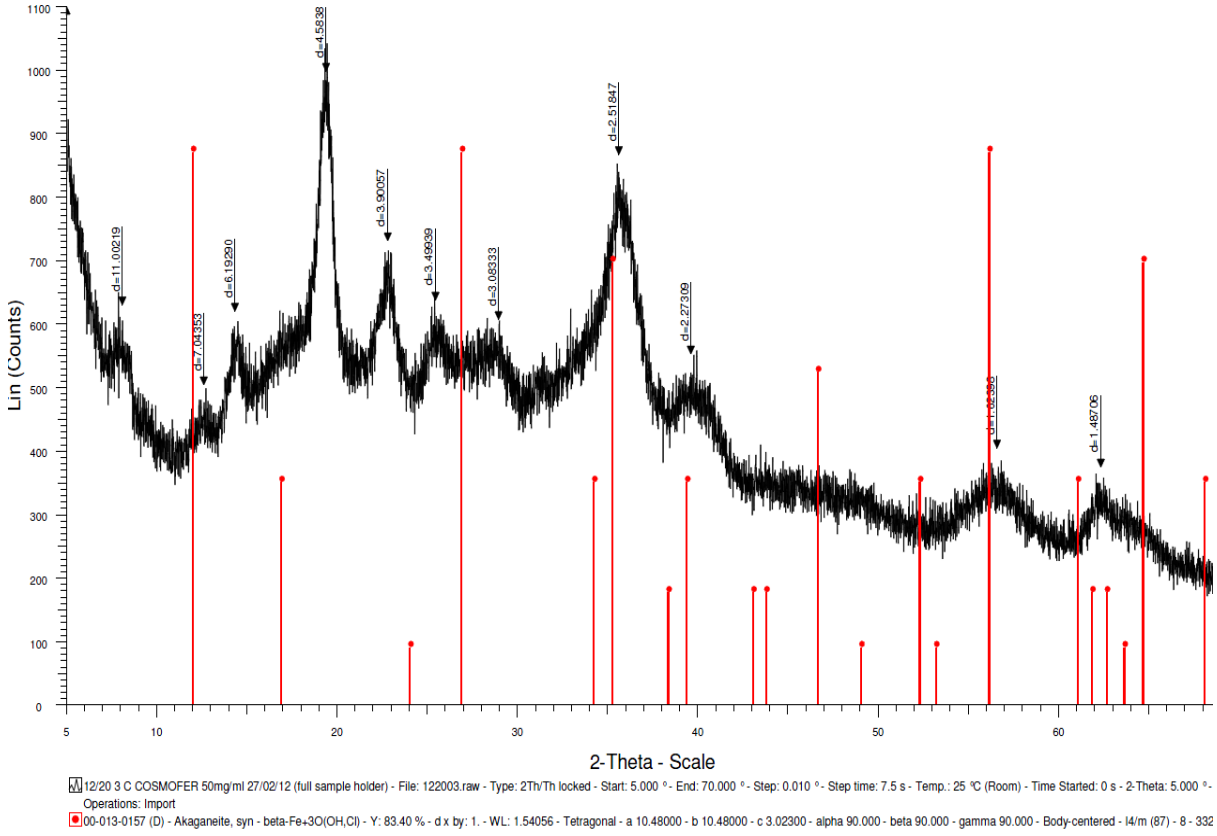

Figure 20 - XRD characterization of Cosmofer powder obtained after drying 2mL of stock solution at 45°C. An akaganeite pattern is represented in red lines.

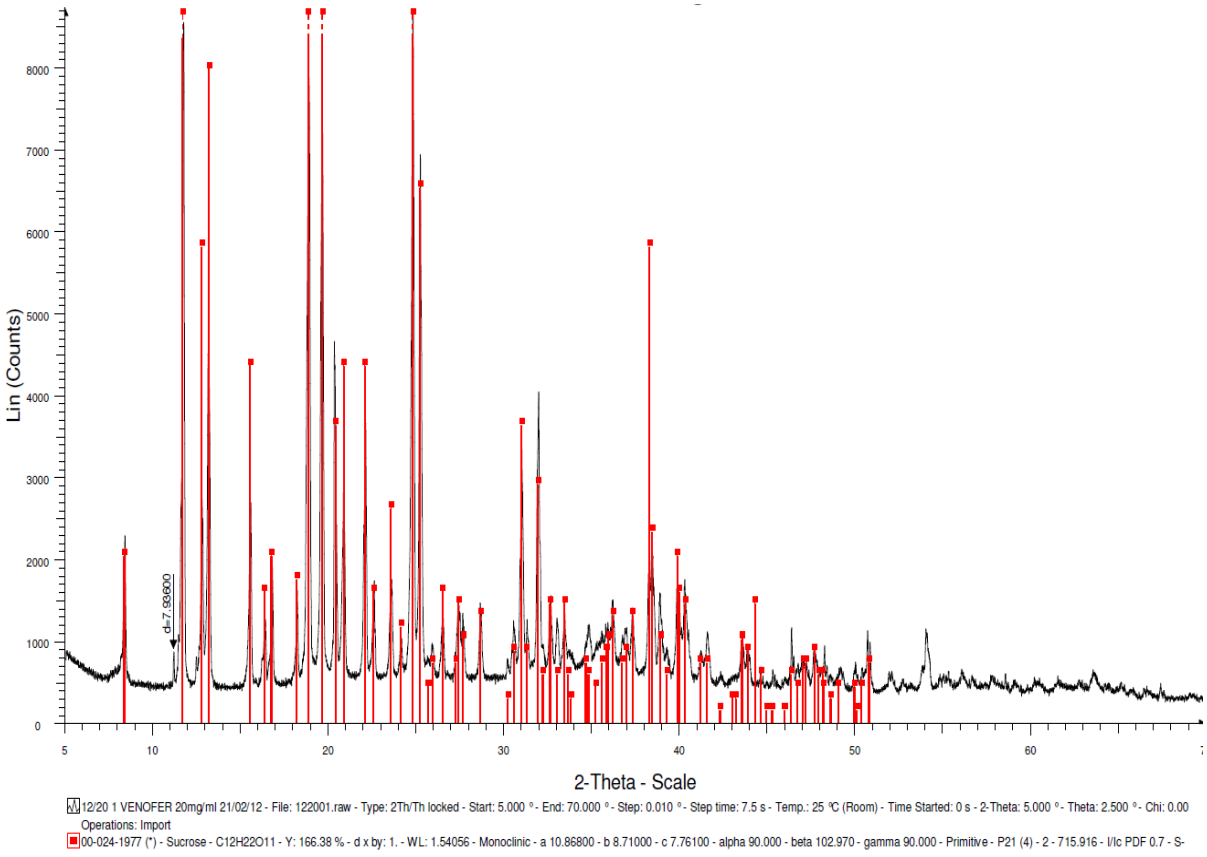

Figure 21 - XRD characterization of Venofer powder obtained after drying 5mL of stock solution at 45°C. An akaganeite pattern is represented in red lines.

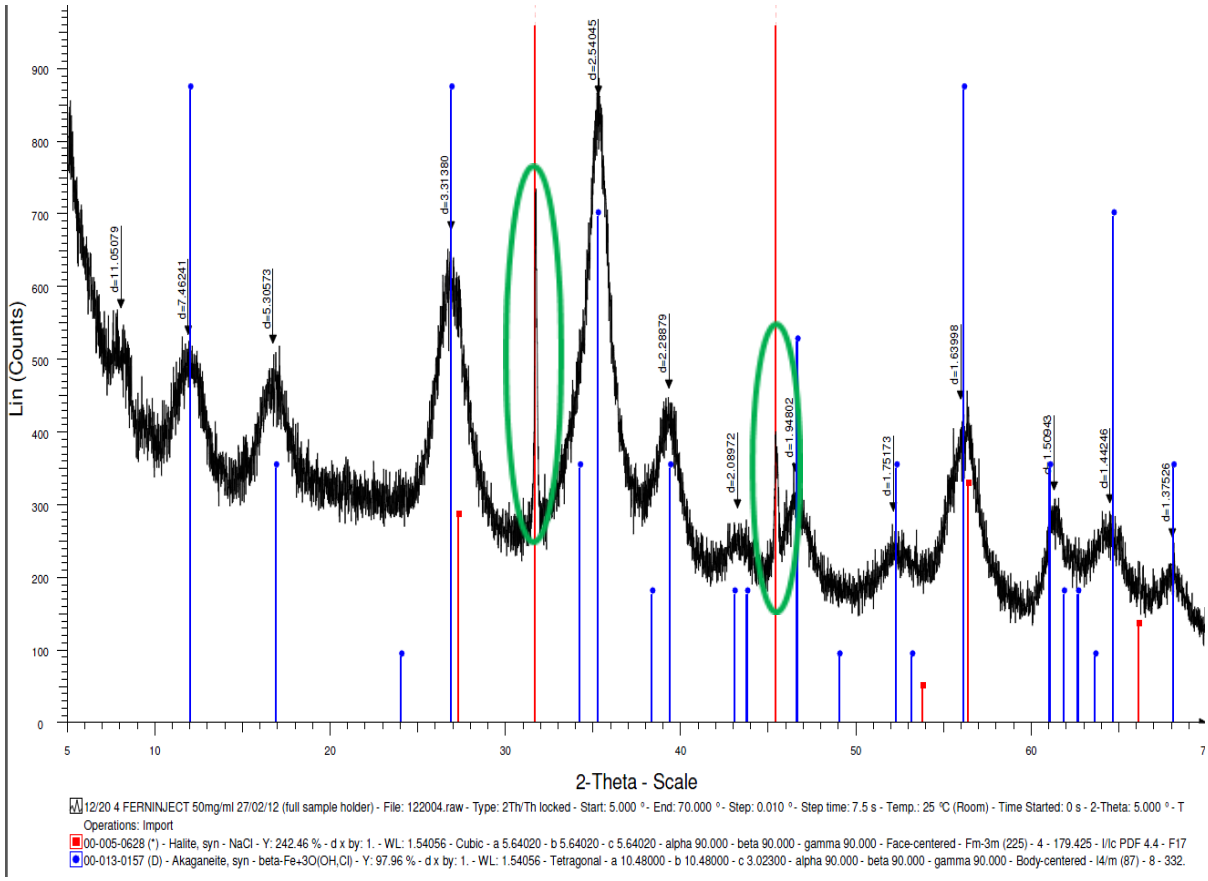

Figure 22 - XRD characterization of Ferinject powder obtained after drying 2mL of stock solution at 45°C. An akaganeite and halite patterns are represented in blue and red lines, respectively. The green circles correspond to the halite (NaCl) peaks detected.

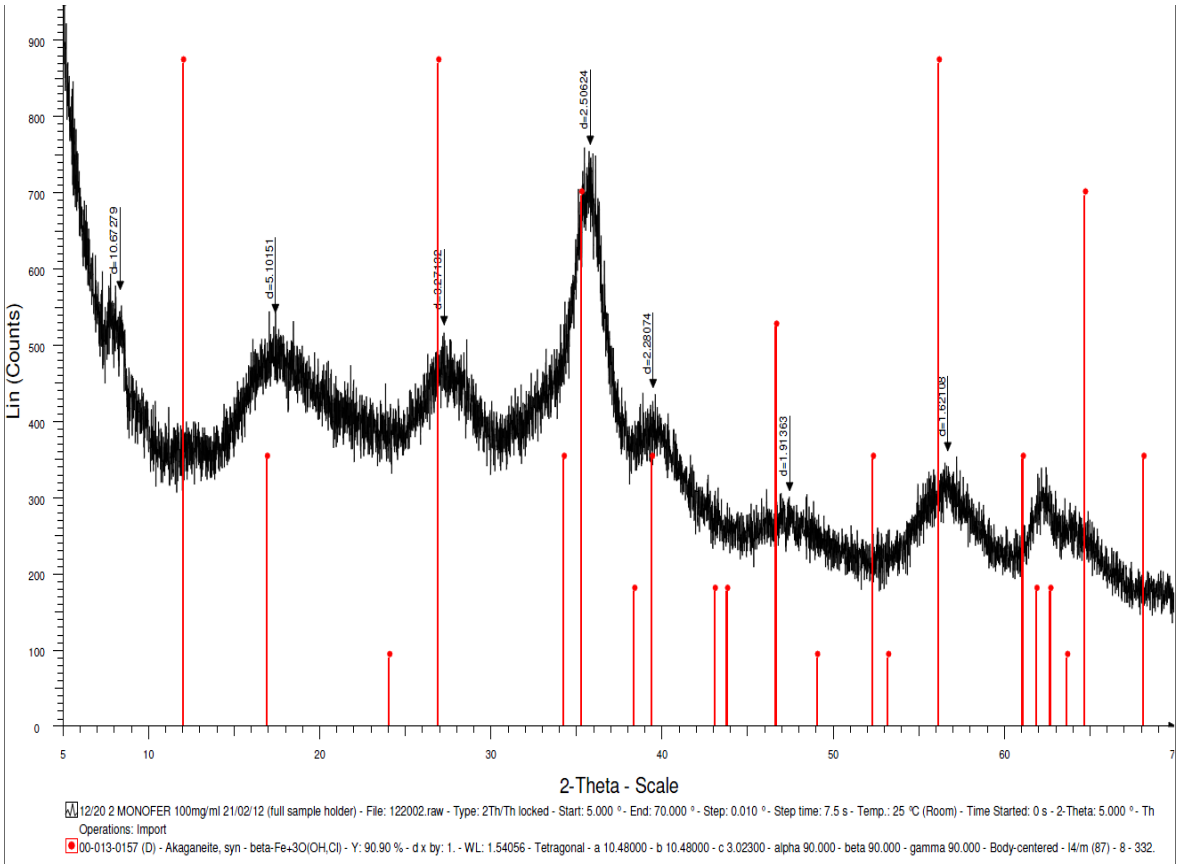

Figure 23 - XRD characterization of Monofer powder obtained after drying 1mL of stock solution at 45ºC. An akaganeite pattern is represented in red lines.

Surprisingly, all four materials should have resembled akaganeite but just Ferinject® spectrum matched the akaganeite peaks more faithfully. Ferinject® spectrum also showed the clear presence of two of halite's peaks (marked as two green circles). This match helped to confirm the presence of akaganeite in Ferinject® because halite is composed by crystals of NaCl, and as mentioned before, chloride is an element present in the structure of akaganeite.

Cosmofer® and Monofer® seem to be more amorphous as their peaks do not match akaganeite ones nor they show the 5000 kDa and 1000 kDa respective dextran peaks (see in Appendix). However, it seems like some of the peaks could have corresponded to the akaganeite ones if they were not blunted which points towards some unidentified cause that could have distorted the original akaganeite structure into another crystalline phase. Such causes could have consisted in the unlikely thermal decomposition of the mineral due to dry heating at 45ºC because akaganeite is easily converted to hematite at 300ºC but it is reported to suffer some transformation below that temperature [117]. The presence of water can also be a variable and the loss of the choride ions leads to a loss of stability and

facilitates the transformation of akaganeite to goethite and hematite [118]. So, the lack of halite's peaks in Cosmofer® and Monofer® spectrums can point towards an unexplained loss of chloride atoms as a possible source of amorphousness. In case of Venofer®, we can confirm the presence of sucrose but its peaks clearly shift the scale up and make de mineral phase identification impossible to determine, although we would expect a mixture of akaganeite and 2-line ferrihydrite [27].

Due to the uncertain explanation for this non resemblance to akaganeite and as the gathering of the powders is quite simple, it is hard to believe that this might be due to bad preparation of the samples. Therefore, we will consider these results in further discussion.

The percentage of solid matter was also calculated from the powders obtained *(Table 10)* to relate it with the iron concentration of each stock suspension.

Table 10 - Percentages of solid matter obtained from the powders of each IV iron material.

Venofer®	**44.8**
Cosmofer®	**28.0**
Ferinject®	**17.9**
Monofer®	**37.3**

At 45ºC, the drying occurred very slowly in a way that after two weeks we had to collected the powder. Consequently, the percentage of solid matter might have been overestimated because of the presence of water in the dried powders. The water contamination might explain why Monofer®, the most iron concentrated material (1000mg/mL), did not have the highest percentage of solid matter when we was supposed to, and why Venofer®, the least iron concentrated IV iron (20 mg/mL), presented the highest percentage (44.8%). Ferinject® and Cosmofer® showed different percentages 28.0% and 17.9%. even though they share the same concentration of iron (50 mg/mL).

5.2 Iron content determination

The concentration of each IV iron suspension was determined, to see if it matched the respective ones described in the vial label (*Figure 24* and *Table 10)*.

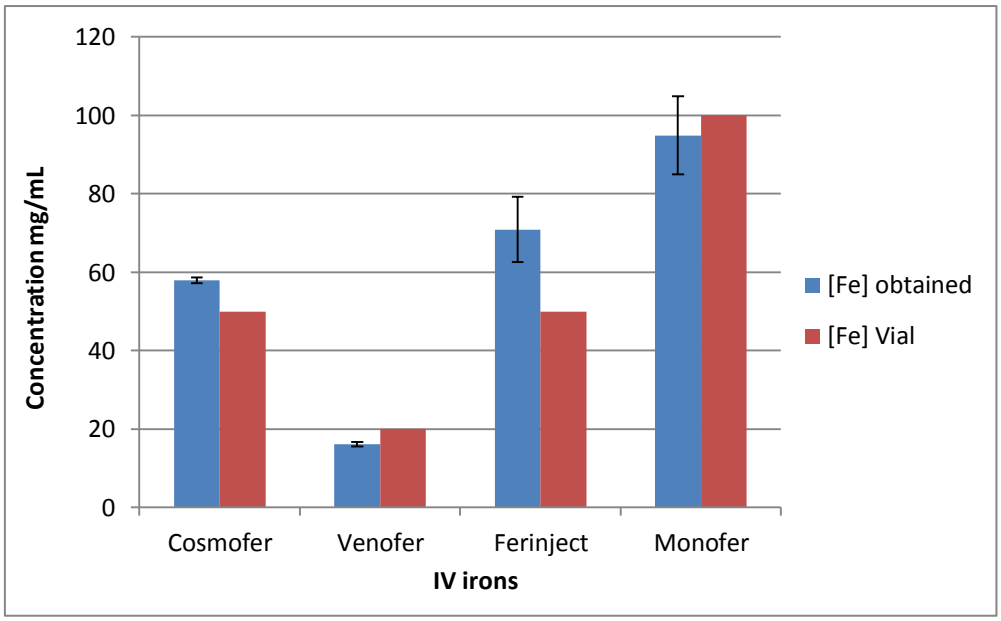

Figure 24 - Comparison of the concentrations (mg/mL) of iron between Cosmofer®, Venofer®, Ferinject® and Monofer® measured by ICP-OES and the concentrations expected (i.e. described in the vials).

Table 10- Concentrations (mg/mL) of iron measured and the ones found in the stock solutions for Cosmofer®, Venofer®, Ferinject® and Monofer®.

IV iron	Average [Fe] measured (mg/mL)	[Fe] expected (mg/mL)
Venofer®	16.08±0.62	20
Cosmofer®	57.97±0.81	50
Ferinject®	70.84±8.34	50
Monofer®	94.91±9.98	100

As we can see in *Figure 24* and *Table 10*, the obtained concentrations of iron showed some deviation from the expected ones in the stock. Although some experimental errors in the dilutions could have happened, these differences are most likely related to manufacturing variability. Venofer® and Cosmofer® presented the most similar concentrations to the respective stock, so the 16.08 mg/mL concentration of iron obtained for Venofer® was considered in the preliminary lysosomal dissolutions to determine the best iron concentration, pH and chelating agent.

5.3 Determination of nanoparticle agglomeration

The particle sizing performed to Venofer®, Cosmofer®, Ferinject® and Monofer®, diluted to 50 ppm of Fe with ultrapure water, gave the actual size of the nanoparticles (*Figure 25* and *Table 11)*. At the same time, it represented the most innocuous scenario that the products would face and the control needed to analyse the results of the particle sizing of the IV iron diluted in a Ca^{2+}/PO_4^{3-} solution.

The 50 ppm concentration was chosen specifically because it is slightly lower than 62.5 ppm, which is the concentration estimated in the blood if the maximum dose of Venofer® was administrated (200 mg) assuming its distribution volume of 3.2 L [57]. This way, we can obtain and compare the possible nanoparticle agglomeration between all the materials in iron concentrations (50 ppm) not considered dangerous for the human with few reports of AEs.

Graphic 25 - Comparison of the particles sizes (nm) measured for the four IV materials at 50ppm of Fe and the ones in literature.

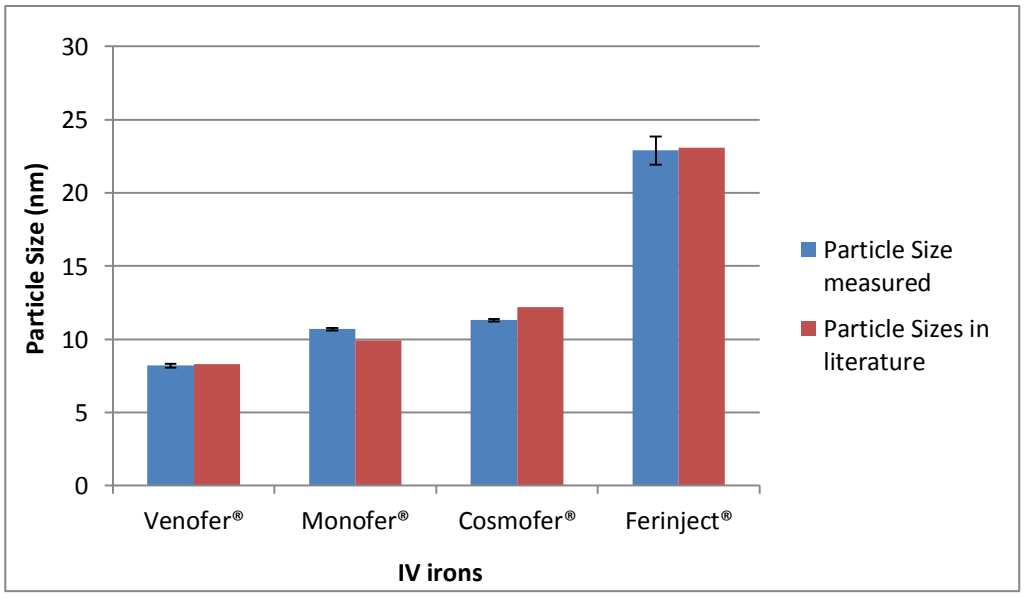

Table 11 - Particle Sizes (nm) obtained for Venofer®, Monofer®, Cosmofer® and Ferinject® diluted in water (50mg/L of iron) and the particle sizes in literature.

IV iron	Average particle sizes measured (nm)	Particle Sizes expected (nm)
Venofer®	8.2±0.12	7-8.3 [26]
Monofer®	10.7±0.08	9.9 [27]
Cosmofer®	11.3±0.09	12.2 [27]
Ferinject®	22.9±0.96	23.1 [27]

In these water conditions, no agglomeration was seen, the particle sizes obtained presented low standard deviations and the peak averages were similar to the ones described in literature (figures of the size distribution in Appendix). As shown in *Table 11*, the average nanoparticles sizes were: Venofer® = 8.2 nm < Monofer® = 10.7 nm < Cosmofer® = 11.3 nm < Ferinject® = 22.9 nm. However, when we measured the particle sizes in the same iron concentration conditions but in a solution with serum concentrations of phosphate (1.3 mM) and total calcium (2.4 mM), the nanoparticle sizes of Cosmofer®, Ferinject® and Monofer® became slightly bigger, ergo diverging from the ones got from the water dilution *(Table 12)*. Venofer® showed many different peaks and the deviation was too high to determine an accurate particle size.

Table 12 - Particle Sizes (nm) of Venofer®, Monofer®, Cosmofer® and Ferinject® diluted in the calcium and phosphate solution (50mg/L of iron).

IV iron	Average particle sizes measured (nm)	Average particle sizes in water (nm)
Venofer®	Not applicable (high deviation)	8.2±0.12
Monofer®	11.7 ± 0.98	10.7±0.08
Cosmofer®	14.3 ± 0.17	11.3±0.09
Ferinject®	23.8 ± 0.47	22.9±0.96

Cosmofer® *(Figures 26)* and Ferinject® *(Figure 29)*, showed large agglomerates, whereas Venofer® *(Figure 27)* showed much higher peak deviations at the lower particle sizes and also a more noticeable presence of large agglomerates. Overall, the presence of these peaks in a bigger particle size range gives evidence of agglomeration between nanoparticles in all the materials but Monofer® *(Figure 28)*.

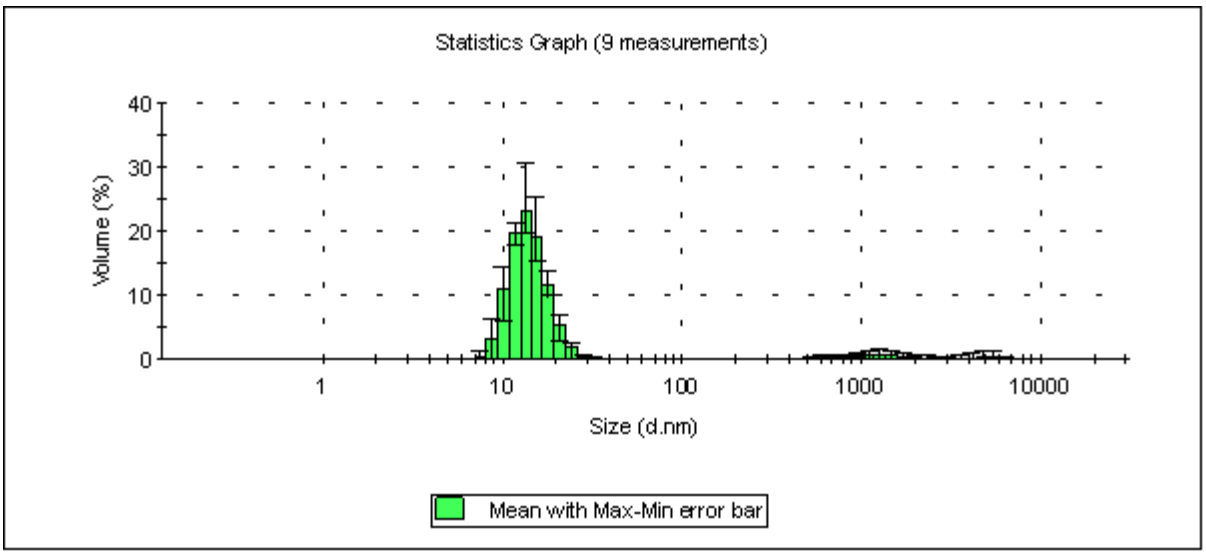

Figure 26 - Statistics graph of the size distribution by volume of Cosmofer® diluted in the calcium and phosphate solution (50mg/L of iron). Total of nine measurements.

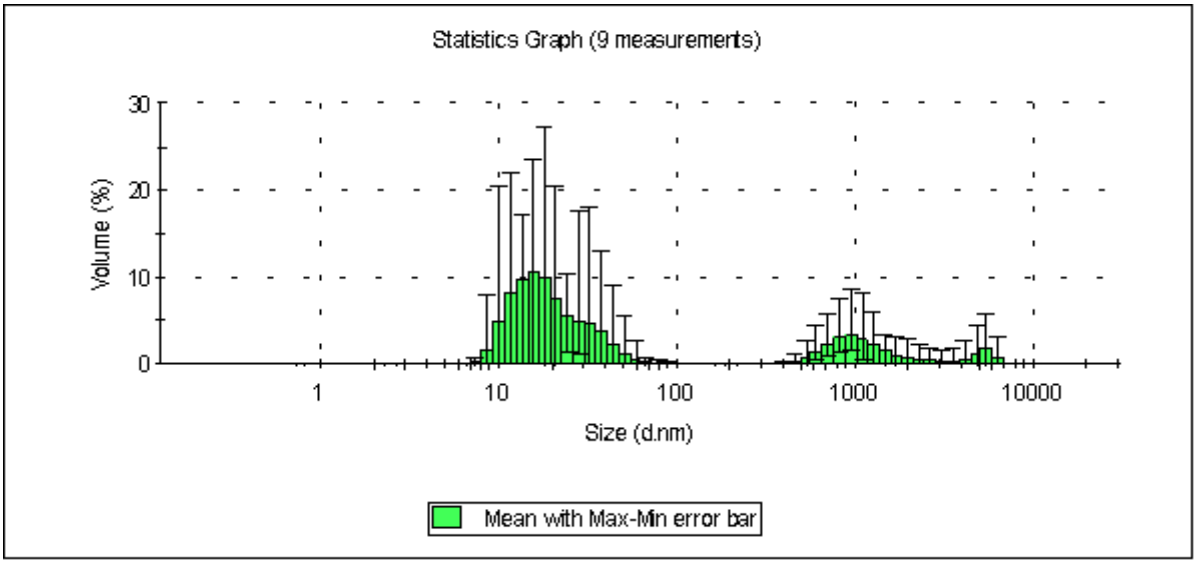

Figure 27 - Statistics graph of the size distribution by volume of Venofer® diluted in the calcium and phosphate solution (50mg/L of iron). Total of nine measurements.

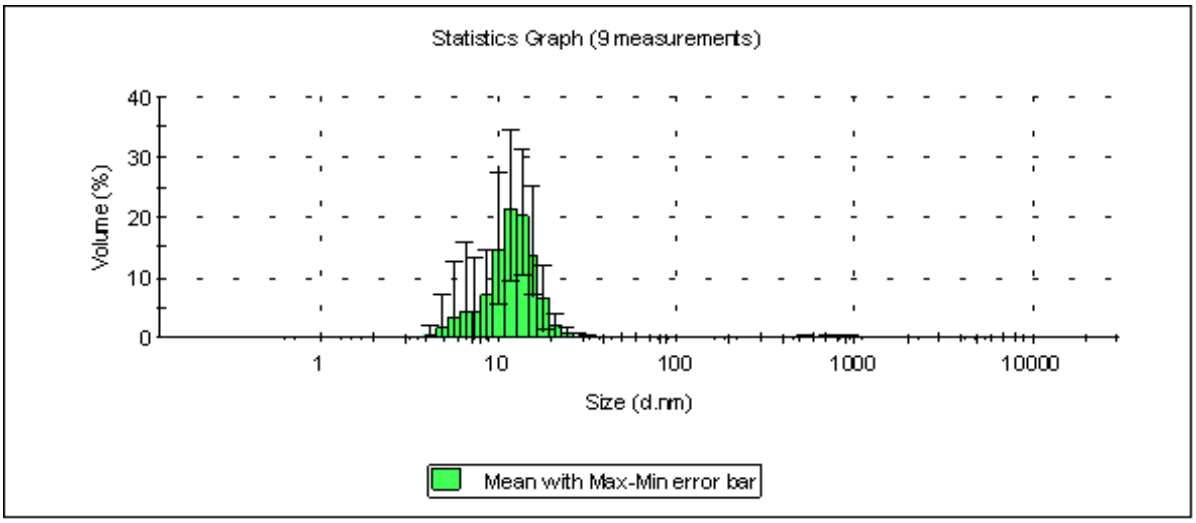

Figure 28 - Statistics graph of the size distribution by volume of Monofer® diluted in the calcium and phosphate solution (50mg/L of iron). Total of nine measurements.

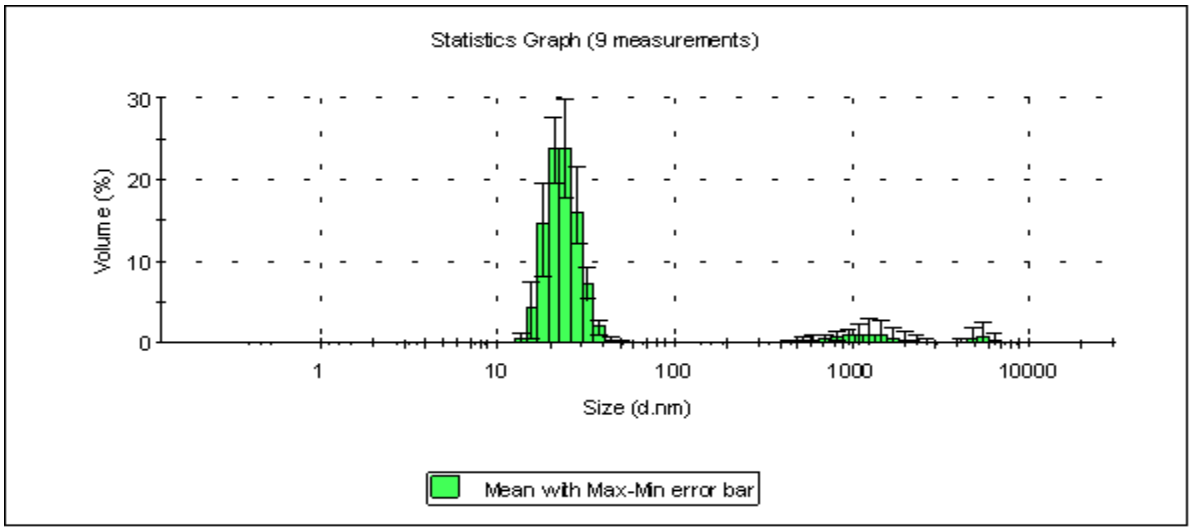

Figure 29 - Statistics graph of the size distribution by volume of Ferinject® diluted in the calcium and phosphate solution (50mg/L of iron). Total of nine measurements.

Further ICP-OES measurements to the same calcium and phosphate solution proved that the agglomeration was not due to the formation of insoluble salts from this solution (*Table 13)*.

Table 13- Concentration of the precipitate, nanoparticulated and soluble fraction of phosphate and total calcium in the already prepared solution.

	Average			
	precipitate mM	**nanoparticle mM**	**soluble mM**	**Total mM**
Phosphate	0.03 ± 0.01	0.04 ± 0.04	1.39 ± 0.03	1.47
Total calcium	0.01 ± 0.01	0.01 ± 0.01	2.14 ± 0.01	2.16

As mentioned before, oxydydroxyes play a significant role in sequestering electrolytes because of their large surface area and strong affinity for some anions such as the affinity of akaganeite for phosphate. This preferable anion adsorption is highly dependent on the pH and on the hydroxyl surface site composition.

In particular, akaganeite has a pH_{PZC} (pH in the point of zero charge, at the core surface) of 7.9 ± 0.1 [119], thus, the core surface of all the IV iron materials should have had a positive charge at the pH 7.4 of the phosphate and calcium solution. In these conditions, the agglomeration evidences in Venofer®, Cosmofer® and Ferinject® can be explained by the electrostatic interaction between the positive charges of the core surface and the negative charged phosphate ions (mechanism described in *Figure 30* [120]).

However, this interaction here proposed is only valid if phosphate can overpass the physical barrier of the carbohydrate shell and the repelling negative charge at physiological pH present in Venofer® and Cosmofer®. Considering the high lability associated to the second generation materials such as Venofer®, it makes sense that the highest evidences of agglomeration in this Venofer® is due to a weak shell-core interaction that allows the phosphate to pass through the sucrose coating and interact with the iron. In case of Ferinject®, it is reported to become more positively charged in the nanoparticle surface with increasingly acid pH [27], so the affinity to phosphate might happen in the surface, even because Ferinject® is a very robust IV iron with strong coating protection.

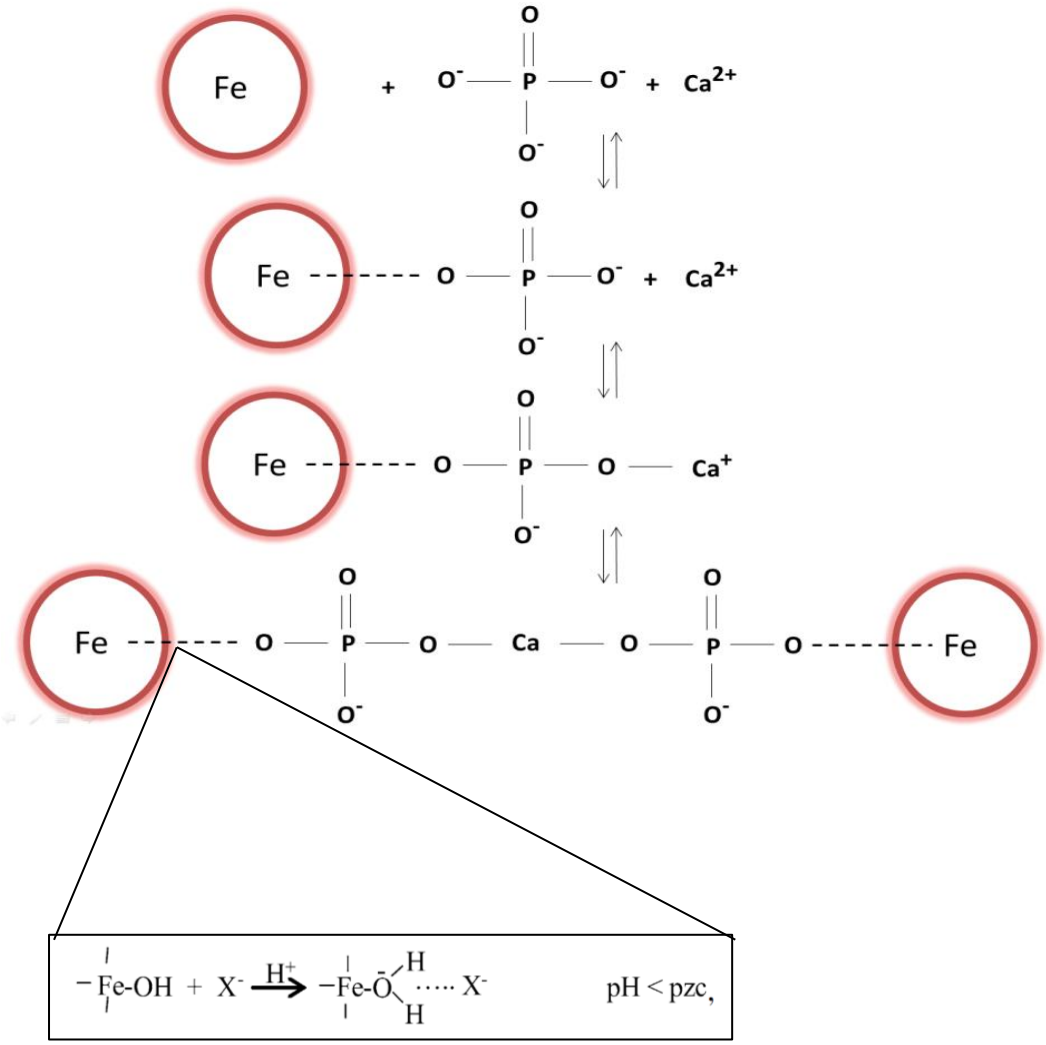

Figure 30 - Scheme of the possible mechanism of agglomeration between the iron nanoparticles and the ions of calcium and phosphate. The standard mechanism of electrostatic adsorption between the phosphate and the oxyhydroxide is described in the box at a pH below the pH of point of zero charge [120].

Conversely, Monofer® shares the same amorphousness and negative surface charge with Venofer® and Cosmofer® and it did not show any sign of agglomeration, so another mechanism of iron core-phosphate adsorption must be the cause, and that might be the ligand exchange for surface OH groups with the formation of inner sphere complex (mechanism described in *Figure 31*) [120]. Moreover, the phosphate adsorption by this mechanism can be enhanced through hydroxyl surface site availability and this last one depends on the level of amorphousness and disorder of the mineral phase. So, although not available in the XRD data, the synthetic 2-line ferrihydrite considered to be present in Venofer® has a much more poor order than akaganeite in a way that its surface is more heterogeneous with a bigger surface area than akaganeite, which gives a number of surface OH group available for adsorption of 12.7×10^2 meq/g while akaganeite has just 4.5×10^2 meq/g [118]. Therefore, the higher evidences of phosphate adsorption in Venofer® can be due to a larger amount of ligand sites to the phosphate ions ergo increasing the affinity between this ion and the core surface.

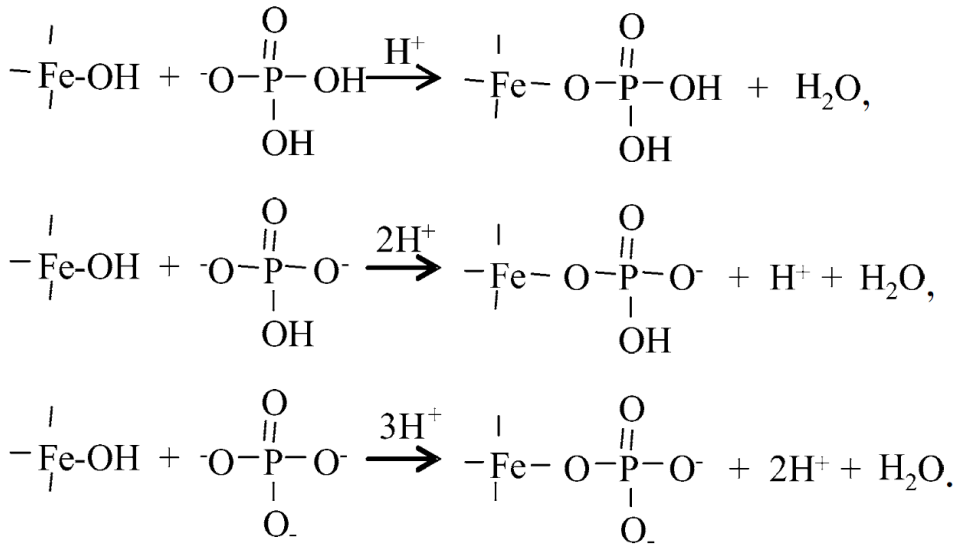

Figure 31 - Mechanism of formation of inner sphere complex by phosphate exchange for hydroxyl groups, as an explanation to the nanoparticle adsorption with phosphate [120].

The phosphate and calcium solution represented just a fraction of the molecules and electrolytes exposed to IV iron materials when these are in the blood, so the agglomeration was also assessed by diluting each IV iron material in FBS (similarity in composition to the Human serum). The main goal was to develop a method that could trap the fraction of agglomerated nanoparticles by filtration and would let all the proteins and the non-

agglomerated nanoparticles pass through the filters. So, 1000 kDa filters were chosen because the largest protein in the human serum is albumin with 67 kDa and the biggest nanoparticles belong to Ferinject® with a molecular weight around 750 kDa [17]. A first assay aimed the determination of the possible agglomeration in the serum conditions the IV iron materials would encounter if they were administrated undiluted, by diluting each material directly with FBS to 300 ppm of Fe. A parallel dilution with saline worked as the control as we do not expect any kind of nanoparticle trapping *(Figure 32)*.

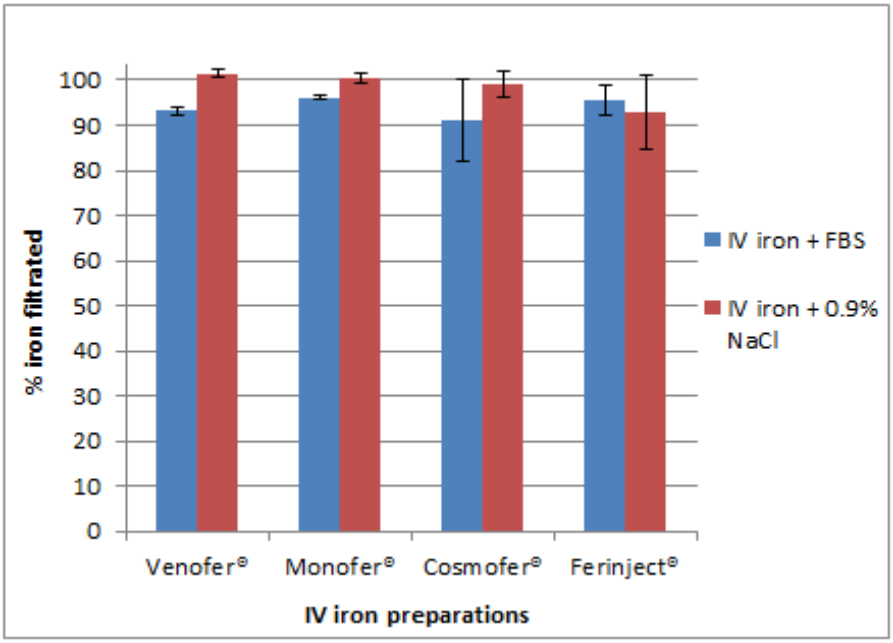

Figure 32 - % of iron filtrated of the 4 IV irons, after 1000kDa filtration by centrifugation, mimicking an undiluted administration. The red bars are the control.

At this high, but permitted concentration, the trapping of iron was only evident in Venofer® (6.79 ± 0.81%) and Monofer® (3.89 ± 0.44%) whereas Cosmofer® and Ferinject® presented large and inconclusive error bars which implicates that a repeat of the assay should be done. Additionally, the high variability obtained with Ferinject® diluted in saline does not confirm agglomeration, but, at the same time, as the IV administration strategy always requires the dilution of the preparation in saline solution immediately before drip infusion, this deviation raises some concerns about the possibility of the Ferinject® nanoparticles agglomerate in saline conditions.

One must consider that the potential agglomeration in Venofer® and Monofer® can also be due to a manifestation of the normal mode of action of the nanoparticles after administration, i.e., the agglomerated nanoparticles might have suffered the normal serum protein coating that is necessary to transport the nanoparticles to the macrophages, where they are processed. Nevertheless, even if this is true, the agglomeration seen in the calcium and phosphate solution make us believe that these percentages of trapped nanoparticles are also due to unwanted binding to serum components such as electrolytes, even not knowing if 6.79 ± 0.81% and 3.89 ± 0.44% are high enough to have a negative impact in the safety.

A second assay aimed the determination of the possible agglomeration in the serum conditions the IV iron materials would encounter if they would be first diluted in saline solution to 1000ppm of Fe and then administrated to the serum to 300 ppm of Fe. The same dilution but with saline worked as the control *(Figure 33)*. This is the most probable outcome that we would find *in vivo* as it is the most safer and ergo frequent administration strategy [65].

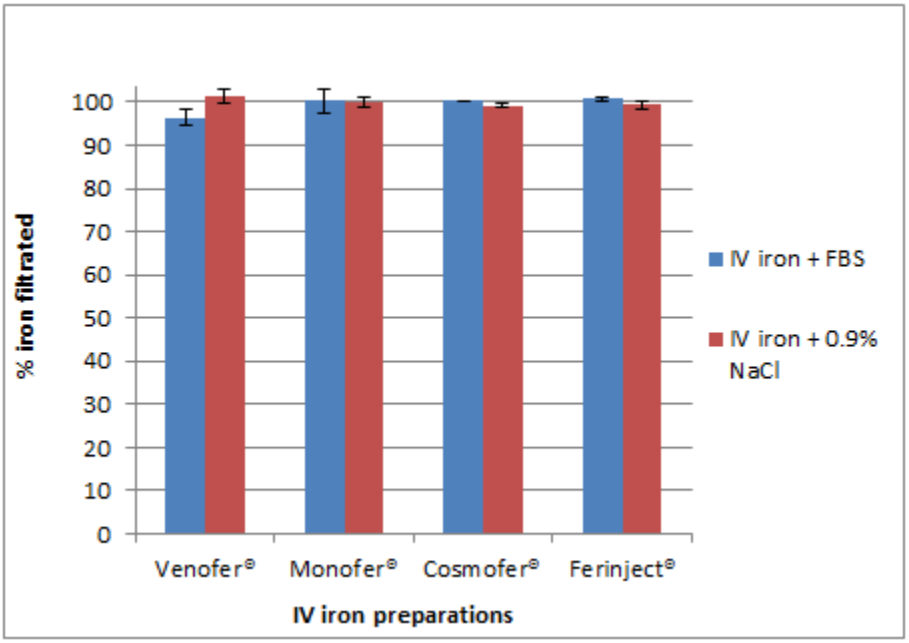

Figure 33 - % of filtrated iron of the 4 IV irons after 1000kDa filtration by centrifugation, mimicking the administration of diluted IV iron to serum. The red bars are the control.

As shown in *Figure 33*, practically all iron from Cosmofer®, Ferinject® and Monofer® passed through the filters, although Venofer® showed the highest percentage of trapped iron (3.54 ± 1.80 %) as it happened in *Figure 32*. Furthermore, the iron from Venofer® trapped in these conditions was lower, because since the saline adjusts the

osmolarity of the suspension to match the blood plasma one (280-300 mOs/kg), we would expect that 300ppm of undiluted Venofer®, typically with higher osmolarity [55], would interact more easily with the serum components, in the same period of time.

The overall results confirm Venofer® as the one with the greatest adherence to serum components, although 300 ppm of Fe would never be encountered *in vivo* after an administration of Venofer®, which proves the importance of the maximum dose of Venofer® being as low as 200 mg and the concentration of iron never exceeding 62.5 ppm (considering the volume of distribution of 3.2 L [57]). Nevertheless, the agglomeration seen at 50 ppm of Fe in the presence of calcium and phosphate confirms that Venofer® has a high affinity for serum components even in lower iron concentrations, which constitutes a concern since at both maximum and low doses, we can assume that Venofer® adsorbs unwanted serum molecules while in circulation till it is completely removed from the blood. Thus, it is conceivable that this unspecific binding to serum electrolytes and possibly to unspecific proteins might be related to some of the side effects related to Venofer®, seen in concentrations below the maximum ones after administration of the maximum dose [85]. In contrast, Monofer® agglomerated in concentrations below the maximum one permitted 533.3 ppm (considering the maximum dose of 1600 mg and its distribution volume of 3 L [69]) which indicate that this material may not be the safest and more reliable IV iron preparation [27].

The zeta potential was measured to all IV irons with 1000 ppm of iron in water at pH ~ 7.4 (*Figure 33*) to try to relate its surface charge to the adherence of the nanoparticles to serum molecules.

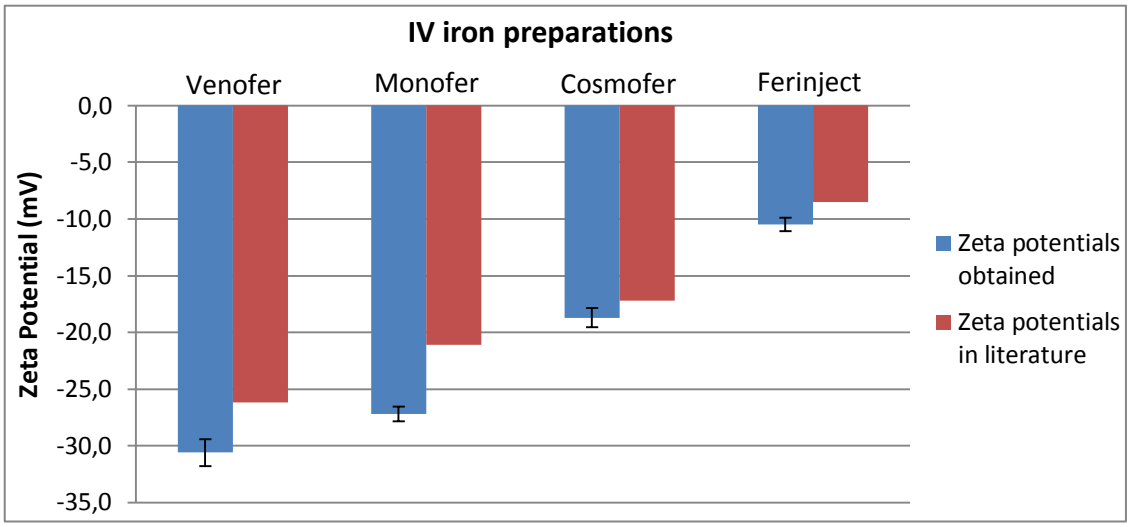

Figure 33 - Zeta Potential obtained for the four IV materials at 1000ppm of iron and pH 7.4 (blue bars). The zeta potential found in literature at similar pH is in red bars.

The 1000 ppm concentration is the lowest that we would find entering the blood stream if the IV iron (Venofer®) was diluted in 0.9% NaCl immediately before administration [62]. In these conditions, all the materials have a negative zeta potential and therefore a negative surface charge which agrees with the data in the literature. Venofer® and Monofer® have the most negative charge due to their large negative zeta potential. This might explain why these had the highest indices of agglomeration with serum, because there is evidence that highly charged nanoparticles have a much higher opsonization (coating by serum proteins) rate than neutral or slightly charged nanoparticles [121]. Although opsonization is required to transport the nanoparticles safely and directly to macrophages, this coating can also be carried out by other than the requested proteins when the conditions are suitable.

Ferinject® is widely reported to induce hypophosphatemia more frequently than the others, due to its reported natural positive charge in acidic pH [50]. But at physiological pH it showed a negative zeta potential which means that, once it is well dispersed in the blood, an electrostatic interaction with negatively charged phosphate might be weak. However, when we diluted Ferinject® to 1000 ppm and 500 ppm of Fe, in acidic pH, the measured zeta potential confirmed the positive charge, in both concentrations with less errors at 500 ppm: pH = 4.71 and zeta potential = + 6.69 ± 0.97 *(Figure 34)*. So, we can assume that Ferinject® has a positive surface charge for a short term in the blood immediately after the administration, during which it can adhere electrostatically to phosphate until the pH is normalized to physiological values. This may also explain why some reports point towards a more transient hypophosphatemia [27, 65]. Plus, maybe with increasing doses of Ferinject®, the enhanced positive charge might exacerbate the severity of the hypophosphatemia.

5.4 Lysosomal dissolution assay

After studying IV iron materials in serum conditions, we analysed them in an intracellular environment by performing a lysosomal dissolution assay. In this assay, we mimicked the conditions that nanoparticles would face after being internalized by the macrophages into the endolysosomes by subjecting the nanoparticles to pH, temperature and chelation conditions of the lysosome to stimulate the actual dissolution of the

nanoparticles by studying the variation of soluble iron with increasing time and, subsequently, determine the relative lability between IV iron products. The first thing needed to do was to find out the best pH, chelating agent and concentration of iron to allow a more efficacious dissolution and to realize which time points are the most representative of the evolution of the iron solubilisation. The best pHs to test are pH 4.5, 5.0 and 5.5 because the pH 4.5 and 5.0 are thought to be the border values of the range within which the common physiological value of lyosomal pH is maintained, that is 4.7 [122]. pH 5.5 occurs for late endosomes when they are acidified after common cellular iron uptake [2]. The most suitable chelates are citrate, isocitrate and phosphate because they are considered to enhance solubilisation of iron in lysosomal conditions [123, 124]. The concentrations selected were 0.1, 0.5 and 1 mM of iron because they allow the detection and quantification of iron concentrations by the ICP-OES in conditions where small percentages of that concentration of iron are dissolved between two time-points.

The kinetics of the evolution iron are not significant for the purpose of selecting the best pH, concentration of iron and chelating agent because we want the conditions that originate the most percentage of soluble iron to get sufficiently different percentages between the four IV irons. With these differences, we can assess their relative lability and study the dissolution kinetics at the same time.

The first experiment selected the iron concentration that yielded the higher percentage of soluble iron after 7 days with pH 5.0 and 10 mM of citrate *(Figures 34* and *35)*.

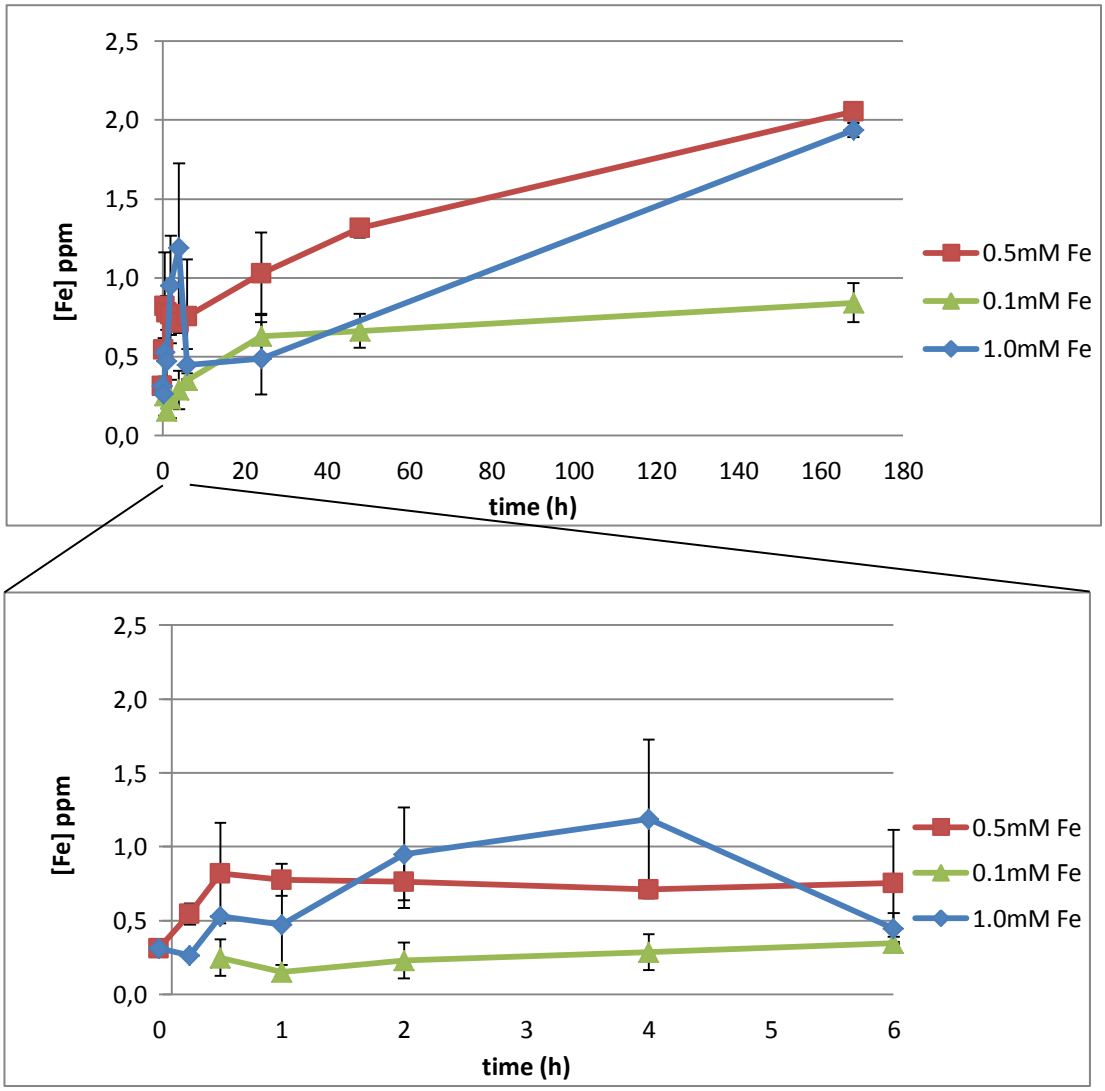

Figure 34 - Variation of the concentration of soluble iron in three different iron concentration conditions at pH 5.0 and 10mM of citrate, during the first 7 days of dissolution, for Venofer. The variation until 6h was expanded.

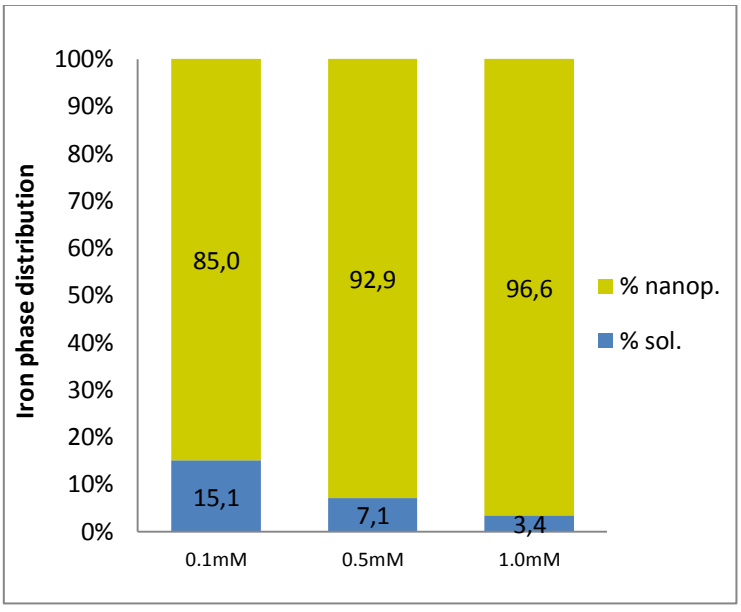

Figure 35 – Distribution of the precipitated, nanoparticulated and soluble iron fraction of Venofer, present in different iron concentrations, at pH 5.0 and 10mM of citrate, after 7 days of dissolution.

0.1 mM of Fe was preferred because although it presented the slowest release of iron and the lowest iron concentration after seven days, it showed a much higher percentage of iron in the soluble form than the other two.

Then, we selected the pH that yielded the higher percentage of soluble iron after 7 days with iron concentration of 0.1mM and 10mM of citrate *(Figure 36 and 37)*.

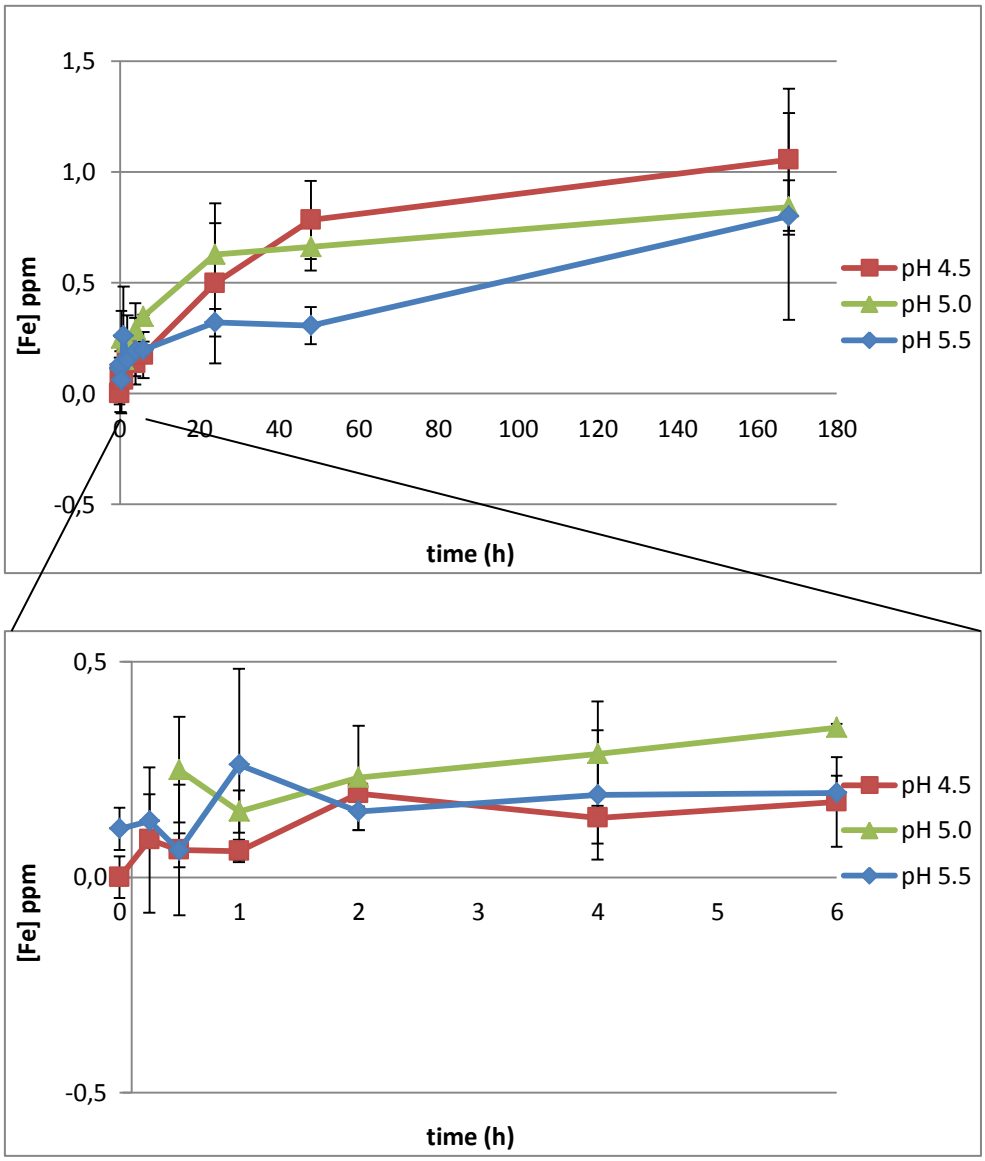

Figure 36 - Variation of the concentration of soluble iron in three different iron pH conditions at 0.1mM of Fe and 10mM of citrate, during the first 7 days of dissolution, for Venofer. The variation until 6h was expanded.

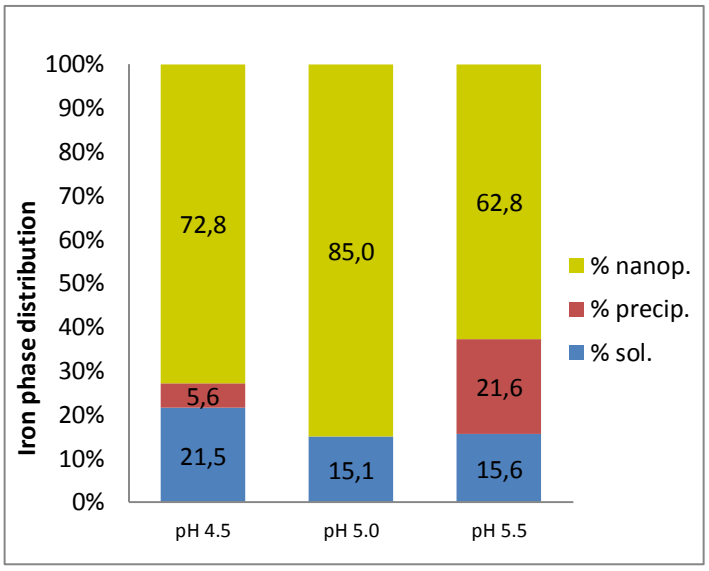

Figure 37 – Distribution of the precipitated, nanoparticulated and soluble iron fraction of Venofer, present in different pH conditions, at 0.1mM of Fe and 10mM of citrate, after 7 days of dissolution.

The pH 4.5 was preferred because not only it presented the fastest release of iron but after 7 days the concentration and percentage soluble iron was bigger than the other two.

Finally, we selected the chelating agent that yielded more percentage of soluble iron after 7 days with iron concentration of 0.1mM and pH 4.5 *(Figure 38 and 39)*.

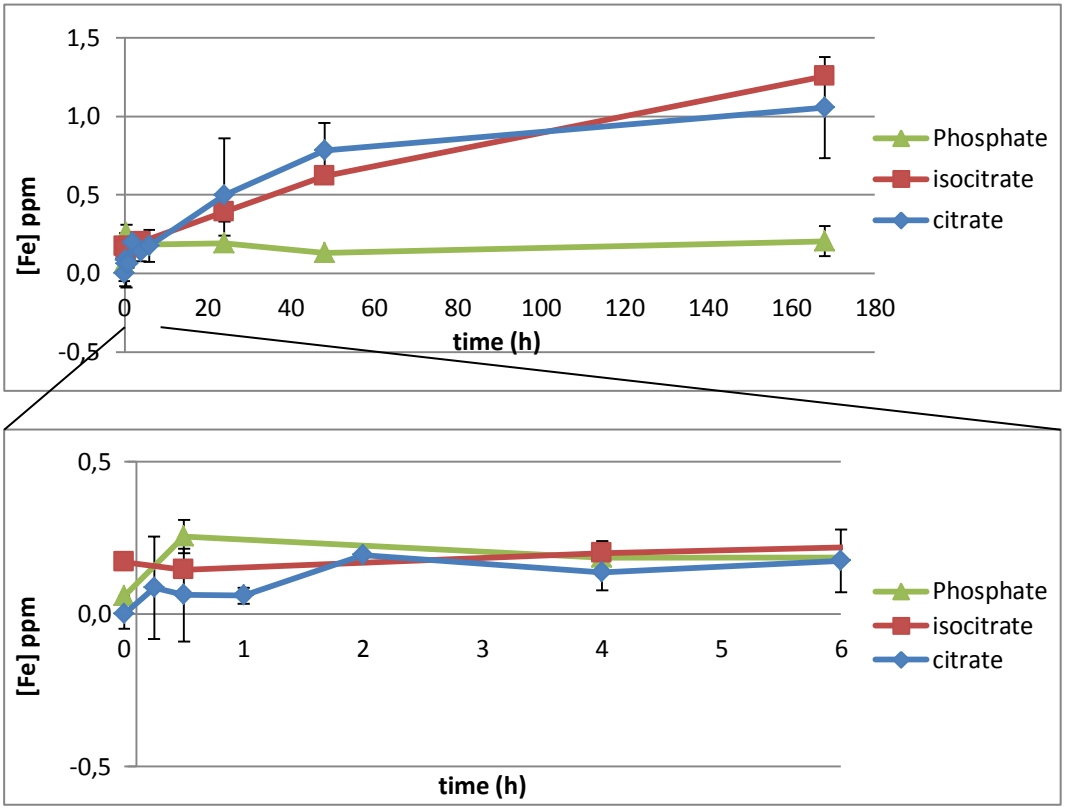

Figure 38 - Variation of the concentration of soluble iron in three different chelating agent buffers, at 0.1mM of Fe and pH 4.5, during the first 7 days of dissolution, for Venofer. The variation until 6h was expanded.

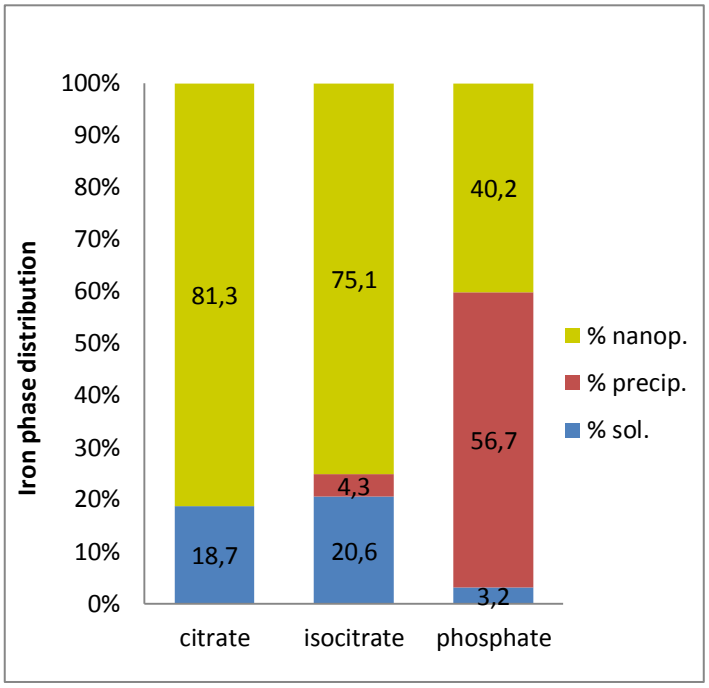

Figure 39 – Distribution of the precipitated, nanoparticulated and soluble iron fraction of Venofer, present in different chelating agents, at 0.1mM of Fe and pH 4.5, after 7 days of dissolution.

Although citrate presented the slowest release of iron and the lowest iron concentration, after seven days, the percentage of soluble iron was quite similar to isocitrate. Therefore, as citrate is much more easily available and cheaper than isocitrate, it was chosen due to its convenience.

Although we have selected the conditions that produce the highest percentage of iron after 7 days of dissolution and, at the same time, correspond to physiological conditions in the lysosome, the percentage is not high enough (< ~20%) to obtain reproducible percentages to all four IV materials. So, a more acidic dissolution was carried out at pH 2.5, 0.1 mM of iron and 10 mM of citric acid (used as the chelating agent and also to adjust initially the pH) to see if we could increase the dissolution performance *(Figure 40 and 41).* This time, two replicates were prepared independently (as well as the blanks) and the only shared step was the incubation of all the vessels in a water bath in the same conditions of temperature and stirring during the seven days of the experiment.

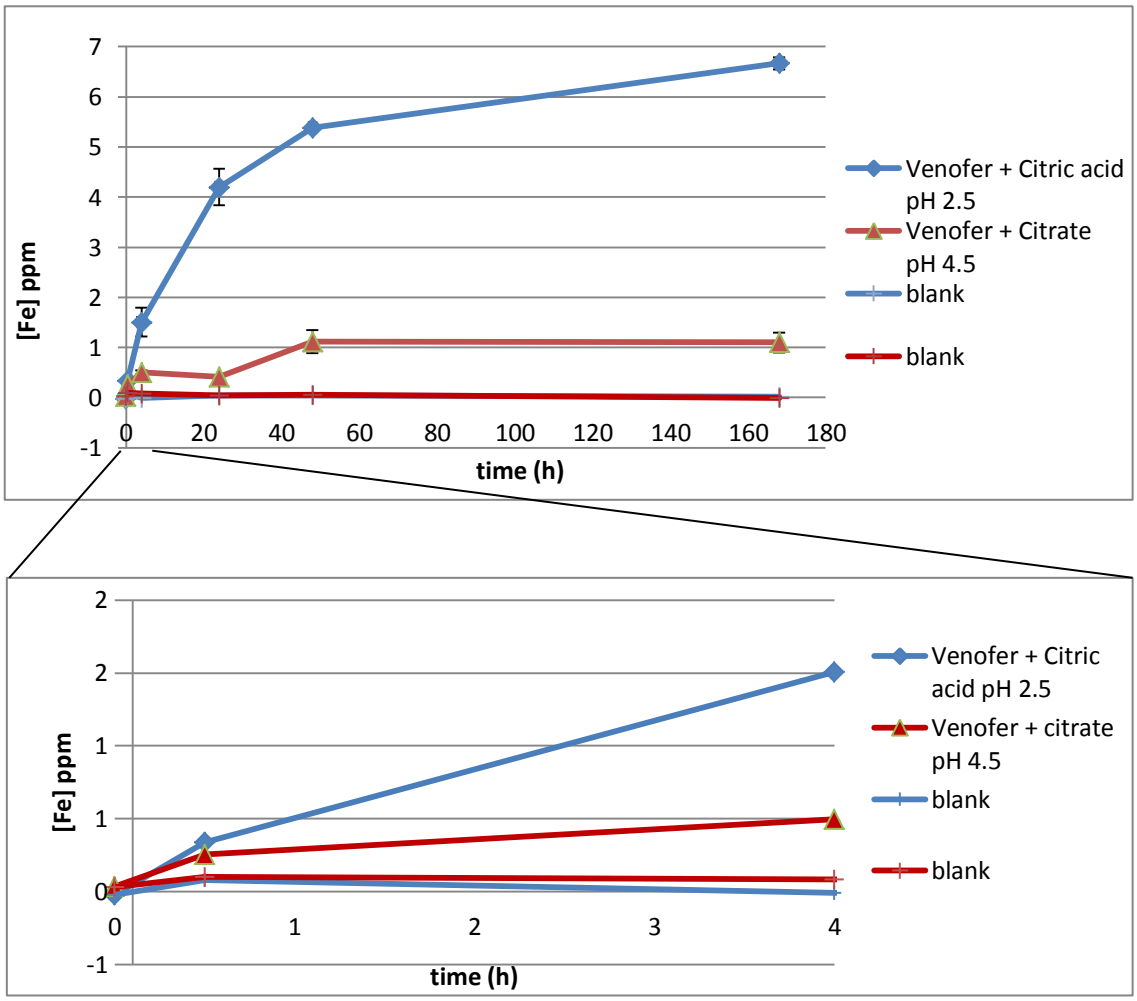

Figure 40 - Variation of the concentration of soluble iron in two pH conditions, at 0.1mM of Fe and 10mM of citrate/citric acid, during the first 7 days of dissolution, for Venofer. The variation until 4h was expanded.

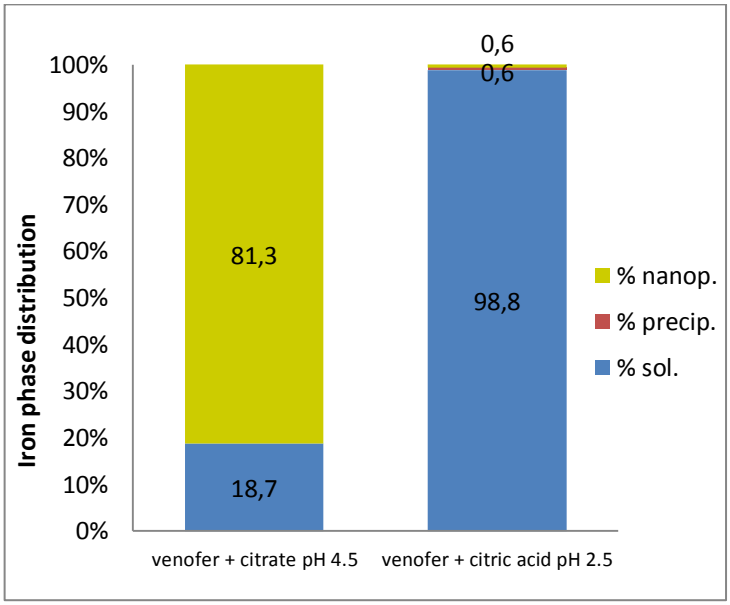

Figure 41 – Distribution of the precipitated, nanoparticulated and soluble iron fraction present in two different pH conditions at 0.1mM of Fe and 10mM of citrate/citric acid, during the first 7 days of dissolution.

The pH remained stable around 2.50 during the incubation. At this pH, the dissolution was much faster and greater than at the conditions with pH 4.5, giving 98.83% of soluble iron after seven days. So, the citric acid at pH 2.50 and the iron concentration of 0.1 mM proved to be the best experimental conditions for the dissolution of iron for a period of seven days. However, it is unknown whether the lower pH or the chelating effect is favouring the dissolution of iron, because the pH 2.50 is slightly below the first pka of citric acid (pka = 3.128) meaning that most of the citric acid is fully protonated giving a weaker chelating effect. Therefore, in a further experiment, the IV iron materials were mixed in water at pH 2.5 without chelating agent (HCl was the pH adjuster) to allow the pH effect on the dissolution of iron *(Figure 42 and 43)*. Two replicates were also prepared independently (as well as the blanks) and the only shared step was the incubation of all the vessels in a water bath in the same conditions of temperature and stirring during the seven days of the experiment. As we got more than 50% of soluble iron after 24h in the citric acid dissolution, the dissolution in water was only conducted during 24h.

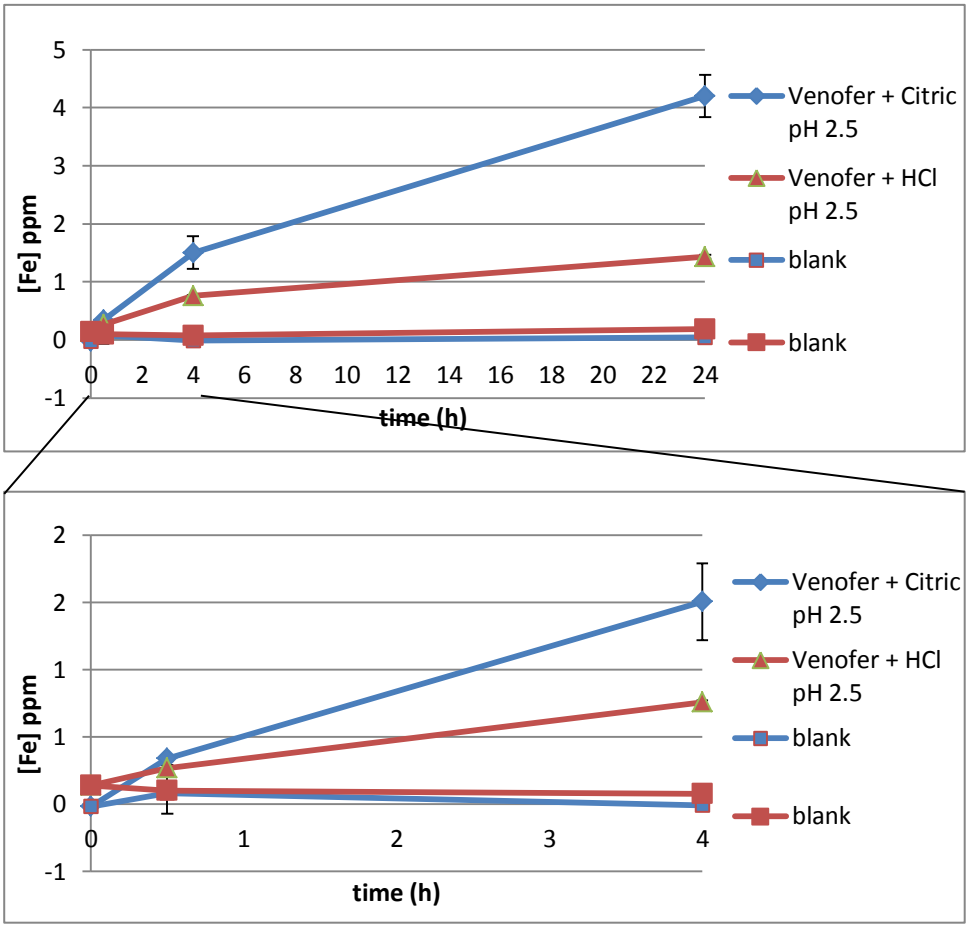

Figure 42 - Variation of the concentration of soluble iron with and without chelating agent, at 0.1mM of Fe and pH 2.5, during the first 24h of dissolution, for Venofer. The variation until 4h was expanded.

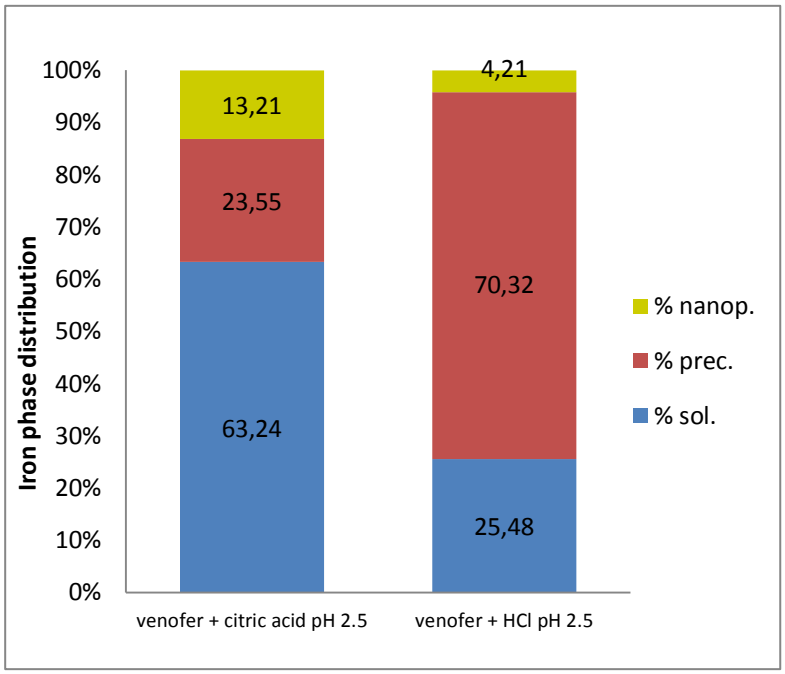

Figure 43 – Distribution of the precipitated, nanoparticulated and soluble iron fraction present with and without chelating agent, at 0.1mM of Fe and pH 2.5, during the first 24h of dissolution.

The pH was thoroughly monitored in each time-point and as HCl does not behave like a buffer, the pH slightly changed during the dissolution, so additions of NaOH to the vessels were made in two different occasions (between 0 min and 24h) due to a slight decrease of the pH. It remained stable around 2.50 after 24h of incubation. With just the pH effect, the dissolution was much slower than at the conditions with citric acid at pH 2.50, giving an average percentage of 33.36 ± 4.238 % of soluble iron after seven days. It proves that at pH 2.50, the citric acid has a substantial buffer effect and also that the 98% of soluble iron observed with the citric acid at pH 2.50, after 7 days, was mainly due to the chelating effect. This being said, we can decrease the time of the experiment and guarantee, at the same time, an appropriate soluble iron percentage. So, the experimental conditions of 0.1mM Fe, 10mM citric acid at pH 2.50 and 24h dissolution period prove to be the best ones for a reproducible dissolution to an extent that allowed a good comparison of the iron lability between all the materials.

With these conditions selected, this method was applied to all the IV irons (*Figure 44, 45 and 46).*

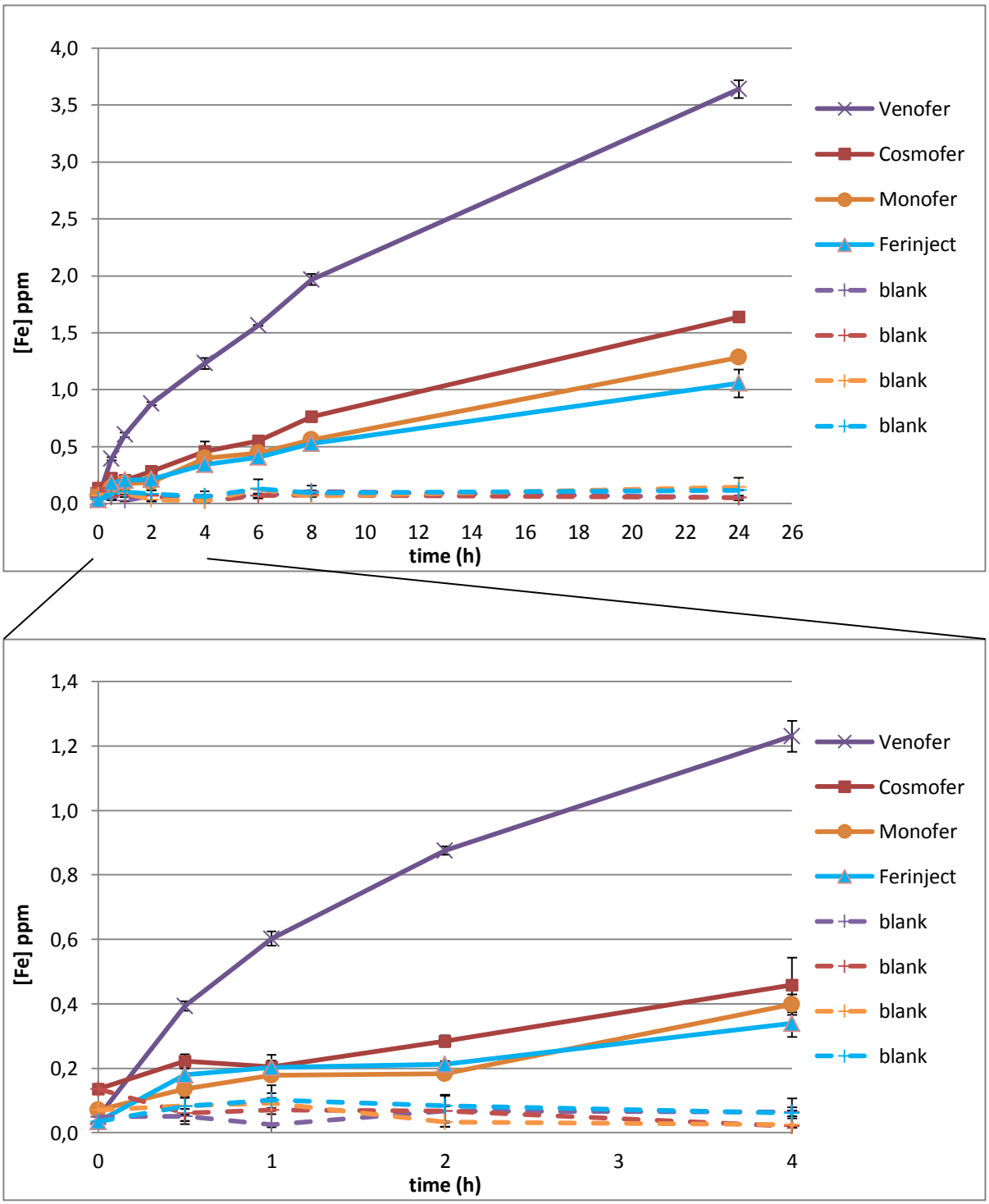

Figure 44 - Variation of the concentration of soluble iron for the four IV materials during 24h, at an iron concentration of 0.1mM, pH 2.5 and 10mM of citric acid. The variation until 4h was expanded. The dashed coloured lines lines are the respective blanks.

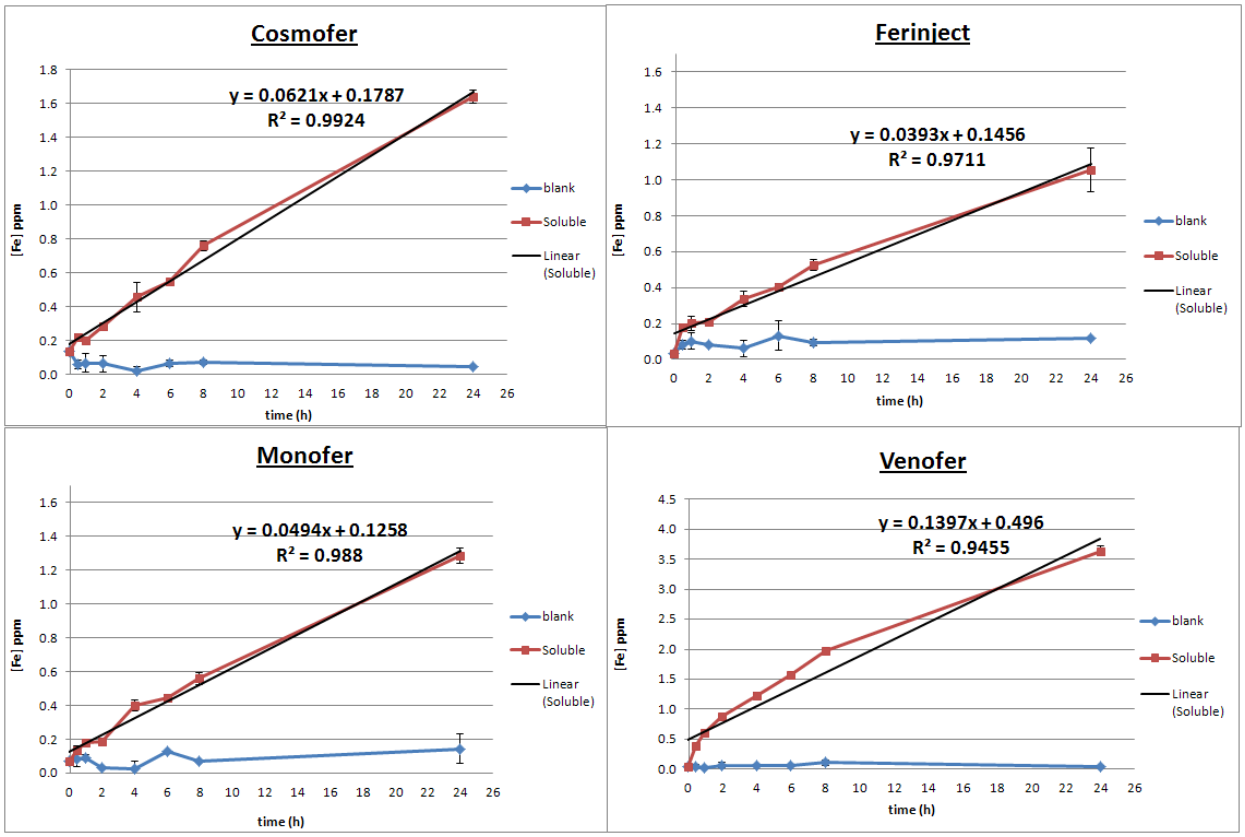

Figure 45 - Variation of the concentration of soluble iron in the four IV materials during 24h, at an iron concentration of 0.1mM, pH 2.5 and 10mM of citric acid. The linear trend was added top each graph.

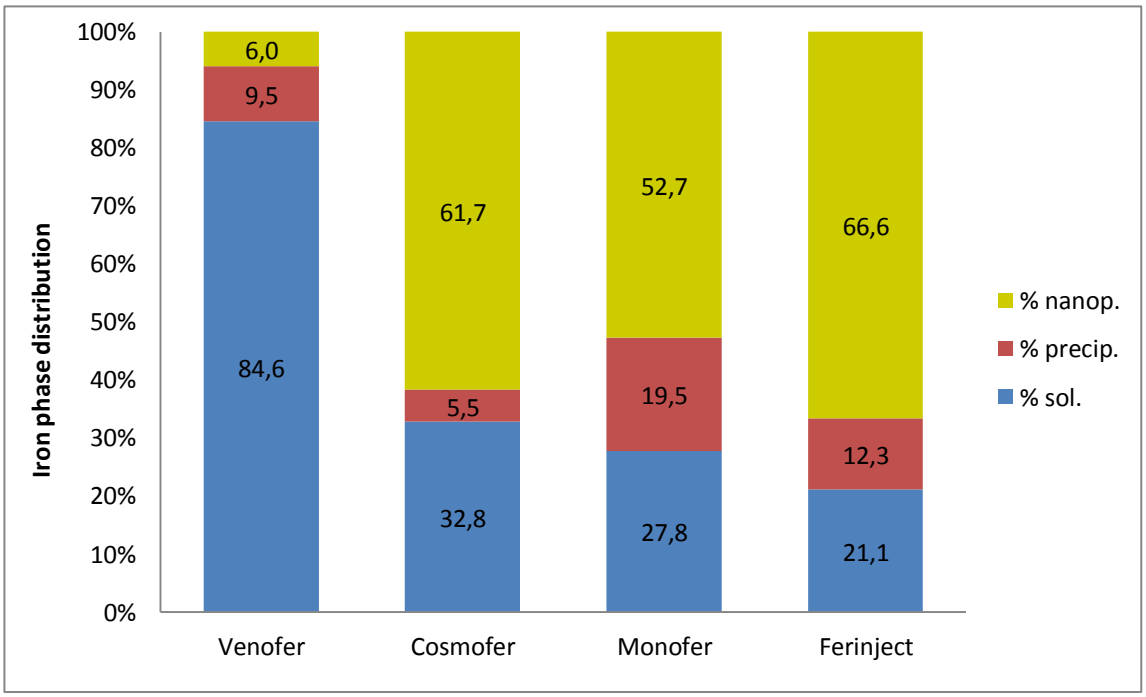

Figure 46 – Distribution of the precipitated, nanoparticulated and soluble iron fraction present in the four materials, after 24h days of dissolution, at an iron concentration of 0.1mM, pH 2.5 and 10mM of citric acid.

When we compare the four IV iron materials in terms of kinetics, Cosmofer®, Ferinject® and Monofer® resemble a linear trend line during all the experiment whereas Venofer® show a softening in the increase of soluble iron with time proved by the highest deviation of the linear trend line (lowest R, 0.9455). Nevertheless, Venofer® shows a higher rate of dissolution during 24h giving a percentage of 84.58% of soluble iron in the end, and also a higher percentage of soluble iron after 4h than the percentages of soluble iron in the other three IV iron materials at 24h. Thus, the dissolution of iron sucrose was fast enough to dissolve most of the iron which explains the slight decrease in the dissolution rate after the 8h. In Cosmofer®, Monofer® and Ferinject®, the concentration of soluble iron increased with time in a linear trend showing that the degradation of these nanoparticles and consequent solubilisation of iron is not saturable till 24h of dissolution. Just 21.07% (Ferinject®), 27.8% (Monofer®) and 32.79% (Cosmofer®) of iron was soluble after 24h, so the dissolution was not fast enough to dissolve most of the iron during this time, giving that in the experimental conditions of 0.1mM Fe, pH 2.5 and 10mM of citric acid, there is enough nanoparticulated iron during 24h to drive the dissolution of Cosmofer®, Ferinject® and Monofer® in a constant rate similar to a 0 order kinetics.

This data supports the notion of different iron core-carbohydrate shell strengths and different particle size as the driving forces to the lability of an IV iron material, as these ones differ in such aspects. Venofer® is the most labile and has the smallest nanoparticles (~8.3nm) while Ferinject® is the least labile and the one with the biggest particle size (~23.1nm). The bigger the particle, the lower is the surface area/volume ratio and the more compact and robust is the iron core ergo the material is less likely to release iron. Monofer® nanoparticles are smaller than Cosmofer® ones but they are less labile. The explanation might reside in the type of interaction between the iron core and the dextran-like carbohydrate shell, which both materials share. But while Cosmofer® has a shell of high length branched polymers surrounding the core, Monofer® has pure linear oligomers arranged in a matrix-like structure with interchanging iron molecules in a strongly bound structure that enables a controlled and slow release of bioavailable iron. This unique robust structure is remarkably core protective because Monofer® is just slightly more labile than Ferinject® and has less than half of the size of it, which makes us conclude that changing the carbohydrate structure is more relevant to alter the lability of these compounds.

As mentioned before, the dissolution profile also depends on the type mineral phase and the presence of amorphous iron increases the dissolution of a iron oxyhydroxide [125]. The 2-line ferryhidrite mineral phase has a higher surface area (225 m^2/g) than akaganeite (77.8 m^2/g) [119] and a higher disordered structure and amorphousness [118]. So, the ferrihydrite crystal structure of Venofer® might have enhanced the dissolution because more weakly bound iron was exposed to the protons in the solution. By the XRD data, we can relate the lowest dissolution performance belonging to Ferinject® with its akaganeite crystallinity and with the certain level of amorphousness observed in Cosmofer® and Monofer®. The lowest lability found in Ferinject® and Monofer® proves the high stability of the third generation materials and their capacity to greatly decrease the incidence of lability-driven anaphylactoid reactions, contrasting with the second generation IV irons such as Venofer®.

A pH driven dissolution (pH 2.5 and 0.1mM of Fe) was carried out to see if the dissolution behaviour resembled the chelating agent + pH-driven dissolution *(Figure 47 and 48)*.

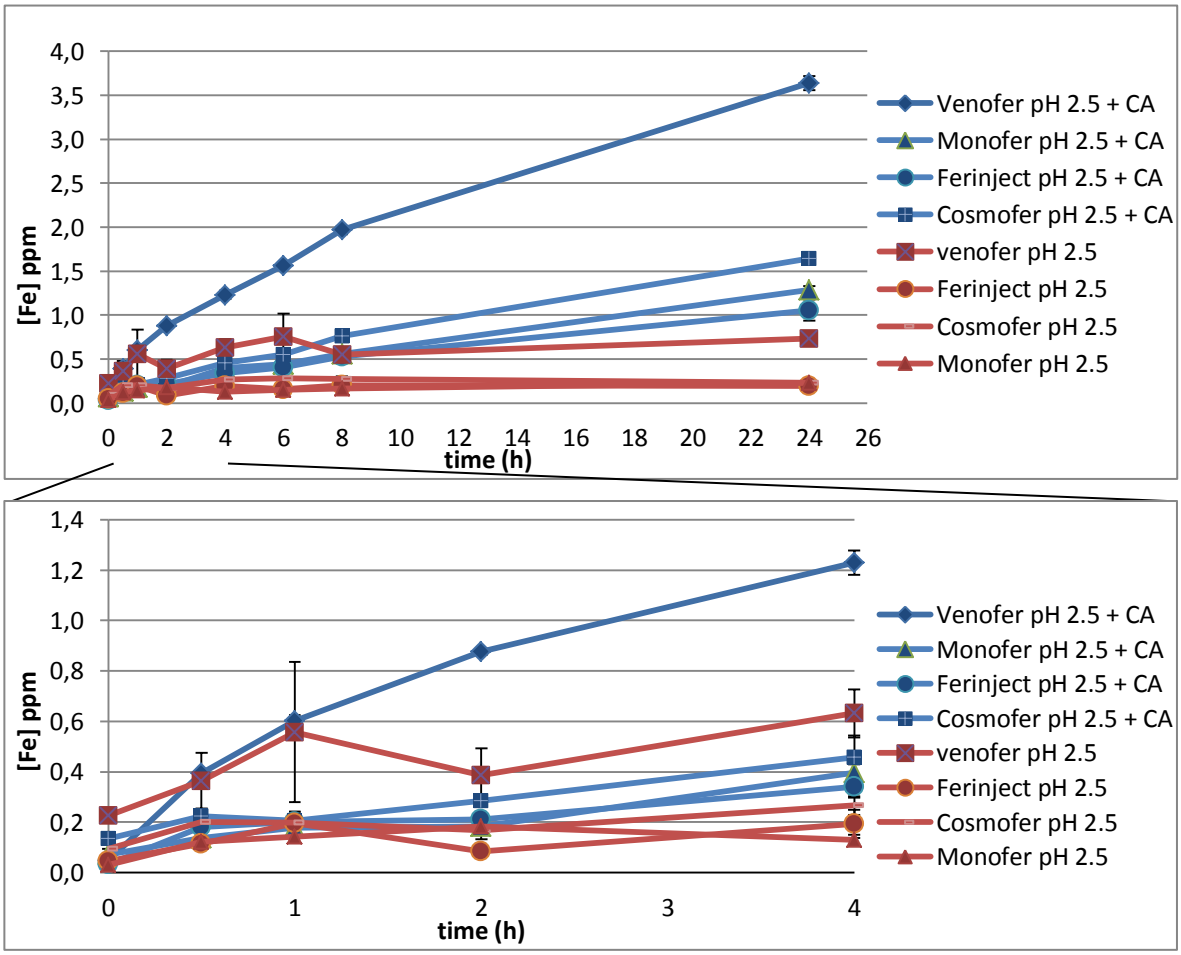

Figure 47 – Chelating agent+ pH-driven dissolution (blue lines) and the pH-driven dissolution (red lines) of the four IV materials during 24h, at an iron concentration of 0.1mM. The variation until 4h was expanded.

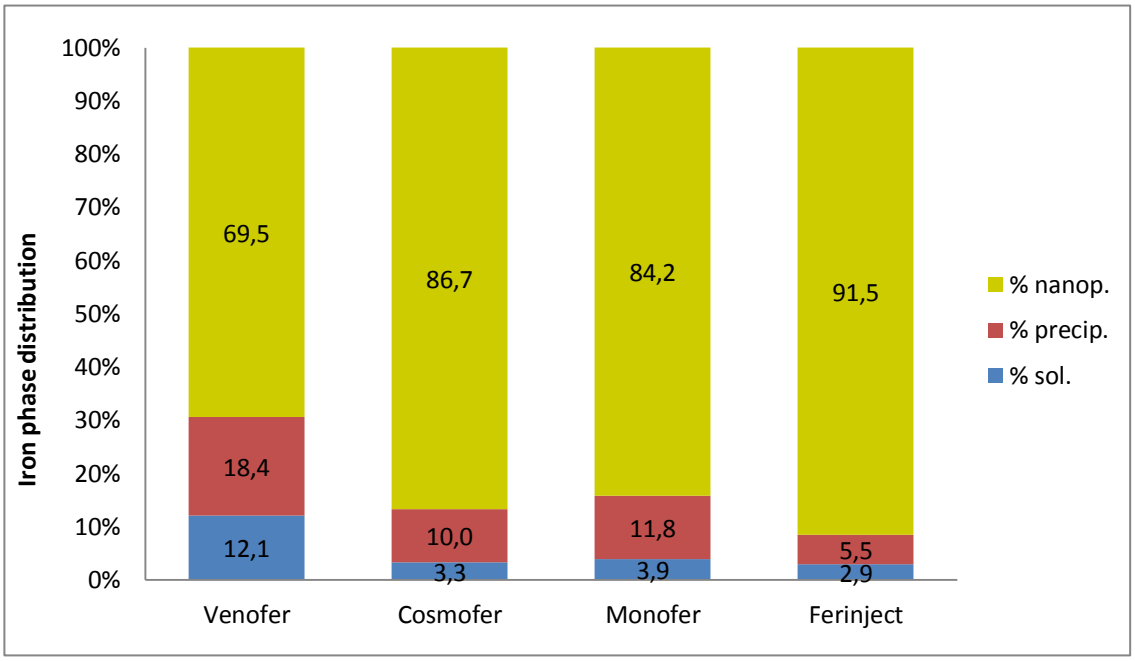

Figure 48 – Distribution of the precipitated, nanoparticulated and soluble iron fraction present in the four materials, after 24h days of pH-driven dissolution, at an iron concentration of 0.1mM and pH 2.5

If we compare the acidic dissolutions of the four IV materials, Cosmofer®, Ferinject® and Monofer® had a similar behaviour during the dissolution as they showed a poor increase of soluble iron with the tendency to stabilize with time in a way that in the end, these three materials shared similar concentration and percentages of iron. Venofer® clearly diverges from the others by showing a faster and higher increase of soluble iron with 12.1% of iron in the soluble form after 24h, even though the progression is quite unclear till 6h due to big standard deviations. The pH driven dissolution was not suitable to study and compare the behaviour of the four IV iron materials because the percentages of soluble iron found in Cosmofer®, Ferinject® and Monofer® do not diverge significantly enough to conclude about their relative lability. So, the addition of citric acid to an acidic environment still provides a more accurate dissolution with more distinguishable kinetic behaviours and, thereby, a more reliable approach to conclude about the relative labilities, also in a more physiological scenario.

To possibly obtain the same dissolution performance as the pH+chelating agent-driven dissolution but maintaining a more physiological scenario, we tried to optimize the assay by increasing the concentration of chelating agent. Two dissolutions of Venofer® were made, both at pH 4.5, 0.1mM of Fe but with 20mM and 50mM of

citrate. 20mM was assumed to be the sum of the concentrations of all the organic acids in the lysosome if we consider 10mM of citrate, whereas 50mM is the concentration of citrate in the lysosomes of the rubber tree [113] *(Figure 49 and 50).*

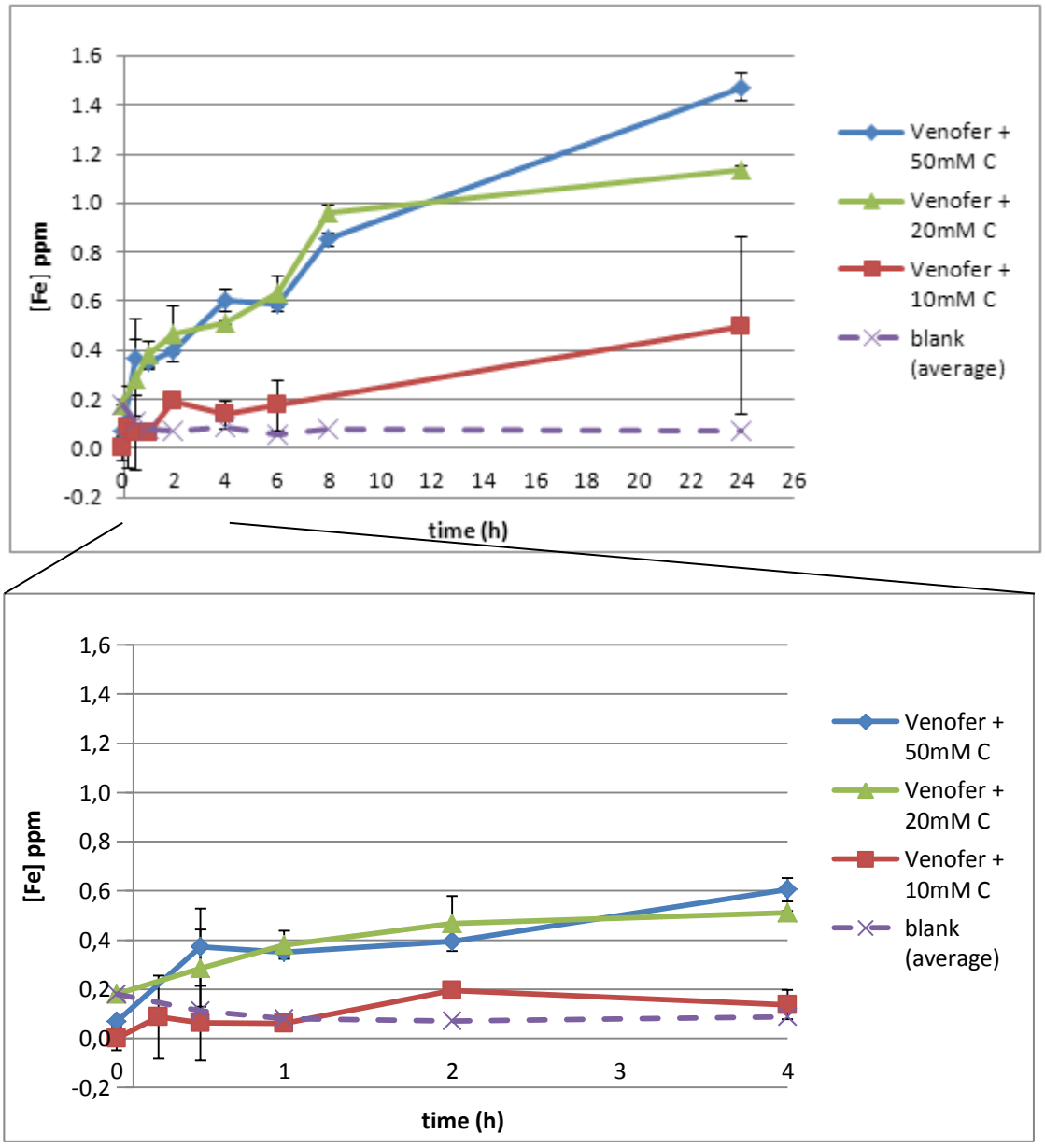

Figure 49 - Variation of the concentration of soluble iron in Venofer during 24h, at an iron concentration of 0.1mM, pH 2.5 and 10mM of citric acid. The variation until 4h was expanded.

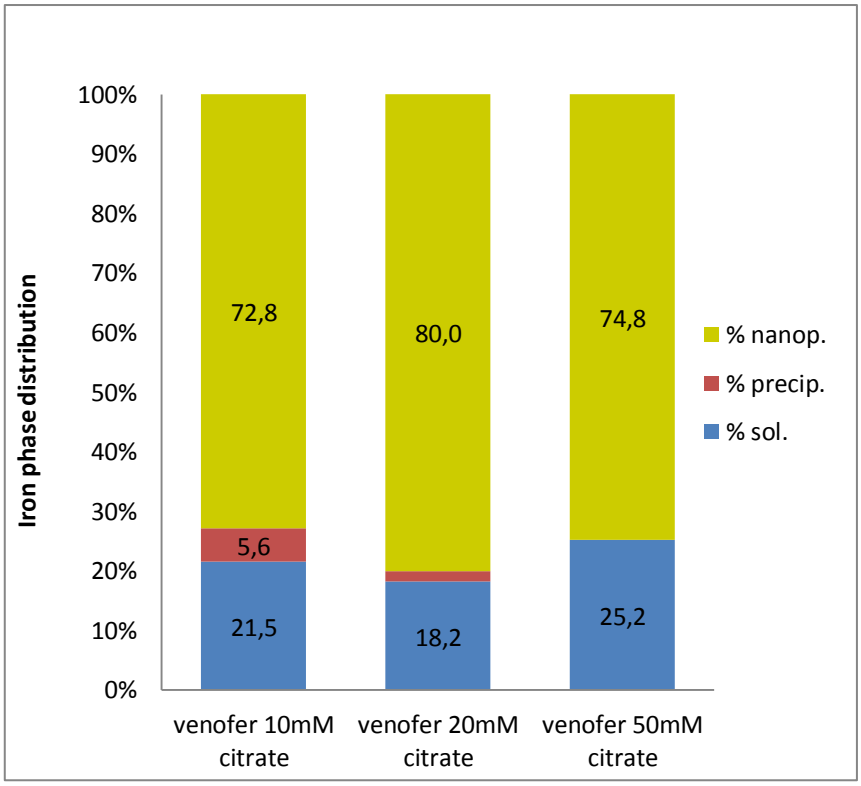

Figure 50 – Percentages of the precipitated, nanoparticulated and soluble iron fraction of Venofer, present in different citrate concentrations conditions, at 0.1mM of Fe pH 4.5, after 24h of dissolution.

During all the incubation period, the dissolution rate with 10mM of citrate was much lower compared to the other two samples. Until 8h, the dissolution with 20 mM of citrate increased the concentration of soluble iron at a similar rate as the one with 50 mM. However, between 8h and 24h, the increase of soluble iron was just 0.18 ppm for the 20 mM solution whereas in the 50 mM of citrate solution the soluble iron continued to rise at the same pace, giving an arise of 0.62 ppm. This difference makes the concentration of 50 mM of citrate the most efficient in releasing soluble iron from the nanoparticles core, with 25.2% of soluble iron after 24h. Ultimately, and based on what was mentioned before, we can assume that with 50 mM of citrate we have the most similar representation of the real dissolution kinetics of 0.1 mM of nanoparticulated iron in the macrophage lysosome, but, although the increase of the concentration of chelating agent increases the dissolution rate, at this best physiological conditions, the percentage of soluble iron is far from the extent obtained after the same period of time at pH 2.5 and 10 mM of citric acid (84.6%), which makes the intracellular mimicking conditions the less suitable to be applied to study the relative labilities between the four IV iron products.

5.5 Voltammetric analysis of ferric and ferrous content in Venofer®.

Voltammetry measurements are important not only to determine the presence of ferrous iron for its own toxicity, but also to relate its presence to the dissolution performance, because the ionic radius of Fe^{2+} (0.74 A) is larger than that of Fe^{3+} (0.64 A), so that the Fe^{2+}-O bond will be longer and weaker than the Fe^{3+}-O bond. Because the dissolution of iron oxides involves the breakdown of Fe-O bonds, the dissolution of IV iron material with ferrous content is expected to be faster [125].

As the concentrations recommended in method V-127 were as low as 20 ppm, we used differential pulse polarography as it is quite sensitive due to the detection limit being as 10^{-7} to 10^{-9} M and because it is less sensitive to changes in the experimental conditions which leads to better precision and accuracy [106].

The first scan of Venofer® showed the presence of both ferric and ferrous iron, represented by the presence of the respective peaks at around -0.9 V and -1.4 V *(Figure 51 and Table 14)*. However, the figure and the table shows a Fe^{2+} peak almost 8 times bigger (in terms of current) than the ferric one, which is in contradiction with the ferric hydroxide form present in the iron core. So, two reasons might explain this: somehow there is considerable amount of ferrous iron in the stock solution of Venofer®, or its peak is enhanced by the permanence of ferrous iron in the vicinity of the working electrode (boundary layer) after being formed by the reduction from the original ferric iron.

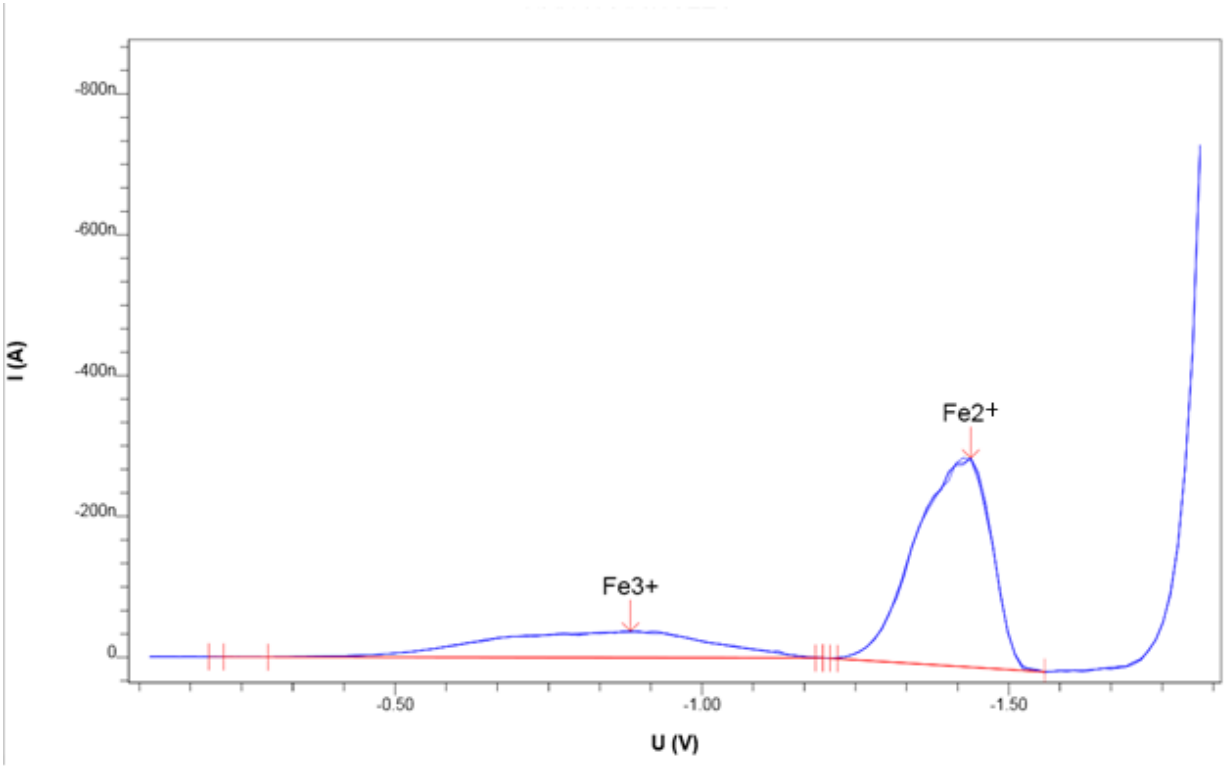

Figure 51 - Linear voltammogram of Venofer when reducing potentials are applied. The first and second peaks correspond to ferric and ferrous species, respectively. *U* is the potential applied (voltage) and *I* is the resulting current (amperes).

Table 14 - Current peak average (nA) and the correspondent average potential (V) for ferrous and ferric species.

Iron specie	Potential (V)	Current (nA)
Fe^{3+}	-0.892 ± 0.020	-37.66 ± 0.295
Fe^{2+}	-1.434 ± 0.006	-296.9 ± 0.228

As the iron core is ferric in nature and as the presence of ferrous iron in a IV iron stock solution has serious safety implications, we tested the method with ferric chloride and ferrous sulphate to determine the origin of the ferrous specie and, subsequently, if the method works *(Figure 52 and 53)*. The results showed one peak when $FeSO_4$ was added, as expected, but it showed two peaks about the same size when $FeCl_3$ was added.

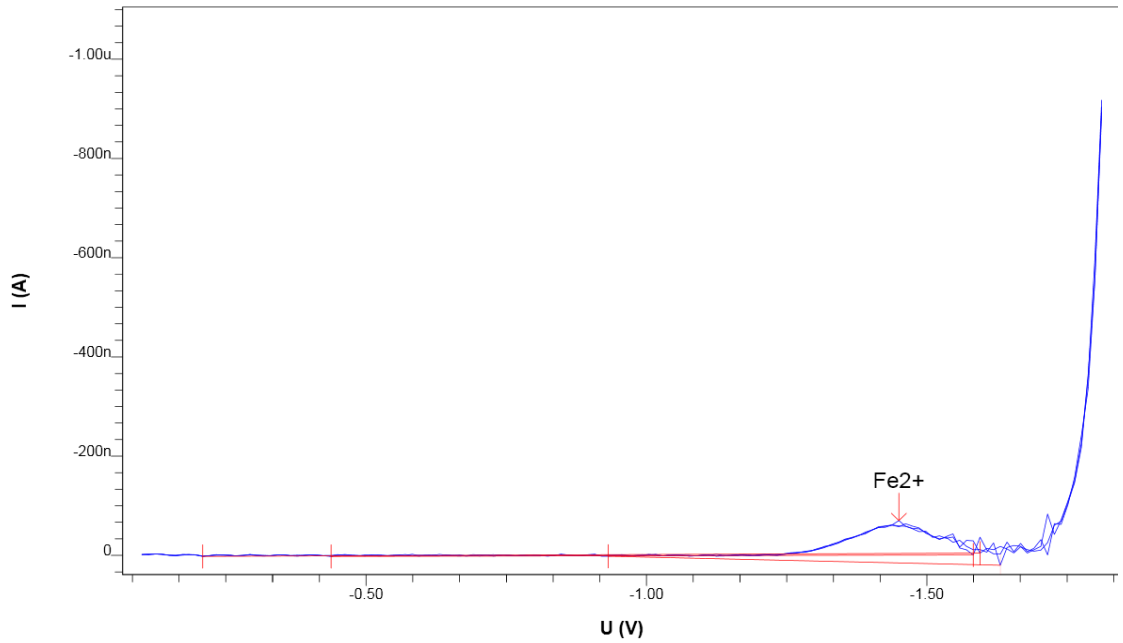

Figure 52 - Linear voltammogram of ferrous sulphate when reducing potentials are applied. The only peak corresponds to the ferrous specie. *U* is the potential applied (voltage) and *I* is the resulting current (amperes).

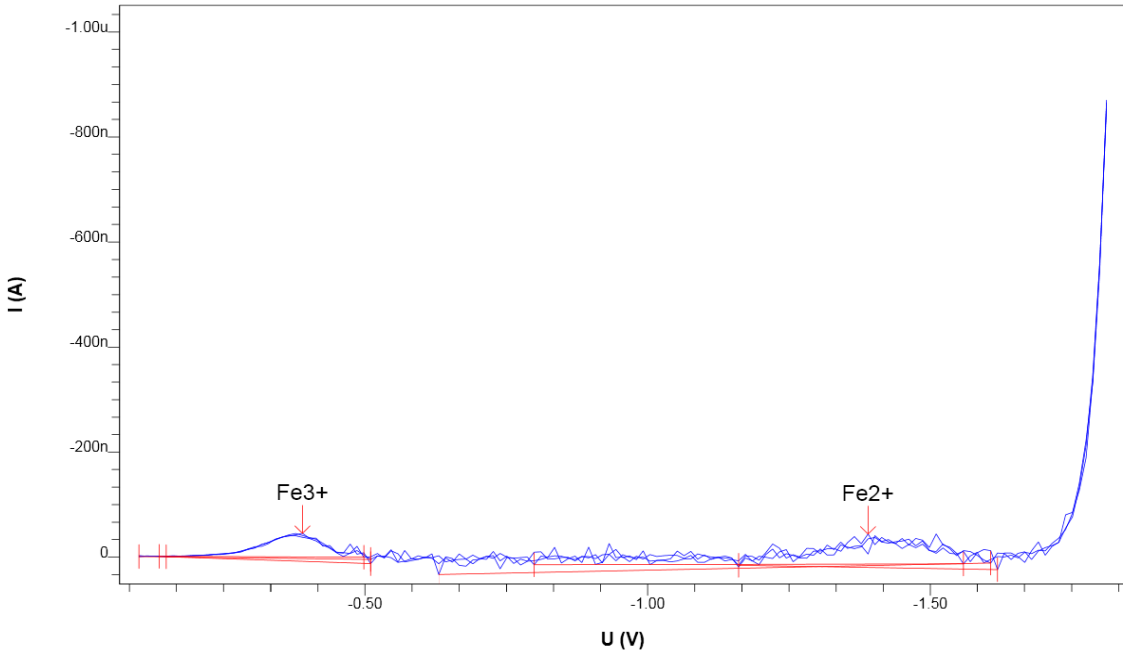

Figure 53 - Linear voltammogram of ferric chloride when reducing potentials are applied. The first and second peaks correspond to the ferric and ferrous specie, respectively. *U* is the voltage applied (voltage) and *I* is the resulting current (amperes).

These results point more towards the formation of the ferrous boundary layer as the explanation of the ferrous content in the Venofer® voltammogram. In fact, although the

dropping mercury has the ability to easily renew the surface of the working electrode by producing a new drop, the electrode is static and, thereby, the mass diffusion between the analytes at the surface of the electrode and in the solution is not carried out. Therefore, the ferrous iron produced in the electrode from the reduction of the ferric iron is not expelled to the bulk solution and it is reduced to Fe^0 at the electrode compromising the detection and quantification of the possible ferrous specie originally in the stock.

Later on, the DME was substituted by a RDE. This solid electrode mechanically stirs the solution in the vicinity of the electrode expelling the reduced products, which avoids the formation of the ferrous layer and still obtains the limiting current from potential pulses. This hydrodynamic voltammetry shows voltammograms identical to those for polarography, except for the lack of current oscillations from the growth of the mercury drops [106]. Although RDE is reported to be less sensitive than the DME, it is sensible enough to provide accurate quantifications at the concentrations used in this experiment because it can restore the sensitivity limit to that of the nearly ideal situation by overcoming the interference from electrode surface adherence or supporting electrolyte reactions to the generation of current, quite common in DME [126].

When we scanned Venofer® using the same concentrations and parameters, just one small ferric peak (around -0.550V) was shown although quite smaller than the ones normally obtained with the DME *(Figure 54 and Table 15)*.

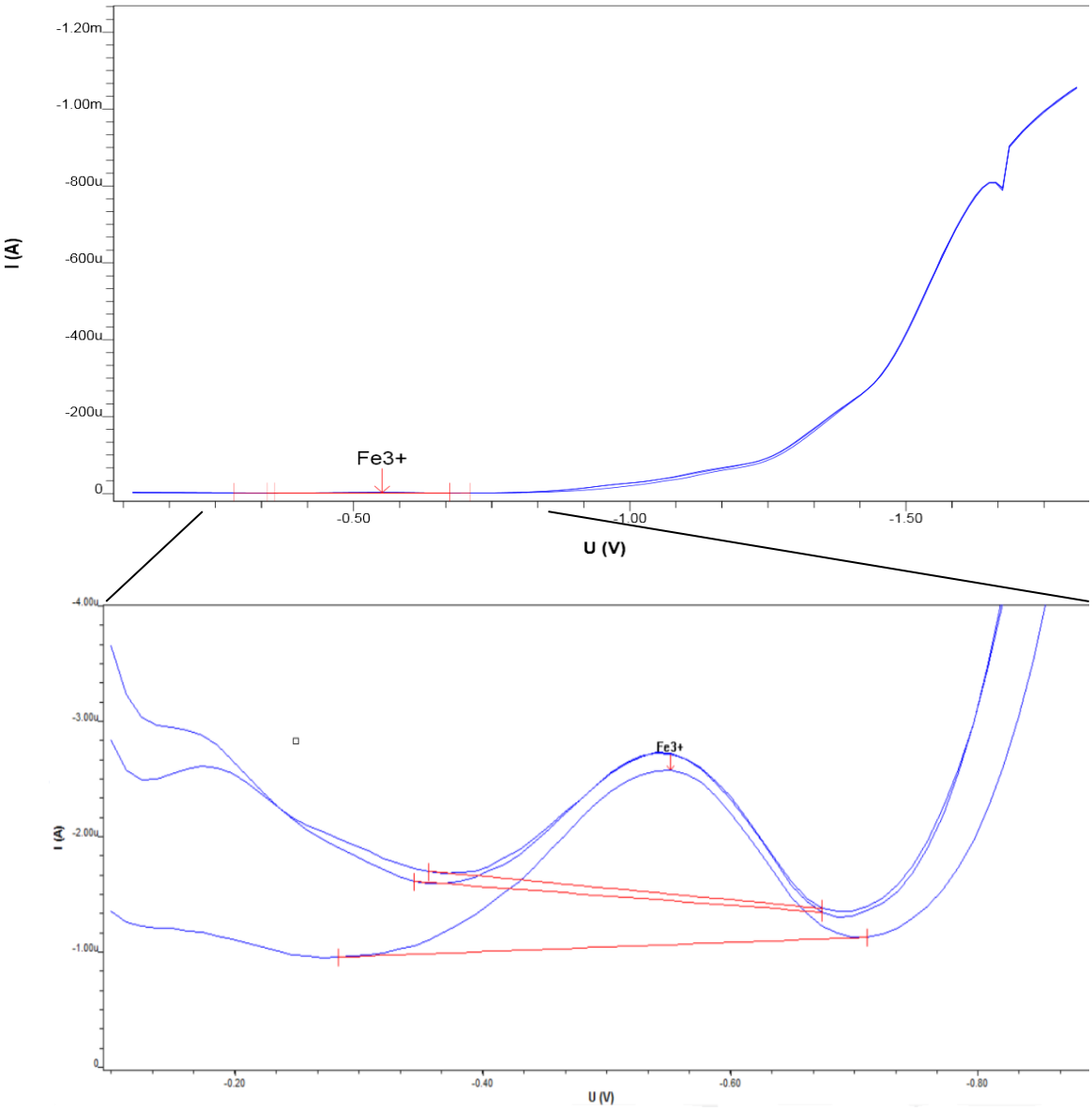

Figure 54 - Linear voltammogram of Venofer (20ppm of Fe) with the RDE as the working electrode, when reducing potentials were applied. The peak was expanded and corresponds to the ferric specie.

Table 15 - Current peak average (uA) and the correspondent average potential (V) for the ferric specie.

Iron species	Potential (V)	Current (uA)
Fe^{3+}	-0.548 ± 0.006	-1.333 ± 0.157

If we consider the results from *Figure 54* as correct, Venofer® seems to have very low soluble iron content in the stock solution, and it is all in the form of ferric iron. So, the side effects associated with Venofer® are most likely not due to the presence of ferrous iron in the stock solution, and the dissolution performance of Venofer® was not influenced by the presence of the weaker Fe^{2+}-O bounds.

The peak is, however, too small, so, to increase the reproducibility, we should have made the bulk solution richer in soluble iron to get a more evident spectrum and a realistic determination of the redox state of the iron. To do so, we could have decreased the pH or used citric acid in the electrolyte solution, based on the success of these parameters in producing soluble iron. We could have also increased the acetate concentration in the electrolytes solution because it has been proved to dissolve iron hydroxide nanoparticles [97], which is evident in the results of four consecutive voltammetry measurements effectuated to Venofer® in RDE conditions. The current peak height increased from -1.333uA A in the first measurement, to -1.417uA in the fourth one, which is an accurate manifestation of the ferric core dissolution and the consequent increase of soluble iron in the solution. This behaviour makes linear voltammetry a potential adequate method to follow the nanoparticle dissolution through time, which would become a novel and a more accurate and progressive way to assess and compare the lability of each material.

Conclusion

The high iron lability and the related anaphylactoid type reactions of Venofer® have been previously reported, and those concerns were corroborated by the dissolution assays. in the current project, which showed that Venofer®, since it has a small particle size, is by far the most labile material, confirming the need for the current practice of administrating it in small doses and as a slow push or infusion, although it can deliver iron faster to Tf, because greater doses or faster rates of administration are associated with serious anaphylactoid type reactions. Moreover, the strong evidence of agglomeration in the calcium/phosphate solution and in FBS showed that Venofer® appears to adsorbe serum compounds indicating that the sucrose contains a weak protection of the iron core, as this affinity is most likely due to the interaction between the iron core and electrolytes and not to the negative surface charge. This has serious implications regarding the safety of Venofer®, as it shows that not only its lability results from the small particle size but also to the weakness of the coating protection.

The safety concerns of Cosmofer® are mostly due to its dextran-induced anaphylaxis, however, Cosmofer® presented a degree of core amorphousness, which could have been the cause of the evidences of agglomeration in the presence of calcium and phosphate and, along with the fact that Cosmofer® was the second highest labile compound, it compromises the supposed robustness of the dextran coating, and rises questions about the adequacy of the high dosage strategy allowed.

Ferinject® presented the lowest lability profile as it has the biggest particle size. Furthermore, it was the only one to show a high level of crystallinity resembling to akaganeite, which demonstrates that not only the particle size and the strength of the carbohydrate shell-core bound are driving forces to the lability and stability of a nanoparticle and, thereby, to the safety of an IV iron material. However, its safety is deeply compromised due to the reports of hypophosphatemia. Although not fully understood, the surface positive charge obtained by the zeta potential might favour a high affinity to the free phosphate and diminish its blood levels once the material is administrated.

Monofer® showed a very low iron lability making it a robust material with a controlled and slow release of bioavailable iron while in serum, which might explain the reports of minimal free iron release. Nevertheless, it joins a robust structure to a small

particle size, explaining why it is rapidly uptaken by the macrophages, as it is characteristic of smaller nanoparticles, avoiding the potential harm associated with long-term circulation times. But, because of its robustness they will donate the iron slowly when being processed by the lysosome. So, these two properties together confer a high level of safety both in circulation and in intracellular environments, which might explain why Monofer® is the safest IV iron available and also why it has a high and fast dosage allowance with the chance of repleting the iron stores in one dose. However, the current paradigm that Monofer® may be the first-line therapy with no safety concerns should be reconsidered as its mineral phase showed high levels of amorphousness which due to its likelihood to facilitate electrostatic interactions and ligand exchange bounds, could have explained the evidences of agglomeration in the presence of serum. Therefore, there is still a need for a prospective work to perform a more thorough characterization of its affinity to serum molecules and to better understand the implications of these findings in the actual *in vivo* scenario.

Overall, Venofer®, Cosmofer®, Ferinject® and Monofer® showed different physicochemical profiles regarding the level of crystallinity of the core, the dissolution performance and consequent lability, and the agglomeration behaviour in the presence of serum or calcium/phosphate solutions. These different physicochemical profiles individualize each IV iron and strikingly demonstrates that a high crystallinity mineral phase, a negative surface charge and a strong and protective non-sucrose polymer carbohydrate shell are the key factors for a stable, safe and ergo, efficient IV iron material for the treatment of anaemia.

Future Work

To accurately assess the nanoparticle agglomeration in the presence of phosphate, we should do elemental analysis by ICP-OES of a mixture containing each IV iron material and a calcium and phosphate solution and link it with the particle sizing results. To do that, we should quantify the phosphate that was adsorbed to the nanoparticles and quantify the agglomerated iron to then relate both of them and get a more quantitative and, thereby, sensible agglomeration scenario. Equivalent serum assays should also be performed to assess the undesirable dissolution of the IV iron preparations under serum conditions that could lead to NTBI. The IV iron preparations could be exposed to citrate, albumin and acetate, instead of calcium and phosphate, as these would mimic the ideal conditions for the formation of NTBI.

A Linear voltammetry method to study the dissolution profile of an IV iron material should be developed because it will enable the direct assessment of the variation of soluble iron in real time during the dissolution and it will not be associated with the errors always associated in the preparation (i.e. pipetting, disrupted filter) and analysis (lab material contamination) of supernatant and ultrafiltrated iron samples when elemental analysis by ICP-OES is being conducted. Another, more relevant mode would be the macrophage stimulation with IV iron followed by ferritin and total protein quantification in several time-points. With the variation of ferritin concentration with time, this *in vitro* assay should represent accurately the *in vivo* dissolution profile and kinetics of each IV iron.

Bibliography

1. Papanikolaou, G., et al, *Iron metabolism and toxicity.* Toxicology and Applied Pharmacology, 2005. 202(2): p. 199-211.
2. Wang, J., et al, *Regulation of cellular iron metabolism.* Biochemical Journal, 2011. 434: p. 365-381.
3. Ganz, T., et al, *Regulation of iron acquisition and iron distribution in mammals.* Biochimica et Biophysica Acta (BBA) - Molecular Cell Research, 2006. 1763(7): p. 690-699.
4. Cook, J., et al *Iron kinetics with emphasis on iron overload.* American Journal of Pathology, 1973. 72(2): p. 337-343.
5. Muñoz, M., et al, *Disorders of iron metabolism. Part 1: molecular basis of iron homoeostasis.* Journal of Clinical Pathology, 2011. 64(4): p. 281-286.
6. Lozoff, B., et al, *Iron Deficiency and Brain Development.* Seminars in Pediatric Neurology, 2006. 13(3): p. 158-165.
7. Ahmad, I., et al, *Management of iron deficiency in patients admitted to hospital: time for a rethink of treatment principles.* Internal Medicine Journal, 2006. 36(6): p. 347-354.
8. Auerbach, M., et al, *Clinical update: intravenous iron for anaemia.* Lancet, 2007. 369(9572): p. 1502-1504.
9. Mani Tiwari, A.K., et al., *Oral iron supplementation leads to oxidative imbalance in anemic women: A prospective study.* Clinical Nutrition, 2010. 30(2): p. 188-193.
10. Trost, L., et al, *The diagnosis and treatment of iron deficiency and its potential relationship to hair loss.* Journal of the American Academy of Dermatology, 2006. 54(5): p. 824-844.
11. Andrews, N., *Disorders of Iron Metabolism.* New England Journal of Medicine, 1999. 341(26): p. 1986-1995.
12. Alastair, F., *Iron and Parenteral Nutrition.* Gastroenterology, 2009. 137(5, Supplement): p. S47-S54.
13. Macdougall, I., *Strategies for iron supplementation: oral versus intravenous.* Kidney international. Supplement, 1999. 69: p. S61-6.
14. JamesD, C., *Iron supplementation: is less better?* The Lancet, 1995. 346(8975): p. 587.
15. Gozzard, D., et al, *When is high-dose intravenous iron repletion needed? Assessing new treatment options.* Drug design, development and therapy, 2011. 5: p. 51-60.
16. Muñoz, M., et al, *Efficacy and safety of intravenous iron therapy as an alternative/adjunct to allogeneic blood transfusion.* Vox Sanguinis, 2008. 94(3): p. 172-183.
17. Auerbach, M., et al, *Clinical use of intravenous iron: administration, efficacy, and safety.* Hematology / the Education Program of the American Society of Hematology. American Society of Hematology. Education Program, 2010. 2010: p. 338-47.
18. Henry, D., et al, *Intravenous Ferric Gluconate Significantly Improves Response to Epoetin Alfa Versus Oral Iron or No Iron in Anemic Patients with Cancer Receiving Chemotherapy.* The Oncologist, 2007. 12(2): p. 231-242.
19. Practitioner, T., *Protocol for the use of IV iron sucrose - Venofer®.* 2008.
20. Reagent, A., *Venofer Prescribing Information.* American Reagent, 2011.
21. University, E., *Iron oxide nanoparticles becoming tools for brain tumor imaging and treatment.* Health & Medicine, 2010.
22. Danielson, B., *Structure, chemistry, and pharmacokinetics of intravenous iron agents.* Journal of the American Society of Nephrology, 2004. 15(12): p. S93-S98.

23. Balakrishnan, V., et al, *Physicochemical properties of ferumoxytol, a new intravenous iron preparation.* European Journal of Clinical Investigation, 2009. 39(6): p. 489-496.
24. London, E., *The molecular formula and proposed structure of the iron–dextran complex, IMFERON.* Journal of Pharmaceutical Sciences, 2004. 93(7): p. 1838-1846.
25. Lazaro, F.J., A. Larrea, and A.R. Abadía, *Magnetostructural study of iron-dextran.* Journal of Magnetism and Magnetic Materials, 2003. 257(2-3): p. 346-354.
26. Kudasheva, D., et al, *Structure of carbohydrate-bound polynuclear iron oxyhydroxide nanoparticles in parenteral materials.* Journal of Inorganic Biochemistry, 2004. 98(11): p. 1757-1769.
27. Jahn, M.R., et al, *A comparative study of the physicochemical properties of iron isomaltoside 1000 (Monofer (R)), a new intravenous iron preparation and its clinical implications.* European Journal of Pharmaceutics and Biopharmaceutics, 2011. 78(3): p. 480-491.
28. Bakoyannakis, D.N., et al., *Akaganeite and goethite-type nanocrystals: synthesis and characterization.* Microporous and Mesoporous Materials, 2003. 59(1): p. 35-42.
29. Singh, B., et al., *Chapter 8 - Applications of Synchrotron-Based X-Ray Diffraction and X-Ray Absorption Spectroscopy to the Understanding of Poorly Crystalline and Metal-Substituted Iron Oxides*, in *Developments in Soil Science*, Elsevier, 2010. p. 199-254.
30. Veiseh, O., et al, *Design and fabrication of magnetic nanoparticles for targeted drug delivery and imaging.* Advanced Drug Delivery Reviews, 2010. 62(3): p. 284-304.
31. Goncalves, C., et al., *Dextrin nanoparticles: Studies on the interaction with murine macrophages and blood clearance.* Colloids and Surfaces B-Biointerfaces, 2010. 75(2): p. 483-489.
32. Sonavane, G., et al, *Biodistribution of colloidal gold nanoparticles after intravenous administration: Effect of particle size.* Colloids and Surfaces B: Biointerfaces, 2008. 66(2): p. 274-280.
33. Skotland, T., et al, *New metal-based nanoparticles for intravenous use: requirements for clinical success with focus on medical imaging.* Nanomedicine-Nanotechnology Biology and Medicine, 2010. 6(6): p. 730-737.
34. Skotland, T., et al, *In vitro stability analyses as a model for metabolism of ferromagnetic particles (Clariscan((TM))), a contrast agent for magnetic resonance imaging.* Journal of Pharmaceutical and Biomedical Analysis, 2002. 28(2): p. 323-329.
35. Van Wyck, D., et al, *Labile iron: Manifestations and clinical implications.* Journal of the American Society of Nephrology, 2004. 15(12): p. S107-S111.
36. Dias, A.M.G.C., et al., *A biotechnological perspective on the application of iron oxide magnetic colloids modified with polysaccharides.* Biotechnology Advances, 2011. 29(1): p. 142-155.
37. Van Wyck, D., et al, *Labile iron in parenteral iron materials: a quantitative and comparative study.* Nephrology Dialysis Transplantation, 2004. 19(3): p. 561-565.
38. Agarwal, R., et al, *Transferrin saturation with intravenous irons: An in vitro study.* Kidney Int, 2004. 66(3): p. 1139-1144.
39. Schlachter, E., et al, *Metabolic pathway and distribution of superparamagnetic iron oxide nanoparticles: in vivo study.* International Journal of Nanomedicine, 2011. 6: p. 1793-1800.
40. Jahn, M.R., et al., *Iron Oxide/Hydroxide Nanoparticles with Negatively Charged Shells Show Increased Uptake in Caco-2 Cells.* Molecular Pharmaceutics, 2012.
41. Geisser, P., et al, *The Pharmacokinetics and Pharmacodynamics of Iron Preparations.* Pharmaceutics, 2011. 3(1): p. 12-33.

42. Laurent, S., et al, *Magnetic Iron Oxide Nanoparticles: Synthesis, Stabilization, Vectorization, Physicochemical Characterizations, and Biological Applications.* Chemical Reviews, 2008. 108(6): p. 2064-2110.
43. Manley, H., et al, *Determination of iron sucrose (Venofer) or iron dextran (DexFerrum) removal by hemodialysis: an in-vitro study.* BMC Nephrology, 2004. 5(1): p. 1.
44. Kletzmayr, J., et al, *High dose intravenous iron: a note of caution.* Nephrology Dialysis Transplantation, 2002. 17(6): p. 962-965.
45. Fletes, R., et al, *Suspected iron dextran-related adverse drug events in hemodialysis patients.* American Journal of Kidney Diseases, 2001. 37(4): p. 743-749.
46. Folb, P., *The Safety of Iron Dextran and a comparison with iron sucrose for intravenous use: a short report to the world health organization advisory committee on the safety of medicines.* 2004.
47. Regent, A., *Dexferrum prescribing Information.* American Regent, 2008.
48. Critchley, J., et al, *Adverse events associated with intravenous iron infusion (low-molecular-weight iron dextran and iron sucrose): a systematic review.* Transfusion Alternatives in Transfusion Medicine, 2007. 9(1): p. 8-36.
49. Pharmacosmos, *Cosmofer® Iron therapy - Product Monography.* 2007.
50. Fishbane, S., et al, *The comparative safety of intravenous iron dextran, iron saccharate, and sodium ferric gluconate.* Seminars in Dialysis, 2000. 13(6): p. 381-384.
51. Yang, Y., et al, *Thermodynamic Stability Assessment of a Colloidal Iron Drug Product: Sodium Ferric Gluconate.* Journal of Pharmaceutical Sciences, 2010. 99(1): p. 142-153.
52. Aventis, S., *Ferrlecit® Prescribing Information.* Sanofi Aventis, 2011.
53. Seligman, P., et al, *Single-dose pharmacokinetics of sodium ferric gluconate complex in iron-deficient subjects.* Pharmacotherapy, 2004. 24(5): p. 574-583.
54. Warady, B., et al, *Single-dosage pharmacokinetics of sodium ferric gluconate complex in iron-deficient pediatric hemodialysis patients.* Clinical Journal of the American Society of Nephrology, 2007. 2(6): p. 1140-1146.
55. Munoz, M., et al, *Intravenous iron in inflammatory bowel disease.* World Journal of Gastroenterology, 2009. 15(37): p. 4666-4674.
56. Maslovsky, I., *Intravenous iron in a primary-care clinic.* American Journal of Hematology, 2005. 78(4): p. 261-264.
57. Regent, A., *Venofer Prescribing Information.* American Regent, 2011.
58. Lu, M., et al, *FDA report: Ferumoxytol for intravenous iron therapy in adult patients with chronic kidney disease.* American Journal of Hematology, 2010. 85(5): p. 315-319.
59. Schwenk, M., et al, *Ferumoxytol: A New Intravenous Iron Preparation for the Treatment of Iron Deficiency Anemia in Patients with Chronic Kidney Disease.* Pharmacotherapy, 2009. 30(1): p. 70-79.
60. Provenzano, R., et al, *Ferumoxytol as an Intravenous Iron Replacement Therapy in Hemodialysis Patients.* Clinical Journal of the American Society of Nephrology, 2009. 4(2): p. 386-393.
61. Macdougall, I., et al, *Current and Upcoming Erythropoiesis-Stimulating Agents, Iron Products, and Other Novel Anemia Medications.* Advances in Chronic Kidney Disease, 2009. 16(2): p. 117-130.
62. Spinowitz, B., et al, *Ferumoxytol for Treating Iron Deficiency Anemia in CKD.* Journal of the American Society of Nephrology, 2008. 19(8): p. 1599-1605.
63. Singh, A., et al, *Safety of Ferumoxytol in Patients With Anemia and CKD.* American Journal of Kidney Diseases, 2008. 52(5): p. 907-915.
64. Pharmaceuticals, A., *Feraheme Prescribing Information.* AMAG Pharmaceuticals, 2011.
65. Administration, T.G., *Australian Public Assessment Report for Ferric Carboxymaltose.* Therapeutic Goods Administration, 2011.

66. González, Z., et al, *Intravenous iron.* Cirugia Espanhola (English Edition), 2009. 86(4): p. 196-203.
67. Pharmacosmos, *Monofer - Summary of Product Characteristics.* Pharmacosmos, 2010.
68. Philip A. Kalra, K.B., Morten Meldal, *Iron isomaltoside 1000: a new high dose option for parenteral iron therapy.* Portuguese Journal of Nephrology and Hypertension, 2012.
69. Nordfjeld, K., H. Andreasen, and L.L. Thomsen, *Pharmacokinetics of iron isomaltoside 1000 in patients with inflammatory bowel disease.* Drug Design Development and Therapy, 2012. 6: p. 43-51.
70. Muñoz, M., et al, *Disorders of iron metabolism. Part II: iron deficiency and iron overload.* Journal of Clinical Pathology, 2011. 64(4): p. 287-296.
71. Knight, B., et al, *Comparison of the core size distribution in iron dextran complexes using Massbauer spectroscopy and X-ray diffraction.* Journal of Inorganic Biochemistry, 1999. 73(4): p. 227-233.
72. Wysowski, D., et al, *Use of parenteral iron products and serious anaphylactic-type reactions.* American Journal of Hematology, 2010. 85(9): p. 650-654.
73. Practice, E., *Ferric carboxymaltose: a breakthrough treatment for iron deficiency anaemia.* Ejhp Practice, 2009. 15(5): p. 62-65.
74. Somsook, E., et al, *Interactions between iron(III) and sucrose, dextran, or starch in complexes.* Carbohydrate Polymers, 2005. 61(3): p. 281-287.
75. Newnham, E., et al, *Safety of iron polymaltose given as a total dose iron infusion.* Internal Medicine Journal, 2006. 36(10): p. 672-674.
76. Johnson, D., et al, *Oral versus intravenous iron supplementation in peritoneal dialysis patients.* Peritoneal Dialysis International, 2001. 21(Suppl 3): p. S231-S235.
77. Zanen, A., et al, *Oversaturation of transferrin after intravenous ferric gluconate (FerrlecitR) in haemodialysis patients.* Nephrology Dialysis Transplantation, 1996. 11(5): p. 820-824.
78. Aisen, P., et al, *Chemistry and biology of eukaryotic iron metabolism.* The International Journal of Biochemistry & Cell Biology, 2001. 33(10): p. 940-959.
79. Gupta, A., et al, *Treatment of iron deficiency anemia: Are monomeric iron compounds suitable for parenteral administration?* Journal of Laboratory and Clinical Medicine, 2000. 136(5): p. 371-378.
80. Liuzzi, J., et al, *Zip14 (Slc39a14) mediates non-transferrin-bound iron uptake into cells.* Proceedings of the National Academy of Sciences, 2006. 103(37): p. 13612-13617.
81. Scheiber-Mojdehkar, B., et al, *Influence of parenteral iron preparations on non-transferrin bound iron uptake, the iron regulatory protein and the expression of ferritin and the divalent metal transporter DMT-1 in HepG2 human hepatoma cells.* Biochemical Pharmacology, 2003. 65(12): p. 1973-1978.
82. Brissot, P., et al., *Non-transferrin bound iron: A key role in iron overload and iron toxicity.* Biochimica et Biophysica Acta (BBA) - General Subjects, 2012. 1820(3): p. 403-410.
83. Parkkinen, J., et al, *Catalytically active iron and bacterial growth in serum of haemodialysis patients after i.v. iron-saccharate administration.* Nephrology Dialysis Transplantation, 2000. 15(11): p. 1827-1834.
84. Deicher, R., et al, *High-dose parenteral iron sucrose depresses neutrophil intracellular killing capacity.* Kidney International, 2003. 64(2): p. 728-736.
85. Dittrich, E., et al., *Efficacy of a low-dose intravenous iron sucrose regimen in peritoneal dialysis patients.* Peritoneal Dialysis International, 2002. 22(1): p. 60-66.
86. Spinowitz, B., et al, *The safety and efficacy of ferumoxytol therapy in anemic chronic kidney disease patients.* Kidney Int, 2005. 68(4): p. 1801-1807.

87. Draeke, T., et al., *Iron Therapy, Advanced Oxidation Protein Products, and Carotid Artery Intima-Media Thickness in End-Stage Renal Disease.* Circulation, 2002. 106(17): p. 2212-2217.
88. Allen, R., et al, *Clinical efficacy and safety of IV ferric carboxymaltose (FCM) treatment of RLS: A multi-centred, placebo-controlled preliminary clinical trial.* Sleep Medicine, 2011. 12(9): p. 906-913.
89. Qunibi, W.Y., et al., *A randomized controlled trial comparing intravenous ferric carboxymaltose with oral iron for treatment of iron deficiency anaemia of non-dialysis-dependent chronic kidney disease patients.* Nephrology Dialysis Transplantation, 2011. 26(5): p. 1599-1607.
90. Wikstrom, B., et al., *Iron isomaltoside 1000: a new intravenous iron for treating iron deficiency in chronic kidney disease.* Journal of Nephrology, 2011. 24(5): p. 589-596.
91. Geisser, P., et al, *Structure, Histotoxicity and relationship of parenteral iron preparations.* Arzneimittel-Forschung/Drug Research, 1992. 42-2(12): p. 1439-1452.
92. Soenen, S., et al, *Cellular toxicity of inorganic nanoparticles: Common aspects and guidelines for improved nanotoxicity evaluation.* Nano Today, 2011. 6(5): p. 446-465.
93. Pawelczyk, E., et al., *Expression of transferrin receptor and ferritin following ferumoxides–protamine sulfate labeling of cells: implications for cellular magnetic resonance imaging.* NMR in Biomedicine, 2006. 19(5): p. 581-592.
94. Gu, J., et al., *The internalization pathway, metabolic fate and biological effect of superparamagnetic iron oxide nanoparticles in the macrophage-like RAW264.7 cell.* SCIENCE CHINA Life Sciences, 2011. 54(9): p. 793-805.
95. Arbab, A.S., et al., *A model of lysosomal metabolism of dextran coated superparamagnetic iron oxide (SPIO) nanoparticles: implications for cellular magnetic resonance imaging.* NMR in Biomedicine, 2005. 18(6): p. 383-389.
96. Simovich, J., et al, *Cellular location of proteins related to iron absorption and transport.* American Journal of Hematology, 2002. 69(3): p. 164-170.
97. Instruments, M., *Dynamic Light Scattering: An Introduction in 30 Minutes.* No year available.
98. Ltd, N., *Nanoparticle Tracking Analysis (NTA) and Dynamic Light Scattering (DLS) - a Comparison.* Nanosight Ltd, 2010.
99. Instruments, L. *Dynamic Light Scattering: Measuring the Particle Size Distribution*. 2009 [cited; Available from: http://www.lsinstruments.ch/technology/dynamic_light_scattering_dls.
100. Dalgleish, D.G., et al, *Dynamic Light-Scattering - Applications to food systems.* Food Research International, 1995. 28(3): p. 181-193.
101. Systems, P.S. *Dynamic Light Scattering*, 2012 [cited; Available from: http://pssnicomp.com/definitions/dynamic-light-scattering.
102. Instruments, M., *Zetasizer Nano Series User Manual*. 2004: Malvern Instruments.
103. Fassel, V., et al, *Inductively coupled plasma. Optical emission spectroscopy.* Analytical Chemistry, 1974. 46(13): p. 1110A-1120a.
104. Hou, X., et al, *Inductively Coupled Plasma-Optical Emission Spectrometry*, in *Encyclopedia of Analytical Chemistry*. 2006, John Wiley & Sons, Ltd.
105. Boss, C., et al *Concepts, instrumentation, and techniques in Inductively Coupled Plasma Optical Emission Spectrometry.* 1997.
106. Harvey, D., *Modern Analytical Chemistry*. 1st Edition. 2000.
107. Methrom, *VA Computrace – 8.757.1013 Software Manual* 1998.
108. M. Noel, K.I.V., *Cyclic Voltammetry and the frontiers of Electrochemistry.* 1990.
109. Scintag, *Chapter 7: Basics of X-ray Diffraction*. 1999: Scintag, Inc.
110. B.E., W., *X-Ray Diffraction.* 1990.

111. Heinrich, S.-G., *Chapter 29 - Measurement of Calcium, Phosphate and Magnesium*, in *Dynamics of Bone and Cartilage Metabolism (Second Edition)*, J.S. Markus, et al., Editors. 2006, Academic Press: Burlington. p. 487-505.
112. Gupta, A. and A.L. Crumbliss, *Treatment of iron deficiency anemia: Are monomeric iron compounds suitable for parenteral administration?* Journal of Laboratory and Clinical Medicine, 2000. 136(5): p. 371-378.
113. Marin, B., M. Marin-Lanza, and E. Komor, *The protonmotive potential difference across the vacuo-lysosomal membrane of Hevea brasiliensis (rubber tree) and its modification by a membrane-bound adenosine triphosphatase.* Biochem. J., 1981. 198(2): p. 365-372.
114. Alonzo, D., et al., *Understanding the Behavior of Amorphous Pharmaceutical Systems during Dissolution.* Pharmaceutical Research. 27(4): p. 608-618.
115. Martin, S., *Precipitation and Dissolution of Iron and Manganese Oxides*, in *Environmental Catalysis*, V.H. Grassian, Editor. 2005.
116. Genz, A., A. Kornmuller, and M. Jekel, *Advanced phosphorus removal from membrane filtrates by adsorption on activated aluminium oxide and granulated ferric hydroxide.* Water Research, 2004. 38(16): p. 3523-3530.
117. Glotch, T. and M. Kraft, *Thermal transformations of akaganeite and lepidocrocite to hematite: assessment of possible precursors to Martian crystalline hematite.* Physics and Chemistry of Minerals, 2008. 35(10): p. 569-581.
118. Cornell, R.M., *Crystal Structure*, in *The Iron Oxides: Structure, Properties, Reactions, Occurrences and Uses*. 2003, Wiley-VCH.
119. Parida, K.M., et al., *Studies on Ferric Oxide Hydroxides: III. Adsorption of Selenite (SeO^{2}_{-3}) on Different Forms of Iron Oxyhydroxides.* Journal of Colloid and Interface Science, 1997. 185(2): p. 355-362.
120. Chitrakar, R., et al., *Phosphate adsorption on synthetic goethite and akaganeite.* Journal of Colloid and Interface Science, 2006. 298(2): p. 602-608.
121. Xiao, K., et al., *The effect of surface charge on in vivo biodistribution of PEG-oligocholic acid based micellar nanoparticles.* Biomaterials. 32(13): p. 3435-3446.
122. Myers, B.M., et al., *Alterations in the structure, physicochemical properties, and pH of hepatocyte lysosomes in experimental iron overload.* The Journal of Clinical Investigation, 1991. 88(4): p. 1207-1215.
123. Skotland, T., P.C. Sontum, and I. Oulie, *In vitro stability analyses as a model for metabolism of ferromagnetic particles (Clariscan((TM))), a contrast agent for magnetic resonance imaging.* Journal of Pharmaceutical and Biomedical Analysis, 2002. 28(2): p. 323-329.
124. Gu, J.L., et al., *The internalization pathway, metabolic fate and biological effect of superparamagnetic iron oxide nanoparticles in the macrophage-like RAW264.7 cell.* Science China-Life Sciences, 2011. 54(9): p. 793-805.
125. Sidhu, P.S., et al., *Dissolution of iron oxides and oxyhydroxides in hydrochloric and perchloric acids.* Clays and Clay Minerals, 1981. 29(6): p. 269-276.
126. Miller, B., Bruckenstein, S., *Submicromolar Analysis with Rotating and Hydrodynamically Modulated Disk Electrodes.* Analytical Chemistry, 1974. 46(13).

Appendix

XRD spectrums of Dextran 1000kDa polymers, Dextran 5000kDa and sucrose:

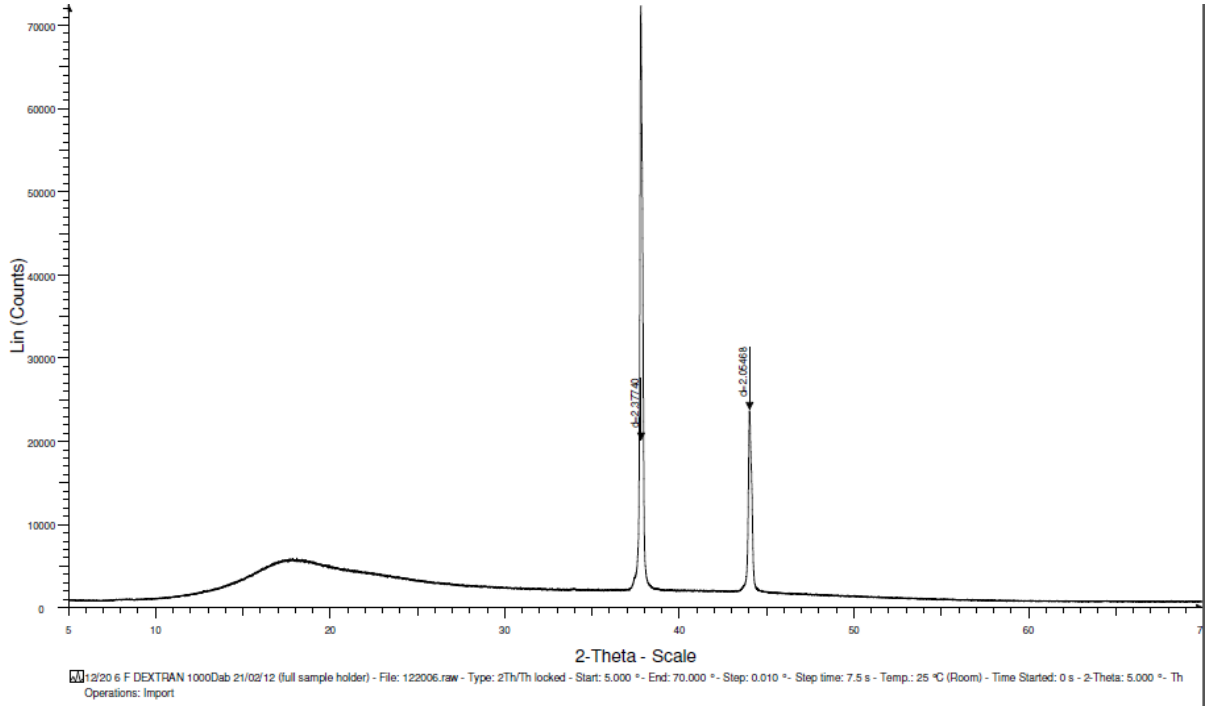

Figure 55 - XRD characterization of Dextran 1000kDa.

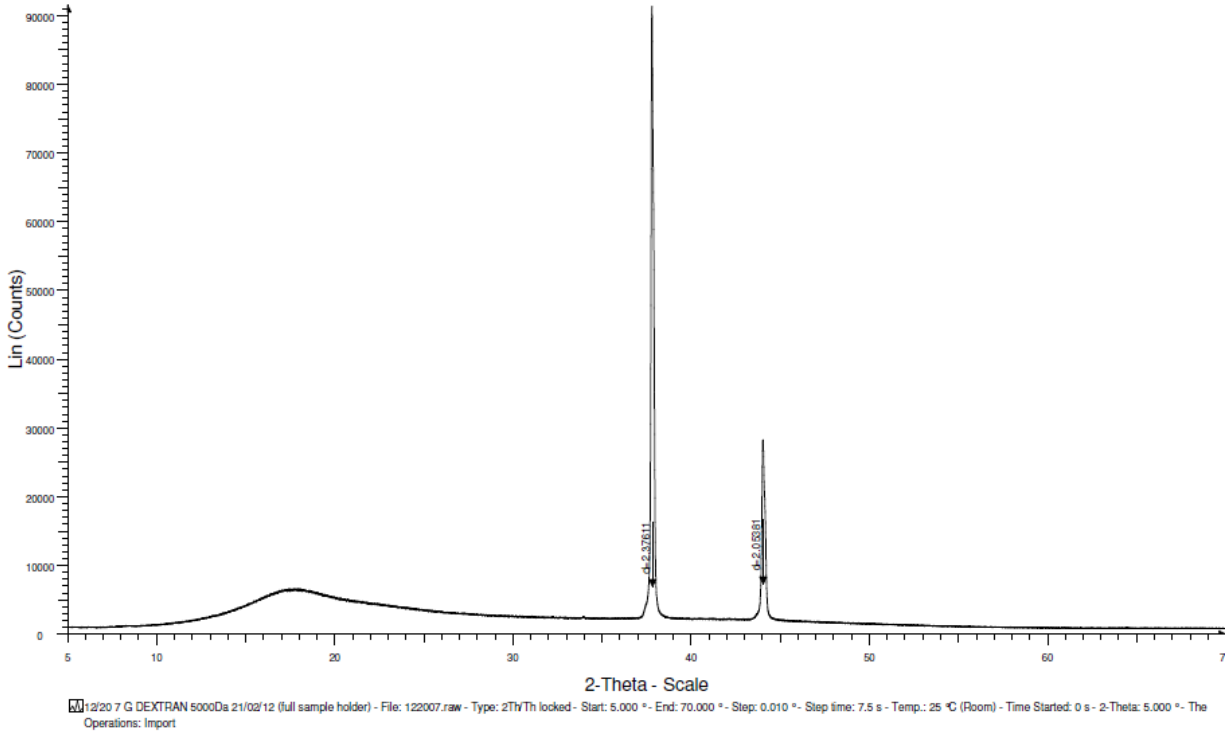

Figure 56 - XRD characterization of Dextran 5000kDa.

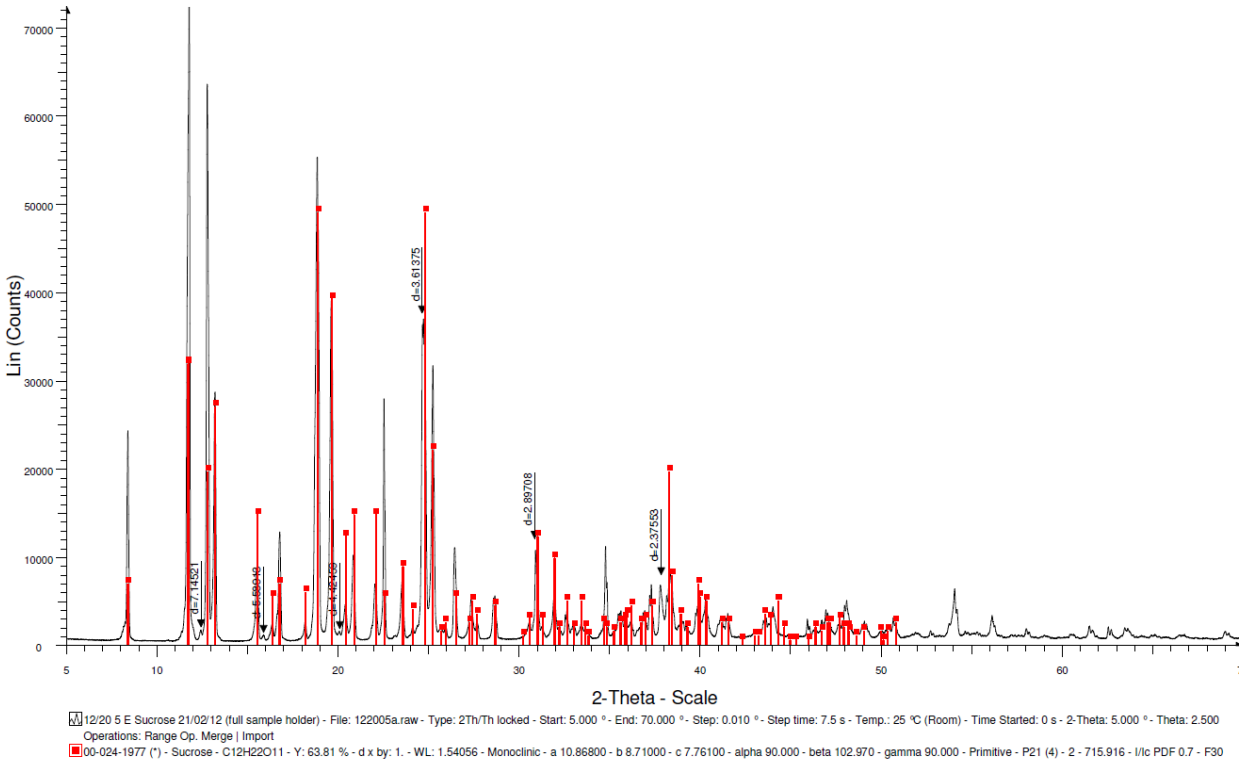

Figure 57 - XRD characterization of Dextran 5000kDa.

The statistic graphs of the particle sizing obtained for Venofer®, Cosmofer® Ferinject® and Monofer® diluted in water (50mg/mL of Fe):

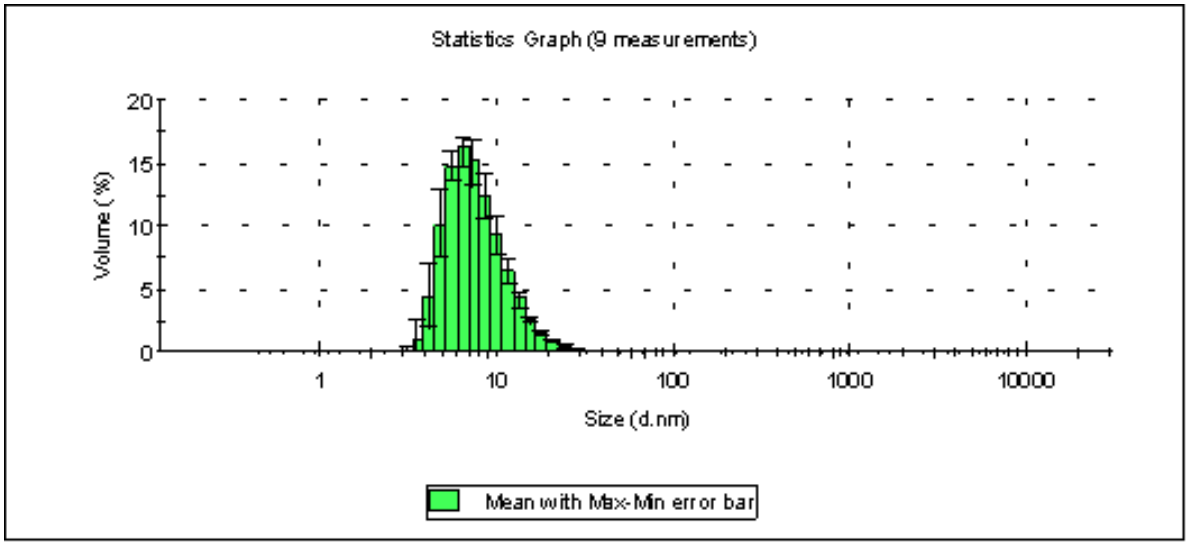

Figure 58 - Statistics graph of the size distribution by volume of Venofer® 50mg/L of iron. Total of nine measurements.

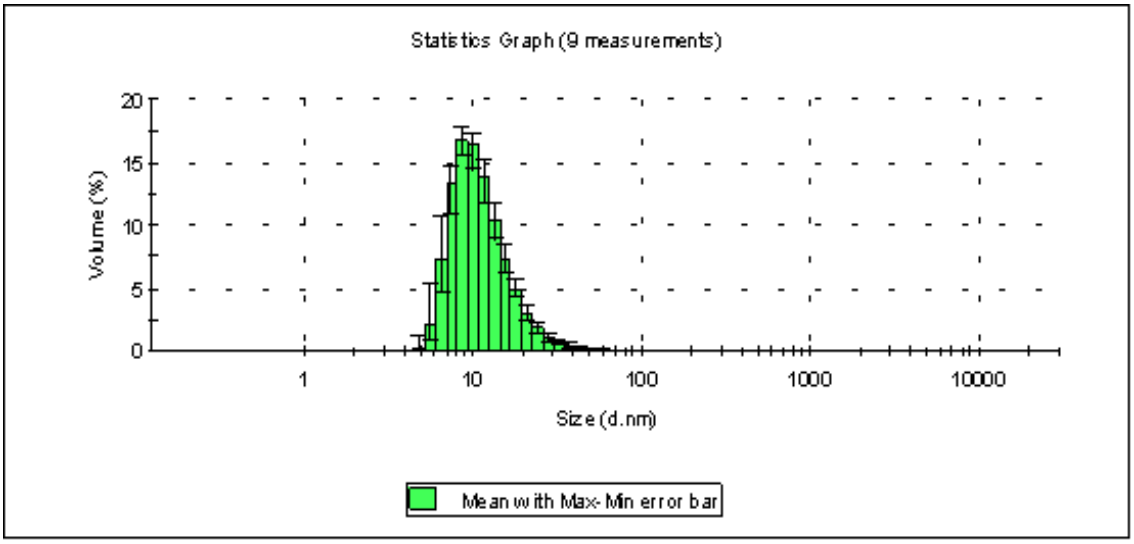

Figure 59 - Statistics graph of the size distribution by volume of Cosmofer® 50mg/L of iron. Total of nine measurements.

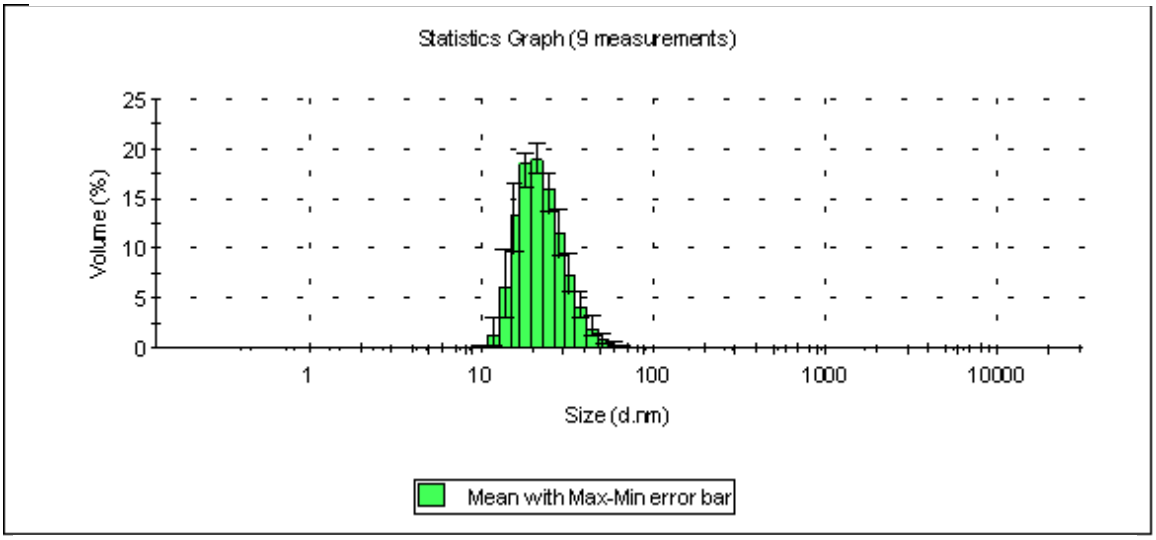

Figure 60 - Statistics graph of the size distribution by volume of Ferinject® 50mg/L of iron. Total of nine measurements.

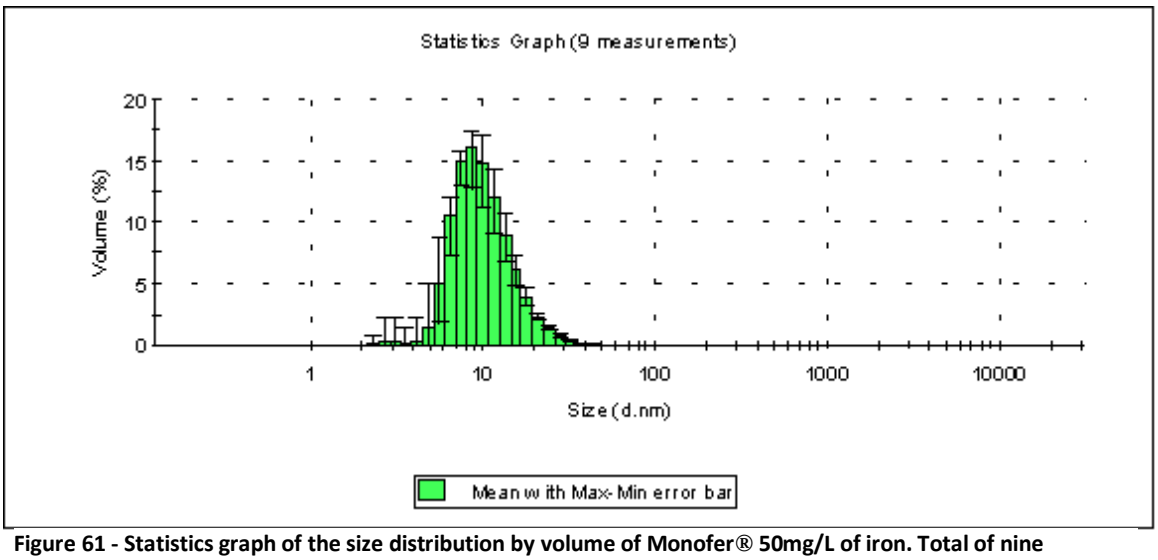

Figure 61 - Statistics graph of the size distribution by volume of Monofer® 50mg/L of iron. Total of nine measurements.

The graphs of the Size distribution by volume obtained for Venofer®, Cosmofer® Ferinject® and Monofer® diluted in the calcium and phosphate solution (50mg/mL of Fe):

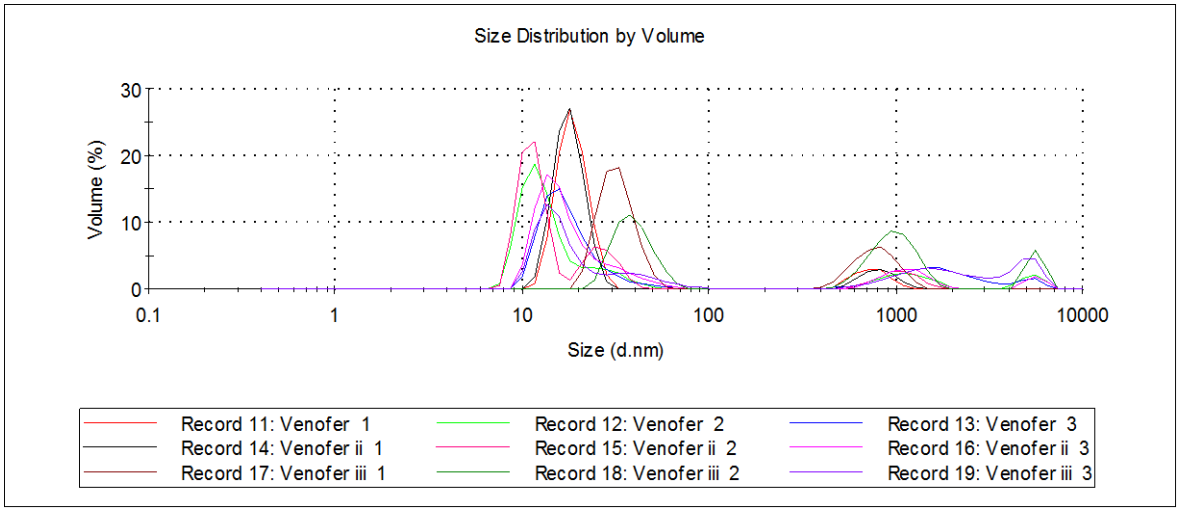

Figure 62 - Size distribution by volume of Venofer® diluted with the calcium and phosphate solution (50mg/L of iron). Total of nine measurements.

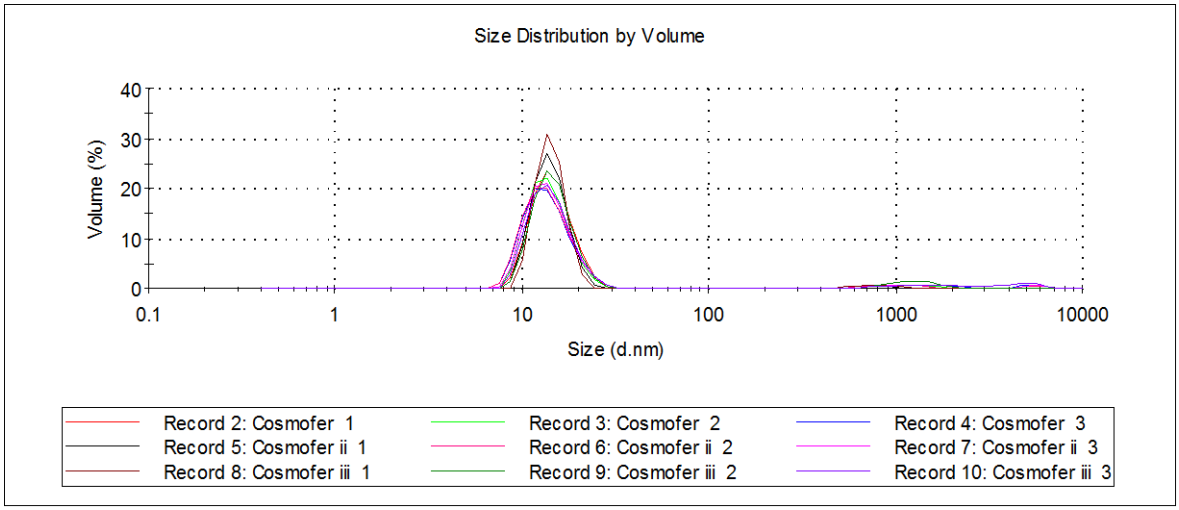

Figure 63 - Size distribution by volume of Cosmofer® diluted with the calcium and phosphate solution (50mg/L of iron). Total of nine measurements.

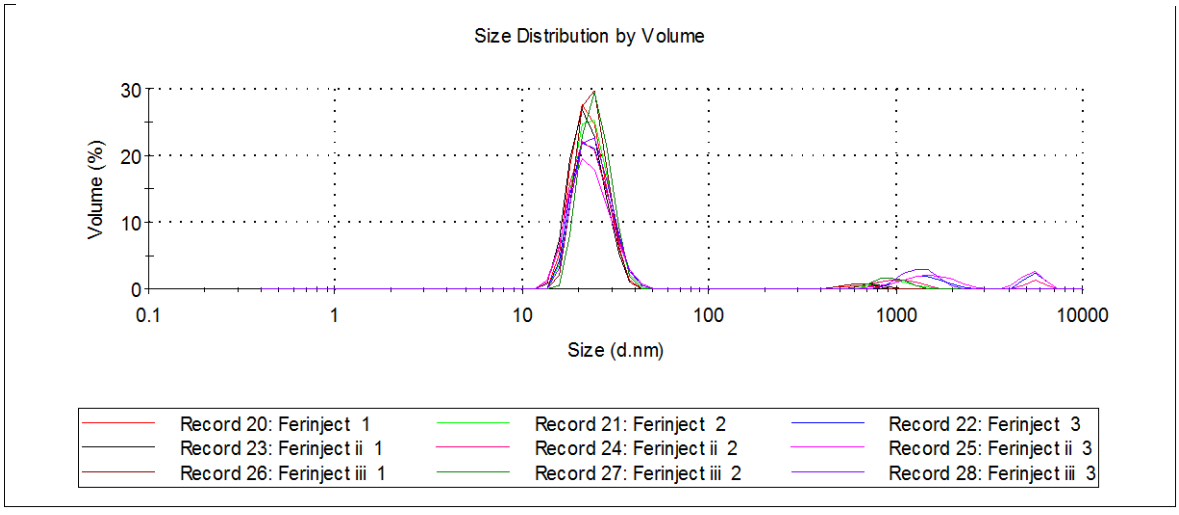

Figure 64 - Size distribution by volume of Ferinject® diluted with the calcium and phosphate solution (50mg/L of iron). Total of nine measurements.

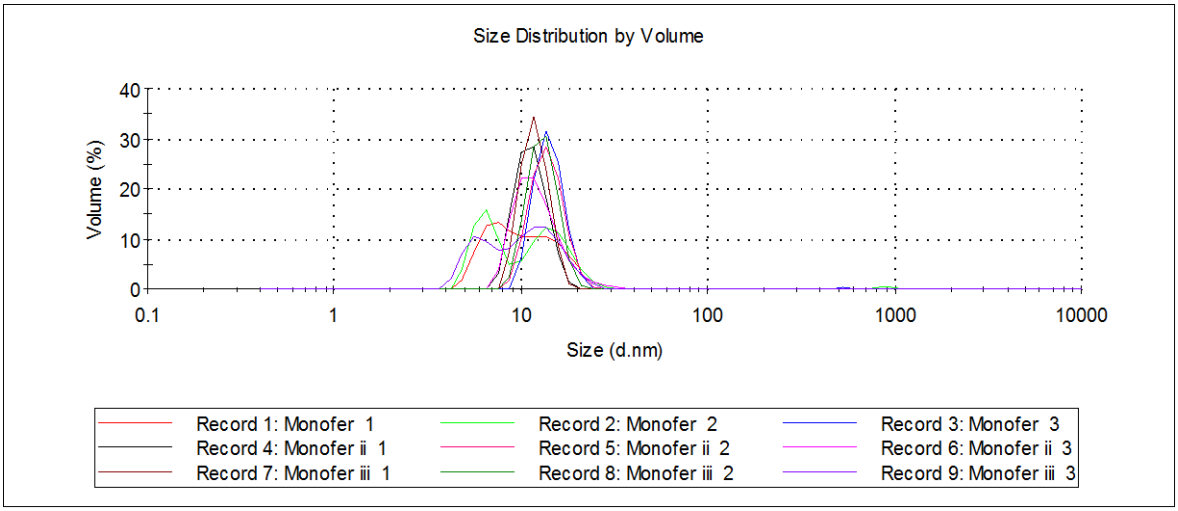

Figure 65 - Size distribution by volume of Monofer® diluted with the calcium and phosphate solution (50mg/L of iron). Total of nine measurements.

The statistic graphs of the zeta potential obtained for Venofer®, Cosmofer® Ferinject® and Monofer® (1000ppm of Fe) at pH ~7.35:

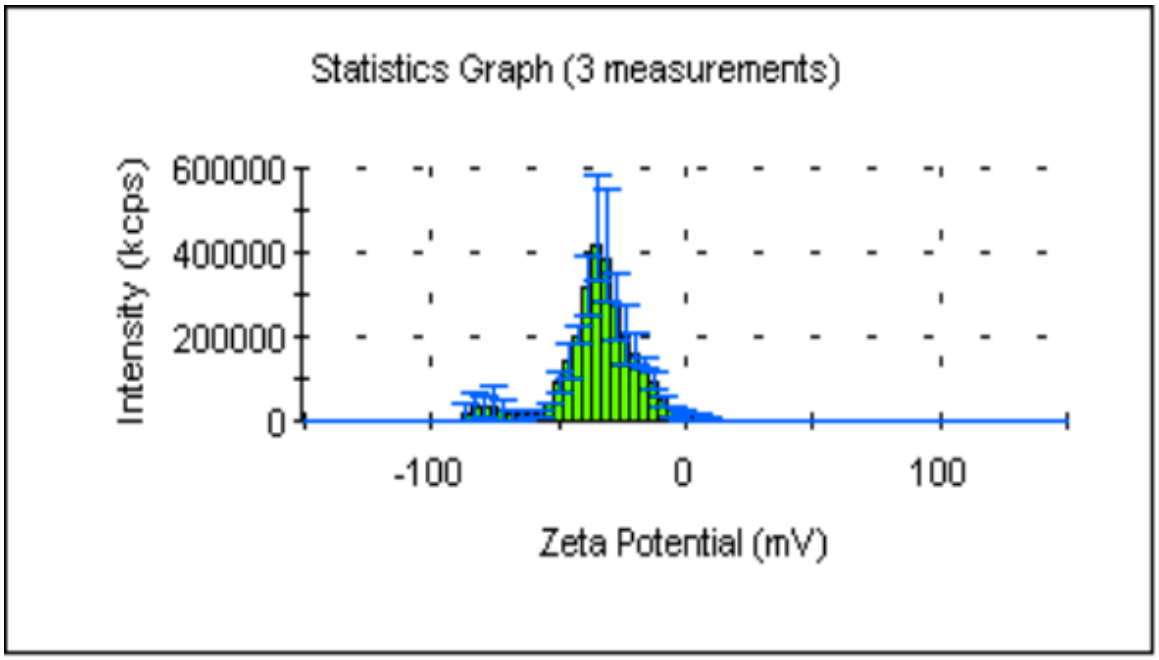

Figure 66 - Statistics graph of the zeta potential distribution by Intensity of Venofer® 1000ppm of iron. Total of three measurements.

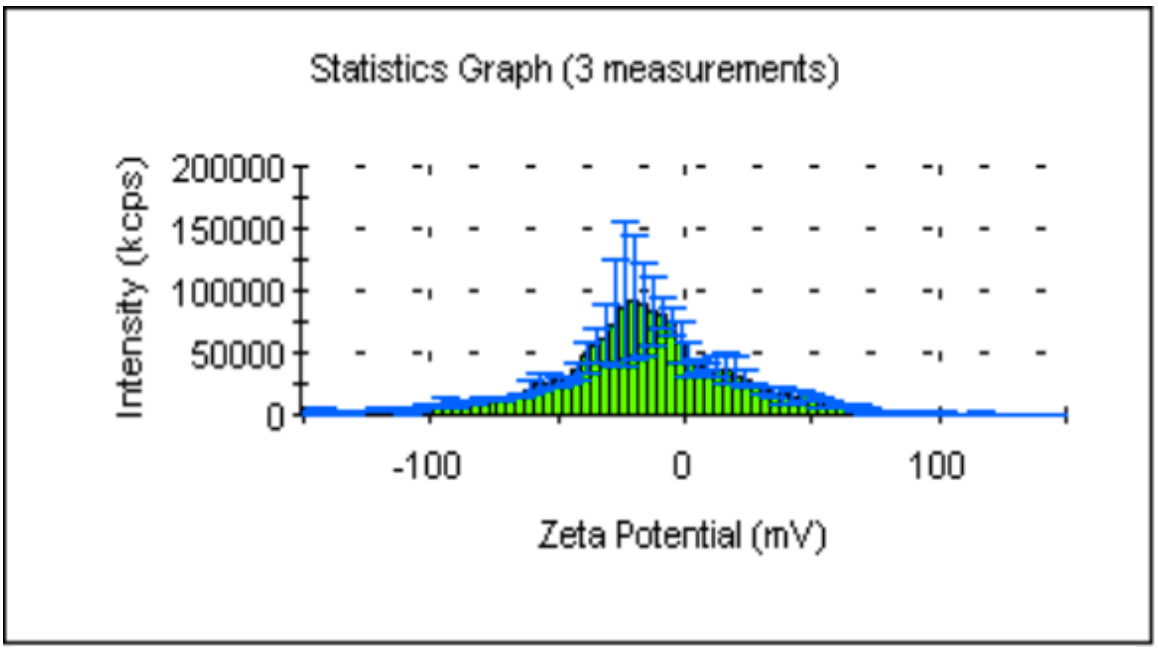

Figure 67 - Statistics graph of the zeta potential distribution by Intensity of Cosmofer® 1000ppm of iron. Total of three measurements.

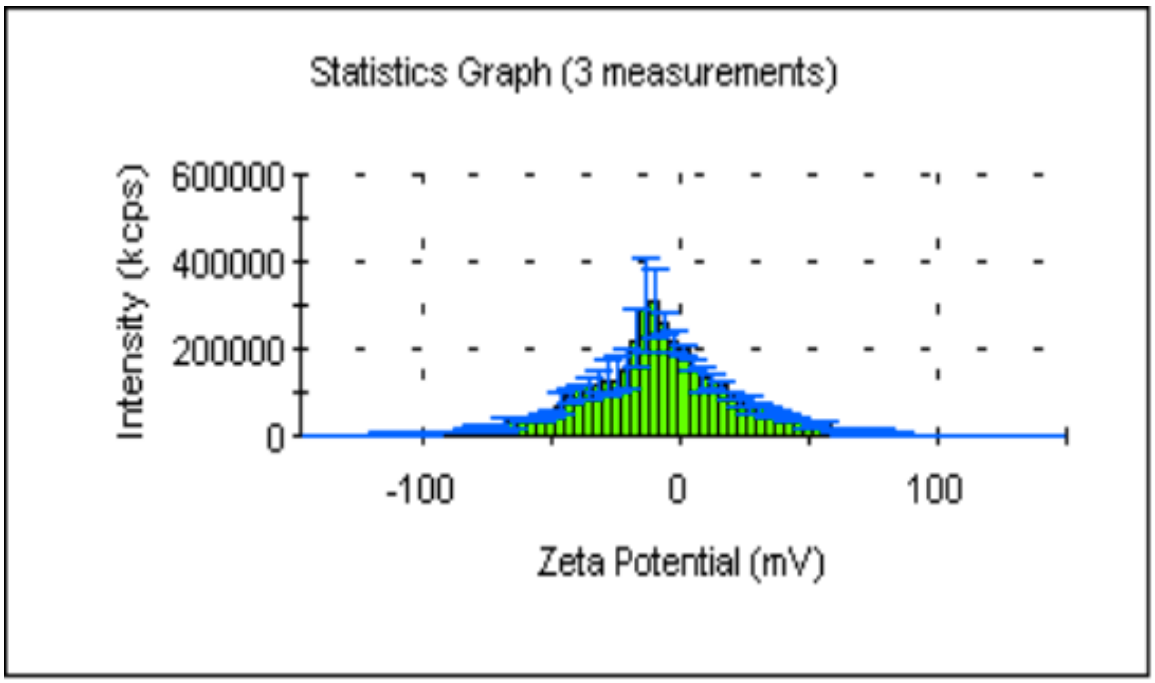

Figure 68 - Statistics graph of the zeta potential distribution by Intensity of Ferinject® 1000ppm of iron. Total of three measurements.

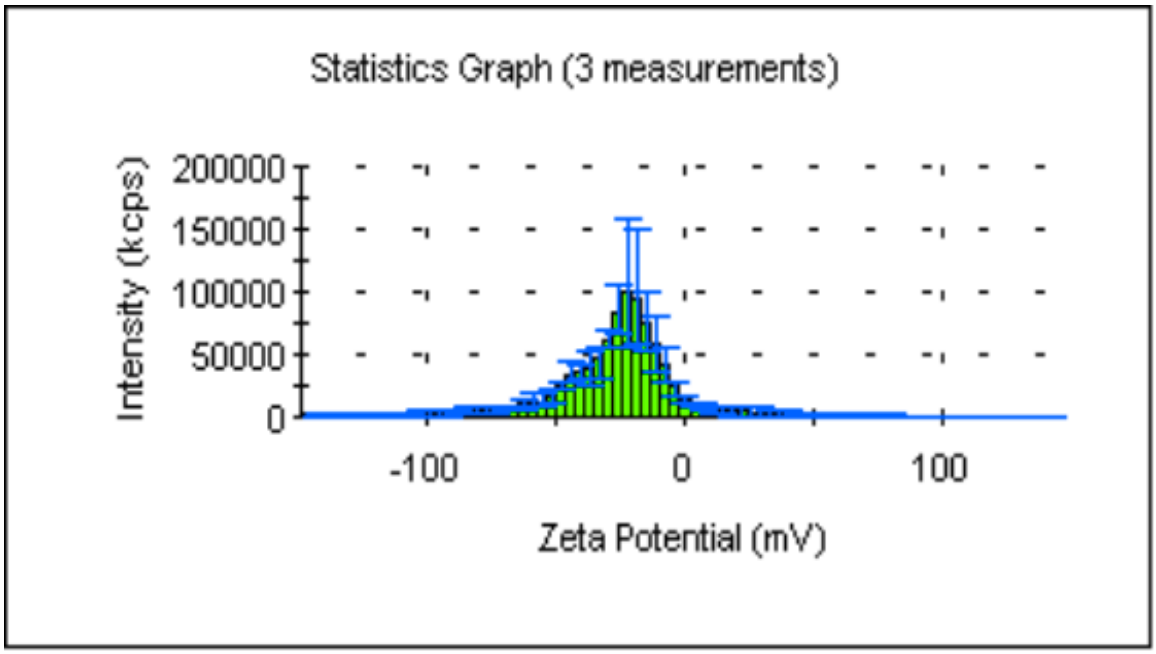

Figure 69 - Statistics graph of the zeta potential distribution by Intensity of Monofer® 1000ppm of iron. Total of three measurements.

The statistic graph of the zeta potential obtained for Ferinject® (500ppm of Fe) without pH adjustment (pH = 4.71):

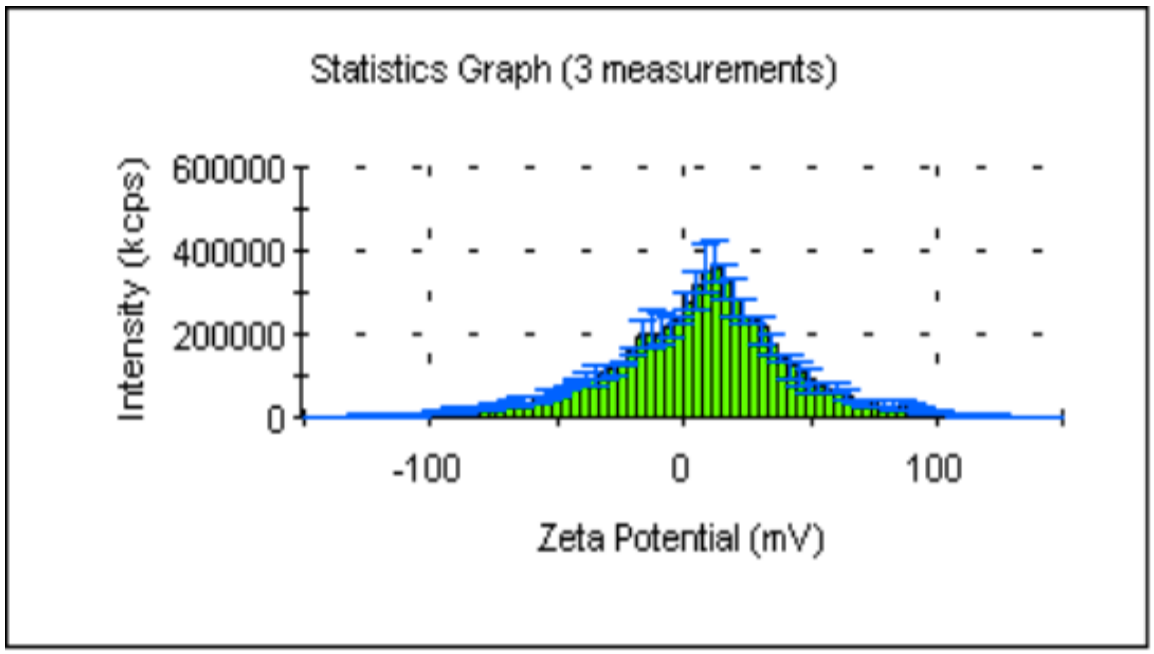

Figure 70 - Statistics graph of the zeta potential distribution by Intensity of Ferinject® 500ppm of iron at pH 4.71. Total of three measurements.

This is a typical calibration graph obtained in one batch of an ICP elemental analysis of iron. The three calibration curves resulted from the measurement of 9 iron standards before starting the measurement of the samples, in between, and after measuring all the samples.

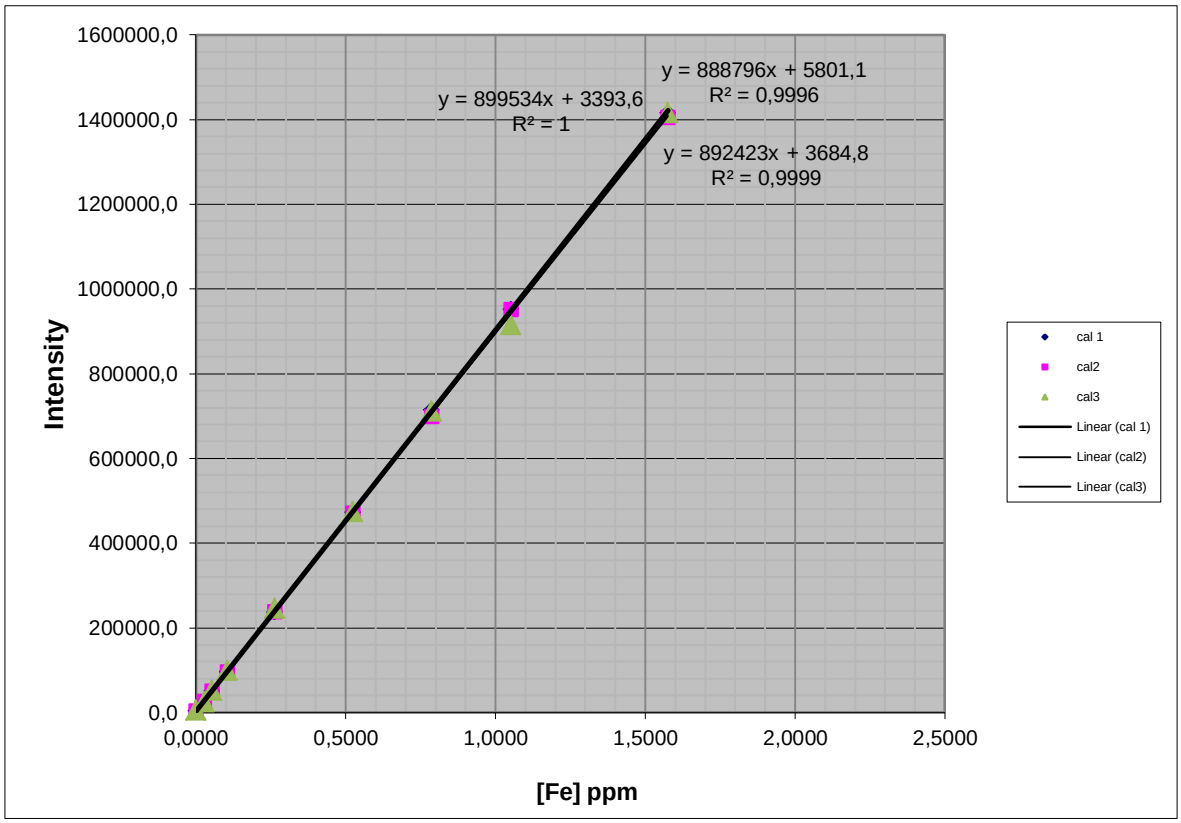

Figure 71 – Three calibration curves obtained during one batch of an ICP elemental analysis of iron.